



THE UNIVERSITY *of* EDINBURGH

Edinburgh Research Explorer

Pathogenic variants in SLF2 and SMC5 cause segmented chromosomes and mosaic variegated hyperploidy

Citation for published version:

Grange, LJ, Reynolds, JJ, Ullah, F, Isidor, B, Shearer, RF, Latypova, X, Baxley, RM, Oliver, AW, Ganesh, A, Cooke, SL, Jhujh, SS, McNee, GS, Hollingworth, R, Higgs, MR, Natsume, T, Khan, T, Martos-Moreno, GA, Chupp, S, Mathew, CG, Parry, D, Simpson, MA, Nahavandi, N, Yüksel, Z, Drasdo, M, Kron, A, Vogt, P, Jonasson, A, Seth, SA, Gonzaga-Jauregui, C, Brigatti, KW, Stegmann, APA, Kanemaki, M, Josifova, D, Uchiyama, Y, Oh, Y, Morimoto, A, Osaka, H, Ammous, Z, Argente, J, Matsumoto, N, Stumpel, CTRM, Taylor, AMR, Jackson, AP, Bielinsky, A-K, Mailand, N, Le Caignec, C, Davis, EE & Stewart, GS 2022, 'Pathogenic variants in SLF2 and SMC5 cause segmented chromosomes and mosaic variegated hyperploidy', *Nature Communications*, vol. 13, no. 1, 6664, pp. 6664. <https://doi.org/10.1038/s41467-022-34349-8>

Digital Object Identifier (DOI):

[10.1038/s41467-022-34349-8](https://doi.org/10.1038/s41467-022-34349-8)

Link:

[Link to publication record in Edinburgh Research Explorer](#)

Document Version:

Peer reviewed version

Published In:

Nature Communications

General rights

Copyright for the publications made accessible via the Edinburgh Research Explorer is retained by the author(s) and / or other copyright owners and it is a condition of accessing these publications that users recognise and abide by the legal requirements associated with these rights.

Take down policy

The University of Edinburgh has made every reasonable effort to ensure that Edinburgh Research Explorer content complies with UK legislation. If you believe that the public display of this file breaches copyright please contact openaccess@ed.ac.uk providing details, and we will remove access to the work immediately and investigate your claim.



1 **Pathogenic variants in *SLF2* and *SMC5* cause segmented chromosomes and**
2 **mosaic variegated hyperploidy.**

3
4 Laura J. Grange^{1*}, John J. Reynolds^{1*}, Farid Ullah^{2,3*}, Bertrand Isidor^{4*}, Robert F. Shearer⁵, Xenia
5 Latypova⁴, Ryan M. Baxley⁶, Antony W. Oliver⁷, Anil Ganesh¹, Sophie L. Cooke¹, Satpal S. Jhujh¹,
6 Gavin S. McNee¹, Robert Hollingworth¹, Martin R. Higgs¹, Toyoaki Natsume⁸, Tahir Khan⁹, Gabriel Á.
7 Martos-Moreno¹⁰, Sharon Chupp¹¹, Christopher G. Mathew¹², David Parry¹³, Michael A. Simpson¹⁴,
8 Nahid Nahavandi¹⁵, Zafer Yüksel¹⁵, Mojgan Drasdo¹⁵, Anja Kron¹⁵, Petra Vogt¹⁵, AnneMarie
9 Jonasson¹⁵, Saad Ahmed Seth¹⁶, Claudia Gonzaga-Jauregui^{17,18}, Karlla W. Brigatti¹⁹, Alexander P.A.
10 Stegmann²⁰, Masato Kanemaki²¹, Dragana Josifova²², Yuri Uchiyama^{23,24}, Yukiko Oh²⁵, Akira
11 Morimoto²⁵, Hitoshi Osaka²⁵, Zineb Ammous¹¹, Jesús Argente^{10,26}, Naomichi Matsumoto²³, Constance
12 T.R.M. Stumpel²⁷, Alexander M.R. Taylor¹, Andrew P. Jackson¹³, Anja-Katrin Bielinsky⁶, Niels Mailand⁵,
13 Cedric Le Caignec^{28#}, Erica E. Davis^{2,29#}, Grant S. Stewart^{1#}

14
15 1. Institute of Cancer and Genomic Sciences, University of Birmingham, Birmingham B15 2TT, United
16 Kingdom.

17
18 2. Advanced Center for Genetic and Translational Medicine (ACT-GeM), Stanley Manne Children's
19 Research Institute, Ann & Robert H Lurie Children's Hospital of Chicago, Chicago, IL 60611, USA

20
21 3. National Institute for Biotechnology and Genetic Engineering (NIBGE-C), Faisalabad; Pakistan
22 Institute of Engineering and Applied Sciences (PIEAS), Islamabad, Pakistan.

23
24 4. Service de Génétique Médicale, CHU Nantes, 9 quai Moncoussu, 44093 Nantes Cedex 1, France

25
26 5. Novo Nordisk Foundation Center for Protein Research, Faculty of Health and Medical Sciences,
27 University of Copenhagen, Copenhagen, Denmark

28
29 6. Department of Biochemistry, Molecular Biology and Biophysics, University of Minnesota,
30 Minneapolis, MN55455 USA

31

32 7. Genome Damage and Stability Centre, Science Park Road, University of Sussex, Falmer, Brighton,
33 BN1 9RQ, United Kingdom

34

35 8. Department of Chromosome Science, National Institute of Genetics, Research Organization of
36 Information and Systems (ROIS), Yata 1111, Mishima, Shizuoka 411-8540, Japan

37

38 9. Center for Human Disease Modeling, Duke University Medical Center, Durham, NC 27701, USA

39

40 10. Universidad Autónoma de Madrid, Hospital Infantil Universitario Niño Jesús, CIBER de
41 fisiopatología de la obesidad y nutrición (CIBEROBN), Instituto de Salud Carlos III. Avenida Menéndez
42 Pelayo, 65; 28009 Madrid, Spain

43

44 11. The Community Health Clinic, 315 Lehman Ave, Ste C, Topeka, Indiana, 46571, USA

45

46 12. Sydney Brenner Institute for Molecular Bioscience, Faculty of Health Sciences, University of the
47 Witwatersrand, Johannesburg, South Africa.

48

49 13. MRC Human Genetics Unit, MRC Institute of Genetics and Molecular Medicine, The University of
50 Edinburgh, Western General Hospital, Crewe Road, Edinburgh EH4 2XU

51

52 14. Department of Medical and Molecular Genetics, Faculty of Life Science and Medicine, King's
53 College London, Guy's Hospital, London, UK

54

55 15. Bioscientia Institute for Medical Diagnostics, Human Genetics, Ingelheim, Germany

56

57 16. King Fahad Military Medical Complex, Dhahran, Saudi Arabia

58

59 17. Regeneron Genetics Center, Regeneron Pharmaceuticals Inc., 777 Old Saw Mill River Road,
60 Tarrytown, New York 10591, USA.

61
62
63
64
65
66
67
68
69
70
71
72
73
74
75
76
77
78
79
80
81
82
83
84
85
86
87
88
89

18. International Laboratory for Human Genome Research, Universidad Nacional Autónoma de México, Querétaro, México

19. Clinic for Special Children, 535 Bunker Hill Road, Strasburg, Philadelphia, USA.

20. Department of Clinical Genetics, Maastricht University Medical Center, Maastricht, the Netherlands

21. Department of Genetics, The Graduate University for Advanced Studies (SOKENDAI), Yata 1111, Mishima, Shizuoka 411-8540, Japan

22. Clinical Genetics Department, Guy's Hospital, Great Maze Pond, London SE1 9RT, UK

23. Department of Rare Disease Genomics, Yokohama City University Hospital, 3-9 Fukuura, Kanazawa-ku, Yokohama 235-0004, Japan

24. Department of Human Genetics, Yokohama City University Graduate School of Medicine, 3-9 Fukuura, Kanazawa-ku, Yokohama 235-0004, Japan

25. Department of Paediatrics, Jichi Medical University School of Medicine, Tochigi, Japan.

26. IMDEA Alimentación/IMDEA Food. Madrid, Spain

27. Department of Clinical Genetics and GROW-School for Oncology and Developmental Biology, Maastricht University Medical Center, Maastricht, the Netherlands

28. Centre Hospitalier Universitaire Toulouse, Service de Génétique Médicale and ToNIC, Toulouse NeuroImaging Center, Université de Toulouse, Inserm, UPS, 31000 Toulouse, France.

90 29. Department of Pediatrics; Department of Cell and Developmental Biology, Feinberg School of
91 Medicine, Northwestern University, Chicago, IL 60611, USA.

92

93

94 * These authors contributed equally

95

96 # Corresponding authors: Grant S. Stewart (g.s.stewart@bham.ac.uk), Erica E. Davis
97 (eridavis@luriechildrens.org), Cedric Le Caignec (lecaignec.c@chu-toulouse.fr)

98

99 **Abstract**

100 Embryonic development is dictated by tight regulation of DNA replication, cell division and
101 differentiation. Mutations in DNA repair and replication genes disrupt this equilibrium, giving rise to
102 neurodevelopmental disease characterised by microcephaly, short stature and chromosomal breakage.
103 Here, we identify biallelic variants in two components of the RAD18-SLF1/2-SMC5/6 genome stability
104 pathway, *SLF2* and *SMC5*, in 11 patients with microcephaly, short stature, cardiac abnormalities and
105 anaemia. Patient-derived cells exhibit a unique chromosomal instability phenotype consisting of
106 segmented and dicentric chromosomes with mosaic variegated hyperploidy. To signify the importance
107 of these segmented chromosomes, we have named this disorder Atelís (meaning - incomplete)
108 Syndrome. Analysis of Atelís Syndrome cells revealed elevated levels of replication stress, partly due
109 to a reduced ability to replicate through G-quadruplex DNA structures, and also loss of sister chromatid
110 cohesion. Together, these data strengthen the functional link between SLF2 and the SMC5/6 complex,
111 highlighting a distinct role for this pathway in maintaining genome stability.

112

113 Introduction

114 Despite the fundamental nature of DNA replication and cell division, inherited variants in genes
115 involved in these processes are an underlying cause of human disease. Whilst these syndromes usually
116 display unique clinical features that define them diagnostically, they typically exhibit common
117 neurodevelopmental deficits, such as severe microcephaly and pre- and post-natal growth retardation¹⁻
118 ³. As such, many of these syndromes can be collectively referred to as microcephalic dwarfism (MD)
119 disorders. This constellation of conditions includes Meier-Gorlin Syndrome, Seckel Syndrome
120 Spectrum Disorders, Bloom Syndrome and Microcephalic Osteodysplastic Primordial Dwarfism type II
121 and can be broadly classified as having deficiencies in one of three cellular processes: DNA replication,
122 DNA repair, and mitotic cell division¹⁻⁴. Although mechanistically distinct, the common clinical
123 phenotypes exhibited by these diseases are thought to result from a reduction in cellular proliferation
124 and/or excessive cell death in the developing embryo, which reduces the number of cells available to
125 maintain normal foetal growth⁵. Cells from these patients often exhibit signs of increased genome
126 instability, such as micronuclei and/or elevated chromosome breakage. A distinct subgroup of these
127 syndromes exhibit rare cytogenetic anomalies, for example, mosaic variegated aneuploidy syndrome
128 (MVA)⁶⁻⁸ caused by variants in the spindle assembly checkpoint genes *BUB1B*, *CEP57* and *TRIP13*, or
129 railroad chromosomes and premature chromatid separation (PCS) associated with Warsaw Breakage
130 Syndrome (WABS) and Cornelia de Lange syndrome, caused by variants in the helicase *DDX11* and
131 components of SMC1/3 cohesin complex respectively^{9,10}. Whilst, the presence of these chromosomal
132 abnormalities is a useful diagnostic tool they can also help dissect the cellular mechanisms underlying
133 the disease pathology.

134 Here, we report 11 patients with a neurodevelopmental disorder overlapping clinically with MVA
135 and Fanconi Anaemia (FA) with pathogenic variants in *SLF2* and *SMC5*, two components of the recently
136 discovered RAD18-SLF1/2-SMC5/6 genome stability pathway¹¹. The precise function of the SMC5/6
137 complex remains enigmatic, however, it has been linked to a number of fundamental processes,
138 including DNA transcription, DNA replication, DNA repair and chromosome segregation^{12,13}. Evidence
139 suggests that the primary function of this complex occurs during DNA replication to stabilise stalled
140 forks, suppress the activity of pro-recombination factors and promote efficient replication through
141 difficult-to-replicate and/or repetitive regions of the genome, such as rDNA and telomeres¹⁴. In contrast,

142 the function of SLF1 and SLF2 remain unclear, other than a reported role in recruiting the SMC5/6
143 complex to sites of DNA damage¹¹.

144 Analysis of SLF2 and SMC5 patient-derived cell lines revealed spontaneous replication stress
145 and multiple mitotic abnormalities that give rise to a unique, diagnostically relevant, genome instability
146 phenotype consisting of segmented, dicentric and railroad chromosomes, and mosaic variegated
147 hyperploidy (MVH). The underlying basis for this chromosomal instability is not fully understood, but our
148 data suggest that it may arise, in part, from the failed resolution of aberrant DNA structures during S-
149 phase, such as G-quadruplexes (G4), potentially leading to a combination of under-replicated DNA and
150 unresolved recombination intermediates persisting through to mitosis. Together, these data
151 demonstrate that despite a hitherto unknown role as a core component of the SMC5/6 complex, SLF2
152 is essential for the SMC5/6 cohesin-like complex to maintain genome stability by regulating both DNA
153 replication and cell division.

154

155 **Results**

156 **Patients with microcephaly and short stature have biallelic *SLF2* (*FAM178A*) and *SMC5* variants**

157 Whole exome sequencing (WES) was carried out on six patients (P1, P2, P3, P4-1, P4-2, P5
158 and P6) from five families, presenting with microcephaly, short stature, mild to severe developmental
159 delay and spontaneous chromosome breakage. After aligning WES reads to the reference genome,
160 variant calling, and filtering for rare variants (MAF <0.005), analysis under a recessive model of
161 inheritance identified biallelic variants in *SLF2* (*FAM178A*) in all six patients. All identified *SLF2* variants
162 segregated amongst family members (with the exception of patients P1 and P5 where parental material
163 was unavailable) and were present at a frequency of <0.5% in the gnomAD database (Figure 1a, 1c;
164 Supplementary Table 1-7; Supplementary Figure 1a). Comparative genomic hybridisation (CGH) array
165 analysis carried out on gDNA from patient P5 confirmed the homozygosity of the identified *SLF2* variant.

166 Given that *SLF2* had been identified previously as part of the RAD18-SLF1/2-SMC5/6 genome
167 stability pathway¹¹, we hypothesised that variants in other components of this pathway may also give
168 rise to a similar neurodevelopmental disorder. By querying gene matching platforms, four patients
169 exhibiting microcephaly and growth retardation that had undergone WES were identified to carry
170 biallelic variants in *SMC5*: patient P7 (c.1110_1112del; p.Arg372del, c.1273C>T; p.Arg425Ter) and
171 patients P8, P9-1 and P9-2 (c.2970C>G; p.His990Asp) (Figure 1a, 1c; Supplementary Table 1;

172 Supplementary Table 8-10; Supplementary Figure 1b). All variants were verified by Sanger sequencing,
173 segregated amongst family members in an autosomal recessive paradigm and were present at a
174 frequency of <0.5% in gnomAD.

175

176 ***SLF2* and *SMC5* variants give rise to neurodevelopmental abnormalities, cardiac defects and**
177 **anaemia.**

178 All individuals with *SLF2* and *SMC5* variants presented with a similar clinical phenotype,
179 including marked microcephaly (-3.57 to -11.88 SD) and a reduction in height (-2.19 to -8.24 SD) (Figure
180 1b; Supplementary Table 1). Moreover, the majority of patients also exhibited a developmental delay
181 along with learning difficulties. Mild skeletal defects (i.e. clinodactyly), skin hyperpigmentation and
182 ocular abnormalities were present in several patients (Supplementary Table 1). Notably, two of seven
183 *SLF2* patients (P4-1, P5) and all four *SMC5* patients (P7, P8, P9-1 and P9-2) displayed cardiac defects
184 (Supplementary Table 1), such as atrial or ventricular defects, a phenotype commonly observed in
185 patients with cohesinopathies^{15,16} but not DNA replication disorders. Furthermore, five of eleven patients
186 (P3, P4-1, P4-2, P5, P9-2) also developed anaemia, with one of these patients (P9-2) subsequently
187 developing myelodysplastic syndrome (Supplementary Table 1). This, coupled with other clinical
188 features, could potentially result in future cases being mistakenly diagnosed with an atypical form of FA
189 in the absence of a clear genetic diagnosis using WES. This is particularly relevant since components
190 of the *SMC5/6* complex have been previously shown to functionally interact with the FA pathway to
191 repair DNA damage¹⁷. Only one patient (P3) developed severe pulmonary disease similar to patients
192 with variants in the *SMC5/6* complex subunit *NSMCE3*^{18,19}, whereas insulin-resistant diabetes and
193 metabolic dysfunction, which are characteristic to patients with *NSMCE2* variants were absent among
194 this cohort²⁰. Collectively, these clinical and genetic observations support the premise that variants in
195 *SLF2* and *SMC5* cause microcephaly and short stature associated with cardiac defects and the
196 development of anaemia.

197

198 ***SLF2* and *SMC5* variants compromise protein stability, interactions with other components of**
199 **the *RAD18-SLF1/2-SMC5/6* pathway and recruitment to sites of DNA damage**

200 To determine the pathogenicity of the identified patient variants, we carried out western blotting
201 on extracts from *SLF2* patient-derived cell lines (*SLF2*-P1, *SLF2*-P2, *SLF2*-P3 and *SLF2*-P4-1) to

202 ascertain if SLF2 protein abundance or stability was compromised. Notably, all four of the SLF2 mutant
203 patient cell lines examined exhibited a reduction or absence of detectable full length SLF2 protein whilst
204 maintaining wild type (WT) levels of RAD18, SMC5, and SMC6 protein (Figure 2a). SLF1 protein level
205 was not tested due to the absence of an available antibody.

206 We next investigated the *SLF2* variants in patients P2 and P3 in more detail. Analysis of cDNA
207 from the SLF2-P3 cell line demonstrated that the synonymous homozygous variant c.3330G>A
208 (p.Arg1110Arg), disrupted splicing leading to an in-frame deletion of exon 17 (Supplementary Figure
209 2a-b). We then analysed the impact of the c.3486G>C (p.Gln1162His) variant, present in patient P2,
210 on splicing. Multiple *SLF2* transcripts are annotated in the human genome and although c.3486G>C
211 (p.Gln1162His) introduces a nonsynonymous change in the two longest transcripts (NM_018121 and
212 NM_001136123), it only affects mRNA splicing of the most abundant *SLF2* transcript (NM_018121) by
213 impairing the exon 19 splice donor splice site (Supplementary Figures 2c, 3a-e). The p.(Gln1162His)
214 variant also displayed compromised protein stability when expressed transiently indicating that this
215 variant disrupts both mRNA and protein stability (Supplementary Figure 3f). Together, these data
216 suggest that most of the identified *SLF2* variants have an adverse effect on protein stability.

217 In contrast, analysis of SMC5 patient cell lines revealed that the homozygous p.(His990Asp)
218 variant present in patients P8, P9-1 and P9-2 had little detectable impact on the protein stability of
219 SMC5, or RAD18, SLF2, and SMC6 (Figure 2b). Only a cell line derived from patient P7 exhibited a
220 reduced abundance of SMC5 protein, presumably due to the presence of a nonsense variant
221 (p.Arg425Ter) on one of the *SMC5* alleles. As loss of Smc5 is embryonically lethal²¹, it is possible that
222 the *SMC5* variants are hypomorphic and that significant disruption of SMC5 protein stability to the extent
223 observed with the SLF2 variants is incompatible with life.

224 SLF1 and SLF2 have been identified as bridging factors between RAD18 and the SMC5/6
225 complex at sites of stalled replication¹¹. To address whether the SLF2 and SMC5 variants compromised
226 their ability to bind components of the RAD18-SLF1/2-SMC5/6 pathway, we initially mapped the binding
227 sites of RAD18, SLF1 and SMC6 on SLF2. Using co-immunoprecipitation analysis with tagged proteins,
228 we determined that the binding of RAD18 and SLF1 to SLF2 requires the C-terminal 471 amino acids
229 (aa702-1173), which also overlapped with the SMC6 binding site located at amino acids 589-810
230 (Supplementary Figure 4a-d). All patient-associated variants in SLF2, with the exception of
231 p.(Gln1162His), are located within or truncate the SLF1/RAD18 binding domain of SLF2 (Figure 1c).

232 Consistent with SLF1 binding being essential for SLF2 to mediate bridging between RAD18 and the
233 SMC5/6 complex, co-immunoprecipitation studies using extracts from hydroxyurea (HU) treated SLF2
234 patient-derived LCLs revealed a failure of all cell lines tested to co-purify SMC6 with RAD18 (Figure
235 2c). Furthermore, all SLF2 mutant proteins, with the exception of p.(Gln1162His), failed to or exhibited
236 a reduced ability to, be recruited to sites of DNA damage induced by laser micro-irradiation
237 (Supplementary Figure 3e).

238 We next extended the co-immunoprecipitation analysis to include SMC5 patient LCLs (Figure
239 2d). The interaction between RAD18 and SMC6 in SMC5-P8 and SMC5-P9-1 cells was observed to be
240 at WT levels, suggesting that p.(His990Asp) had no discernible impact on the integrity of the RAD18-
241 SLF1/2-SMC5/6 complex, whereas the association of RAD18 with SMC6 was partially affected in
242 SMC5-P7 cells. However, both the p.(Arg372del) and p.(His990Asp) SMC5 mutants failed to re-localise
243 efficiently to sites of laser micro-irradiation induced damage, with the latter being more severely affected
244 (Supplementary Figure 4f). These observations indicate that whilst these variants largely do not appear
245 to compromise their binding to components of the RAD18-SLF1-SLF2-SMC5/6 pathway, they do affect
246 their re-localisation to and/or retention at sites of damage.

247 To gain insight into why the SMC5 mutants affected stability of the SMC5/6 complex at sites of
248 damage, we carried out co-immunoprecipitation analysis to assess if these mutations affected binding
249 to other components of the complex. Interestingly, whilst the p.(His990Asp) mutation did not
250 significantly affect binding to other components of the SMC5/6 complex, the p.(Arg372del) significantly
251 compromised binding to SLF2, SMC6 and NSMCE2 (Figure 2e). Moreover, endogenous NSMCE2
252 exhibited reduced binding to SMC5 in cells from patient SMC5-P7 (Figure 2f). Consistent with these
253 observations, the Nse2 binding site on yeast Smc5 lies in close proximity to Lys368, which is the yeast
254 functional equivalent of human SMC5 Arg372 (Supplementary Figure 5). This suggests that the failure
255 of the p.(Arg372del) mutant SMC5 to be recruited to sites of laser damage may be due to this mutation
256 compromising the binding of other key components of the SMC5/6 complex.

257 To explore the possibility that the p.(His990Asp) may have a deleterious impact on the structure
258 of the SMC5/6 complex, we compared the AlphaFold model for human SMC5 to the X-ray crystal
259 structures for the head domain of *Pyrococcus furiosus* Rad50 (*Pf.Rad50*) in both the unliganded and
260 ATP-bound forms²³. Notably, His990 lies just upstream of the ATP-binding cassette (ABC) signature
261 motif of Smc5 (Supplementary Figure 6a), a region of the protein implicit in both binding ATP and

262 mediating the complex set of conformational changes that occur when SMC proteins bind nucleotide²².
263 Interestingly, His990 sits in a position functionally equivalent to Phe791 of *Pf.Rad50* – a residue known
264 to interact directly with the adenine moiety of bound ATP²³. Whilst mutation of His990 to aspartic acid
265 would appear to be tolerated and unlikely to cause any gross-misfolding of the protein, as judged by
266 the lack of steric clashes produced by the mutation (Supplementary Figure 6b), it removes an aromatic
267 amino acid and replaces it with one carrying a negative charge. As such, this would alter the overall
268 charge of a region that normally functions to accept the adenine moiety. Therefore, it is likely that the
269 p.(His990Asp) mutation perturbs the ability of the complex to either bind or turnover ATP, in turn
270 affecting its association with, or retention on chromatin²⁴.

271

272 **Cell cycle arrest and increased apoptosis in the developing brain underlies the development of** 273 **microcephaly in zebrafish lacking *slf2* and *smc5***

274 To gain insight into how SLF2 and SMC5 patient associated variants affect neurodevelopment,
275 we utilised CRISPR-Cas9 genome-editing to ablate the single zebrafish orthologs of each of *slf2* and
276 *smc5* in zebrafish embryos. Single guide (sg) RNAs targeting the primary isoforms of *slf2* and *smc5*
277 (Supplementary Figure 7a, 7f) were injected, with or without recombinant Cas9 protein, into -
278 *1.4col1a1:egfp* reporter embryos at the single-cell stage, which were allowed to develop until 3 days
279 post-fertilisation (dpf) (Supplementary Figure 7b-c, 7g-h). This reporter allows visualisation of
280 craniofacial patterning during embryonal development²⁵. Bright field lateral images were acquired to
281 measure head size and ventral fluorescent images of GFP-positive cells allowed visualisation of the
282 pharyngeal skeleton. Similar to the clinical phenotype exhibited by SLF2 and SMC5 patients, zebrafish
283 embryos lacking *slf2* and *smc5* displayed a significant reduction in head size and aberrant craniofacial
284 patterning, as indicated by a broadening of the angle of the ceratohyal cartilage; a major mandibular
285 structure (Figure 3a-f). Furthermore, unlike *smc5*, which is an essential gene²¹, we were able to
286 generate stable F2 *slf2* mutants possessing a frameshifting 8 bp deletion allele in *slf2* exon 7
287 (c.515_522del; p.Ser172_Ser174fsTer191; Supplementary Figure 7d-e). Consistent with our
288 observations from F0 embryos injected with sgRNA and Cas9, stable F2 *slf2* null mutants also exhibited
289 microcephaly and aberrant craniofacial patterning (Figure 3g).

290 To validate these findings, we used morpholinos (MO) to suppress the expression of *slf2* and
291 *smc5* in zebrafish embryos. Splice blocking MO targeting the single zebrafish ortholog of each gene,

292 *slf2* (exon 11) and *smc5* (exon3), were designed and depletion of *slf2* and *smc5* mRNA was confirmed
293 by RT-PCR after injection into zebrafish larvae (Supplementary Figure 8a-b). MO were injected into -
294 *1.4col1a1:egfp* reporter embryos at the single-cell stage. Injected embryos were reared to 3 dpf and
295 then bright field images were acquired to measure head size and ventral fluorescent images of GFP-
296 positive cells to visualise the pharyngeal skeleton. Comparable to our observations from the zebrafish
297 embryos lacking *slf2* and *smc5*, zebrafish embryos depleted of *slf2* and *smc5* using MO also displayed
298 a significant reduction in head size and aberrant craniofacial patterning in the pharyngeal skeleton
299 (Supplementary Figure 8e-h, Supplementary Figure 9a-f), which could both be rescued by re-
300 expression of WT human *SLF2* or *SMC5* mRNA.

301 To confirm the pathogenicity of the *SMC5* disease associated variants we utilised our *smc5*
302 morphant zebrafish model to ascertain whether the three patient-associated *SMC5* variants could
303 rescue the developmental abnormalities caused by loss of *smc5* expression. Neither the p.(Arg425Ter),
304 p.(Arg372del) nor p.(His990Asp) variants could complement the reduced head size and increased
305 ceratohyal angle resulting from *smc5* depletion (Supplementary Figure 9g-i), reinforcing that they confer
306 a loss of function effect. In contrast, both the head size and ceratohyal angle could be restored to normal
307 following expression of WT human *SMC5* or a polymorphic *SMC5* variant, p.(Arg733Gln), identified
308 from gnomAD.

309 To investigate the two principal underlying causes of microcephaly, slowed cell cycle
310 progression and/or increased apoptosis in the developing brain^{2,26-28}, fixed wholemount *slf2* and *smc5*
311 depleted zebrafish embryos were stained with markers of cell cycle stage (G2/M: phospho-histone H3
312 serine-10) and apoptosis (TUNEL). F0 CRISPR embryos injected with either *slf2* or *smc5* sgRNA with
313 recombinant Cas9 (Figure 4) exhibited a pronounced increase in both phospho-histone H3 and TUNEL
314 staining in the developing brain when compared to control zebrafish. Importantly, this phenotype was
315 recapitulated in zebrafish embryos transfected with *slf2* or *smc5* MO, which could be complemented by
316 re-expression of the orthologous WT human mRNA (Supplementary Figure 10). Together, these in vivo
317 data confirm that a functional RAD18-SLF1/2-SMC5/6 pathway is required for normal development of
318 the brain and cartilaginous structures, and compromising this pathway triggers a G2/M cell cycle arrest
319 and the onset of apoptosis leading to microcephaly.

320

321 **SLF2/SMC5 mutant patient-derived cell lines exhibit increased spontaneous replication stress**

322 Although the SMC5/6 complex has been implicated in regulating numerous DNA repair and
323 replication pathways, it is thought that its primary function is to promote efficient replication^{14,29}.
324 Therefore, we used DNA fibre analysis to study the impact of SLF2 and SMC5 variants on replication
325 dynamics. All *SLF2* and *SMC5* mutant LCLs examined exhibited a significant increase in spontaneous
326 replication fork stalling and fork asymmetry comparable to that observed in an LCL derived from an
327 ATR-Seckel Syndrome patient (Figure 5a-d). Importantly, this increased spontaneous replication fork
328 stalling was also observed in patient-derived fibroblasts and could be suppressed by re-expressing WT
329 *SLF2* or *SMC5* (Figure 5e-f; Supplementary Figure 11a-b). Unlike the ATR-Seckel cell line, all the *SLF2*
330 mutant LCLs and one of the *SMC5* mutant LCLs exhibited WT levels of replication fork speed
331 (Supplementary Figure 11c-d). In contrast, LCLs carrying the homozygous p.(His990Asp) exhibited a
332 moderate reduction in replication fork speed.

333 To confirm these observations, we used CRISPR-Cas9 gene editing in U-2 OS cells to generate
334 *SLF2* knockout clones. Despite several attempts we were unable to generate complete *SLF2* knockout
335 clones. Rather, we generated two hypomorphic (HM) clones, each with one expressed mutant allele of
336 *SLF2* in conjunction with one or more truncating mutant alleles: *SLF2* HM cl.1 (p.Asn411Lysfs16,
337 p.Ser403Ter, p.Asn411LysfsTer3) and *SLF2* HM cl.2 (p.Asp398_Ser404del, p.Ser403ThrfsTer14).
338 These clones were subsequently complemented by re-expressing WT *SLF2* (Supplementary Figure
339 12). Importantly, DNA fibre analysis of these *SLF2* HM clones demonstrated that the vector
340 complemented *SLF2* HM cell lines exhibited significantly elevated levels of spontaneous fork stalling
341 compared to the WT *SLF2* complemented clones (Figure 5g).

342 Since spontaneous replication stress exhibited by cells can be attributed to defective ATR-
343 dependent DNA damage signalling, we used DNA fibre analysis and western blotting to monitor
344 activation of the ATR-dependent stress response^{30,31}. In contrast to the ATR-Seckel syndrome cell line,
345 all the *SLF2* or *SMC5* patient cell lines were capable of activating ATR or the intra-S phase checkpoint
346 in response to HU and MMC (Supplementary Figure 11e-f, Supplementary Figure 13) indicating that
347 dysregulation of the ATR stress response pathway does not account for the observed DNA replication
348 defects. This is consistent with previous work demonstrating that loss of the SMC5/6 pathway does not
349 affect activation of the ATR-dependent DDR¹⁷.

350 We next investigated the cellular impact of the increased spontaneous replication fork instability
351 observed in the patient cell lines using different markers of replication stress. Significantly, both *SLF2*

352 and SMC5 patient cell lines exhibited elevated signs of spontaneous replication stress including the
353 presence of DNA double strand breaks (DSBs) in S-phase cells (53BP1 foci in EdU positive cells), an
354 increased frequency of mitotic cells undergoing mitotic DNA synthesis (MiDAS), elevated levels of
355 53BP1 G1 bodies and the formation of micronuclei (Figure 6a-d, Supplementary Figure 14a-d)^{17,29}.
356 Crucially, all these phenotypes could be complemented by re-expressing either WT *SLF2* or *SMC5*
357 (Figure 6). Moreover, the U-2 OS *SLF2* HM cell lines also exhibited elevated levels of micronuclei
358 compared to the corrected WT *SLF2* expressing clones (Figure 6e).

359

360 **Hypomorphic variants in *SLF2* and *SMC5* are associated with mitotic abnormalities, segmented** 361 **chromosomes, cohesion defects and mosaic variegated hyperploidy**

362 Consistent with the elevated levels of spontaneous replication stress, LCLs derived from *SLF2*
363 and *SMC5* mutant patients all exhibited increased levels of chromosomal aberrations (such as
364 chromosome and chromatid gaps/breaks and chromosome radials) comparable to that observed in an
365 ATR Seckel Syndrome LCL (Figure 6f-g). Notably, this phenotype was not significantly exacerbated by
366 exposure to either APH or MMC, unlike LCLs from an ATR-Seckel Syndrome patient (Supplementary
367 Figure 15a-b). Importantly, the elevated spontaneous levels of chromosomal aberrations in the
368 *SLF2/SMC5* patient fibroblasts and the U-2 OS *SLF2* HM cells, was rescued by re-expression of either
369 WT *SLF2* or *SMC5* (Figure 6h-i).

370 In addition to the spontaneous chromosomal aberrations, metaphase spread analysis of both
371 the peripheral blood and patient-derived LCLs of *SLF2* and *SMC5* patients revealed that a significant
372 subset of cells exhibited large increases in chromosome numbers, with some metaphases having >100
373 chromosomes (Figure 7a; Supplementary Figure 16a-b; Supplementary Figure 17a). Unlike MVA,
374 which typically involves the loss/gain of small numbers of chromosomes, the cytogenetic abnormality
375 observed in *SLF2* and *SMC5* patient cells predominantly involved huge chromosomal gains. Therefore,
376 we have termed this cytogenetic abnormality mosaic variegated hyperploidy (MVH), i.e. chromosome
377 number >46.

378 To investigate the cause of the MVH, we explored whether *SLF2* or *SMC5* patient-derived cell
379 lines exhibited spontaneous mitotic abnormalities. Both *SLF2* and *SMC5* patient fibroblast cell lines,
380 and U-2 OS *SLF2* HM cells, displayed a significant increase in mitotic cells with lagging chromosomes
381 in empty vector complemented cells compared to cells re-expressing WT protein (Figure 7b-d),

382 consistent with previous reports^{17,29,32}. Additionally, when we examined the origins of these lagging
383 chromosomes/micronuclei using CENPA as a marker of centromeres, it was evident that a significant
384 proportion of the micronuclei were positive for CENPA, suggesting that they could have resulted from
385 failed mitotic segregation (Supplementary Figure 16c-d). This is supportive of the RAD18-SLF1/2-
386 SMC5/6 pathway playing an important role in promoting proper chromosomal segregation.

387 Since SMC5/6 forms a cohesin-like complex and has been implicated in facilitating centromeric
388 and sister chromatid cohesion^{21,32-35}, we analysed metaphase spreads from SLF2 and SMC5 patient-
389 derived cells for the presence of cohesion defects. SLF2 and SMC5 peripheral blood lymphocytes
390 showed loss of sister chromatid cohesion as evidenced by the presence of railroad chromosomes
391 (Figure 7e; Supplementary Figure 17b). Moreover, SLF2 and SMC5 patient-derived LCLs exhibited
392 PCS after treatment with the proteasome inhibitor MG132, which is known to induce cohesion fatigue
393 by preventing the metaphase-to-anaphase transition³⁶ (Figure 7f). Together, these observations
394 suggest that the MVH characteristic to SLF2 and SMC5 patient cells may also be caused by PCS
395 resulting from cohesion fatigue.

396 However, given the extent of the karyotypic abnormalities it seemed plausible that other cellular
397 defects may contribute to the large increases in chromosome number seen in SLF2 and SMC5 mutant
398 cell lines in addition to PCS. Replication stress can trigger centrosome amplification via fragmentation
399 of the pericentriolar material (PCM)³⁷ or premature centriole disengagement, which can lead to mitotic
400 arrest and aneuploidy-induced cell death and microcephaly³⁸. To investigate whether centrosome
401 abnormalities could contribute to the cellular pathology associated with SLF2 and SMC5 dysfunction,
402 patient-derived cell lines were subjected to immunofluorescence with antibodies to PCNT1 (a
403 component of the PCM) and mitotin/CENPF (marker of S/G2 cells) before and after incubation with
404 aphidicolin (APH). Notably, following APH exposure a significant proportion of S/G2 cells possessed
405 more than two centrosomes (Figure 7g). We also observed that APH treatment had a profound effect
406 on mitosis with >10-50% of SLF2 and SMC5 patient-derived LCLs exhibiting multi-polar spindles during
407 mitosis (Figure 7h, Supplementary Figure 16e). This increase in centrosome number and multi-polar
408 spindles is not due to higher levels of replication stress in the APH treated patient cells as quantification
409 of APH-induced G1 53BP1 bodies revealed no difference between empty vector and WT SLF2/SMC5
410 complemented cells (Figure 7i). Therefore, it is likely that the MVH observed in SLF2 and SMC5 patient

411 cells arises as a consequence of multiple defects including unresolved replication stress, PCS,
412 chromosome mis-segregation and centrosome amplification.

413

414 **SLF2/SMC5 mutant cells are unable to replicate efficiently in the presence of stabilised G-**
415 **quadruplex structures.**

416 During our analysis of metaphase spreads of peripheral blood lymphocytes from SLF2 and
417 SMC5 patients, we noted that among the increased levels of spontaneous chromosomal damage, two
418 distinct types of chromosome abnormality were evident (Figure 8a; Supplementary Figure 18). The first
419 type of abnormal chromosome, which we termed segmented chromosomes, contained one or more
420 chromosome gaps/breaks along the body of the chromosome (type 1). Type 1 segmented
421 chromosomes with two or more gaps/breaks were particularly evident in SLF2-P1 and SLF2-P3, whilst
422 most of the segmented chromosomes in SLF2-P2 and SMC5-P7 possessed one gap/break. The
423 second type of abnormal chromosomal structure resembled a dicentric chromosome, which was
424 confirmed by the presence of two centromeres using centromere specific FISH probes (type 2) (Figure
425 8b).

426 The type 1 segmented chromosomes were reminiscent of the chromosomal abnormalities
427 resulting from combined inactivation of GEN1 and either MUS81 or SLX4, suggesting that they may be
428 caused by an inability to resolve recombination intermediates^{39,40}. Accordingly, both SLF2 and SMC5
429 patient-derived cell lines exhibited elevated levels of recombination as indicated by increased levels of
430 spontaneous RAD51 foci and sister chromatid exchanges (SCEs) in the patient-derived fibroblasts and
431 LCLs respectively (Figure 8c, Supplementary Figure 19a-b, Supplementary Figure 15c-d). This is in line
432 with previous work demonstrating a role for the SMC5/6 complex in resolving recombination
433 intermediates⁴¹⁻⁴⁴. We also observed an increased frequency of telomeric SCEs in SLF2 mutant LCLs
434 (Supplementary Figure 19c), which could, in part, contribute to the generation of the observed dicentric
435 chromosomes. To investigate whether the spontaneous chromosomal aberrations observed in
436 SLF2/SMC5 mutant cells could arise as a consequence of the presence of unresolved HR
437 intermediates, we examined the effect of stably expressing the bacterial Holliday junction resolvase,
438 RusA, in patient-derived cell lines on genome stability⁴⁰. In line with SLF2 and SMC5 dysfunction
439 causing unresolved HR intermediates to accumulate and this leading to increased genome instability,
440 expression of WT RusA increased the level of spontaneous chromosome aberrations in SLF2/SMC5

441 mutant cells lines complemented with an empty vector but not with WT SLF2 or SMC5 (Supplementary
442 Figure 19c).

443 It is known that the SMC5/6 complex is important for the dissolution of replication stress-
444 induced recombination, especially at repetitive regions prone to forming secondary structures and
445 natural replication pause site intermediates^{41,43-46}. This is consistent with our observations that the
446 replication stress phenotype observed in SLF2/SMC5 mutant cells was not markedly exacerbated by
447 exposure to MMC, APH and HU (Figure 5; Supplementary Figures 11 and 13). Recently, it has been
448 shown that RNF168, which promotes the recruitment of the RAD18-SLF1/2-SMC5/6 pathway to
449 damaged replication forks, is important for signalling the presence of G-quadruplex (G4) DNA structures
450 stabilised by the RNA polymerase I inhibitor, CX5461⁴⁷. Since cells deficient in BRCA1/2 and the
451 cohesin-associated helicase DDX11 are also hypersensitive to this agent^{48,49} and DDX11 was shown
452 to function with SMC5/6 to repair DNA damage^{17,50,51}, we hypothesised that the RAD18-SLF1/2-
453 SMC5/6 pathway might play a role in suppressing replication stress at sites of stabilised G4 structures.
454 To test this possibility, we first investigated the effects of CX5461 on DNA replication using DNA fibre
455 analysis. This revealed that whilst WT SLF2 and SMC5 expressing patient fibroblasts could replicate
456 normally in the presence of CX5461, SLF2 and SMC5 patient fibroblasts complemented with an empty
457 vector exhibited a significant reduction in replication fork speed when incubated with this G4-stabilizing
458 compound (Figure 8d). Additionally, SLF2 and SMC5 patient-derived fibroblasts, LCLs and U-2 OS
459 SLF2 HM cells treated with CX5461 exhibited increased levels of G1 phase 53BP1 bodies and
460 chromosome aberrations (Figure 8e, Supplementary Figure 20a, c). In keeping with this, LCLs from
461 SLF2-P1 and SMC5-P8 displayed an increased sensitivity to CX5461 (Figure 8f). Strikingly, we also
462 observed that CX5461 treatment induced a significant increase in the levels of type 1 segmented
463 chromosomes in the SLF2 and SMC5 patient LCLs, but not in the WT LCLs (Supplementary Figure
464 20b). These data suggest a role for SLF2 and the SMC5/6 complex in resolving replication stress at
465 sites of stabilised G4 structures.

466 Whilst CX5461 is known to inhibit RNA polymerase I and stabilise G-quadruplexes, more
467 recently it has also been identified as a TOP2 poison^{52,53}. Given the pleiotropic nature of CX5461, we
468 sought to identify which genotoxic lesion induced by CX5461 was causing the increased replication
469 stress in cells deficient in components of the SMC5/6 complex. In this respect, we carried out DNA fibre
470 and chromosomal aberration analysis on patient-derived cell lines following exposure to pyridostatin (a

471 G-quadruplex stabiliser), etoposide (a TOP2 poison) and BMH21 (an RNA polymerase I inhibitor).
472 Interestingly, only exposure to pyridostatin caused a significant reduction in replication progression and
473 an increase in the levels of chromosome aberrations in SLF2 and SMC5 mutant cell lines (Figure 8g,
474 Supplementary Figure 20d).

475 Taken together, these observations support the notion that the spontaneous replication stress
476 and chromosomal instability displayed by cells from patients with SLF2/SMC5 mutations is caused, in
477 part, by an inability to resolve a specific subset of replication-associated recombination intermediates
478 arising at sites of G4 structures.

479

480 Discussion

481 Disrupting the delicate balance between stem cell proliferation and differentiation profoundly
482 affects embryonic development, particularly body growth and brain development. Rapidly proliferating
483 pluripotent stem cells exhibit constitutively high levels of replication stress and as such are heavily
484 reliant on replication-associated DNA damage response pathways to maintain genome stability.
485 Unsurprisingly, patients with pathogenic variants in genes encoding components of the replisome, the
486 DNA damage response (DDR) and factors that maintain sister chromatid cohesion exhibit
487 developmental abnormalities including severe microcephaly and dwarfism. Furthermore, variants in
488 centrosome components and regulators of the microtubule-spindle network can also result in these
489 developmental abnormalities by affecting the orientation of the spindle pole and/or triggering excessive
490 cell death through the generation of aneuploid cells¹. However, it is often difficult to determine whether
491 the cellular pathology underlying the development of these neurodevelopmental disorders results
492 primarily from the presence of aberrant replication or defective mitosis^{38,54,55}.

493 Here we report the clinical and genetic characterization of 11 patients with biallelic variants in
494 two components of the newly described RAD18-SLF1/2-SMC5/6 DDR pathway, *SLF2* and *SMC5*,
495 exhibiting microcephaly, short stature, cardiac defects and anaemia. However, in contrast to FA and
496 other known disorders, cells from these patients exhibit a unique chromosomal instability phenotype,
497 hallmarked by segmented and dicentric chromosomes and mosaic variegated hyperploidy, arising from
498 a combination of replication stress- and mitosis-associated cellular pathologies. Given that the
499 segmented chromosomes seen in *SLF2* and *SMC5* patient cells represent a chromosome instability
500 phenotype not previously associated with any known DNA repair or replication deficiency disorder, we
501 have named this syndrome, Atelís Syndrome (ATS), after the Greek word for incomplete to signify the
502 importance of these atelic or segmented chromosomes as a diagnostic marker of the disease.

503 The *SMC5/6* complex has been shown to have many functions in the cell, including regulating
504 homologous recombination (HR)-dependent DNA repair, stabilising and restarting stalled replication
505 forks, maintaining replication through highly repetitive regions of the genome, maintaining rDNA
506 stability, elongating telomeres by ALT and controlling the topology of unusual DNA structures^{12,14,56,57}.
507 In contrast, little is known about the functions of *SLF1* and *SLF2*, which were identified during a large
508 proteomic screen of proteins associated with damaged replication forks¹¹. However, it has been
509 suggested that *SLF1* and *SLF2* are functional orthologs of the yeast *Nse5* and *Nse6* proteins,

510 respectively, which are important for localising the SMC5/6 complex to DNA damage and regulating its
511 ATPase activity^{11,58-60}.

512 Pursuant to the role of the SLF1/2-SMC5/6 complex in maintaining replication fork stability, we
513 demonstrate that cells from ATS patients exhibit elevated levels of spontaneous replication stress,
514 although this was not exacerbated significantly following exposure to replication stress-inducing agents
515 (HU, MMC or APH). This suggests that the clinical phenotype resulting from variants in *SLF2* and *SMC5*
516 may not simply arise from elevated levels of replication stress, but rather from deficits with a subset of
517 replication forks, such as those replicating through difficult-to-replicate regions of the genome or
518 encountering specific types of endogenous DNA lesions. Consistent with this hypothesis, ATS cells fail
519 to replicate efficiently in the presence of stabilised G4 structures and accumulate chromosomal
520 damage, suggesting that the RAD18-SLF1/2-SMC5/6 pathway functions to resolve replication
521 intermediates occurring at these lesions. Since G4 structures have been shown to be enriched at
522 telomere repeat sequences⁶¹, a defect in the ability to replicate through these lesions could result in
523 genome instability at telomeres, potentially explaining the presence of dicentric chromosomes in ATS
524 patient cells.

525 ATS patients exhibit overlapping clinical and cellular features with WABS patients, including
526 microcephaly, growth restriction, skin hyper-pigmentation, ocular abnormalities and heart defects.
527 Moreover, cell lines derived from both ATS and WABS patients exhibit loss of sister chromatid cohesion
528 and premature chromatid separation⁴⁹. Interestingly, the loss of sister chromatid cohesion in WABS cell
529 lines is exacerbated upon exposure to replication stress-inducing genotoxins, including G4 stabilising
530 agents⁴⁹. Notably, cells from *Ddx11* null mice display loss of sister chromatid cohesion, chromosome
531 segregation errors and aneuploidy, which has been shown to induce a G2/M cell cycle delay and
532 apoptosis⁶². This suggests that a failure to resolve specific endogenous DNA lesions, such as G4
533 structures, in ATS cells may directly compromise cohesion, or exacerbate a pre-existing cohesion
534 defect, thus giving rise to chromosome segregation defects and aneuploidy that triggers cell death in
535 highly proliferative tissues, such as the developing brain.

536 It is clear that the RAD18-SLF1/2-SMC5/6 pathway plays additional cellular roles beyond
537 promoting replication through G4 lesions. In yeast, the *smc5/6* complex restrains recombination at
538 programmed fork pause sites, for example, in the rDNA locus^{43,44,63} and, in mammalian cells, SMC5/6
539 is involved in suppressing HR at highly repetitive sequences, e.g. rDNA, centromeres and

540 telomeres^{14,63}. Consistent with this, ATS cells exhibit elevated levels of RAD51 in S-phase cells and
541 spontaneous SCEs and tSCEs. Interestingly, segmented chromosomes have been observed in cells
542 that have a combined defect in both the Holliday junction dissolution and resolution pathways⁶⁴,
543 indicating that the gaps in the type 1 segmented chromosomes may result from a failure to
544 dissolve/resolve recombination intermediates⁴¹.

545 Cells from *NSMCE2* and *NSMCE3* mutant patients are not known to display segmented or
546 dicentric chromosomes, and whilst *NSMCE3* patient-derived cells exhibit aneuploidy and structural
547 chromosome abnormalities, hyperploidy to the extent seen in ATS cells was not reported^{18,20}. This
548 indicates that neither *NSMCE2* nor *NSMCE3* subunits are essential for this SMC5/6 function, or that
549 the hypomorphic variants in these genes retain sufficient function to suppress these chromosomal
550 phenotypes. Consistent with the latter scenario, *Nsmce2* transgenic mice lacking SUMO E3 ligase
551 activity developed normally, whereas a complete loss of *Nsmce2* resulted in early embryonic lethality
552 associated with chromosome segregation defects⁶⁵. Notably MEFs derived from the *Nsmce2* knockout
553 mice exhibited increased spontaneous replication stress and genome instability due to a failure to
554 detangle recombination intermediates similar to ATS patient cell lines (e.g. elevated levels of BRCA1
555 foci, increased sister chromatid and telomeric SCEs and chromosomal segregation errors)⁶⁵ indicating
556 that ATS represents a more severe form of SMC5/6 dysfunction.

557 Interestingly, the clinical phenotype exhibited by patients with variants in the SMC5/6 complex
558 components *NSMCE2* and *NSMCE3* are different from each other, with the former being associated
559 with microcephalic primordial dwarfism and insulin resistance²⁰ and the latter being associated with
560 severe pulmonary disease and immunodeficiency^{18,19}. It is unclear why these clinical presentations are
561 different, especially as the cellular phenotype resulting from *NSMCE2* and *NSMCE3* variants are
562 similar^{18,20}. One possible important cellular difference between the two disorders is that the patient-
563 associated missense variants in *NSMCE3* result in the destabilization of the SMC5/6 complex to a much
564 greater extent than the nonsense variants present in *NSMCE2* patients^{18,20}. It is notable that the clinical
565 phenotype of ATS patients more closely resembles that of *NSMCE2* patients than *NSMCE3* patients,
566 and like *NSMCE2* patient variants, *SLF2* and *SMC5* patient variants do not destabilise the SMC5/6
567 complex to any significant degree.

568 Taken together, we have demonstrated that variants in two components of the RAD18-SLF1/2-
569 SMC5/6 pathway give rise to a FA/MVA-like disorder, termed Atelis Syndrome, with clinical and cellular

570 features overlapping with WABS, MVA, NSMCE2 variants and FA. In vivo ablation of *sif2* and *smc5* in
571 zebrafish recapitulate patient phenotypes including microcephaly and craniofacial patterning defects,
572 likely due to concomitant cell cycle defects and apoptosis. We show that cells from ATS patients display
573 a unique and complex chromosomal instability phenotype consisting of atelic (segmented) and dicentric
574 chromosomes coupled with MVH, which should allow for cytogenetic diagnosis of patients with this
575 disorder.
576

577 **Methods**

578

579 **Research subjects.**

580 Informed consent was obtained from all participating families to take clinical samples and to
581 publish clinical information in accordance with local approval regulations and in compliance with the
582 Declaration of Helsinki principles. This study was approved by the West Midlands, Coventry and
583 Warwickshire Research Ethics Committee (REC: 20/WM/0098), the Scottish Multicentre Research
584 Ethics Committee (REC: 05/MRE00/74), the Lancaster General Hospital Institutional Review Board and
585 the Institutional Review Boards of Yokohama City University Graduate School of Medicine (ID:
586 A190800001) and Jichi Medical University (ID: G21-V06). A collaboration to study the pathological
587 significance of the identified *SLF2* and *SMC5* variants was established via GeneMatcher⁶⁶.

588

589 **Exome sequencing.**

590 Genomic DNA from affected children and family members was extracted from peripheral blood
591 using standard methods. Whole exome capture and sequencing was performed as described to a
592 minimum of 30x coverage⁶⁷. Exome sequencing for families 8 and 9 was conducted in collaboration
593 with the Regeneron Genetics Center as previously described⁶⁸. Briefly, DNA was sheared (Covaris S2),
594 exome capture performed using the Agilent SureSelect v5 enrichment kit according to manufacturer's
595 instructions, and libraries were sequenced with 125 bp read-pairs using the Illumina HiSeq 2500 V4
596 platform. All analyses were performed as described⁶⁹. Variants were confirmed by bidirectional capillary
597 dye-terminator sequencing and annotated using the reference sequences, GenBank: NM_018121.4,
598 NM_001136123.2 and NM_015110.4. Capillary sequencing was performed in the MRC Human
599 Genetics Unit, Edinburgh, UK, the University of Birmingham, UK, the Bioscientia Institute for Medical
600 Diagnostics, Germany, the Rare Disease Genomics Department, Yokohama City University Hospital,
601 Japan and the Regeneron Genetics Center, Regeneron Pharmaceuticals Inc., USA.

602

603 **Cell lines**

604 Patient-derived lymphoblastoid cell lines (LCLs) were generated from peripheral blood samples
605 with Epstein Barr virus (EBV) transformation using standard methods and were maintained in
606 RPMI1640 medium (Life Technologies) supplemented with 10% FBS, L-glutamine and penicillin-

607 streptomycin. The ATR-Seckel LCL used in this study was reported previously³¹. Dermal primary
608 fibroblasts were grown from skin-punch biopsies and maintained in Dulbecco's modified Eagle's
609 medium (DMEM; Thermo Fisher Scientific) supplemented with 20% FCS, 5% L-glutamine and 5%
610 penicillin-streptomycin. Primary fibroblasts were immortalized with a lentivirus expressing human
611 telomerase reverse transcriptase (hTERT) that was generated by transfecting 293FT cells (Thermo
612 Fisher Scientific) with the plasmids: pLV-hTERT-IRES-hygro (Addgene #85140), psPax2 (Addgene
613 #12260) and pMD2.G (Addgene #12259). Selection was performed using Hygromycin (Thermo Fisher
614 Scientific) at 70 µg/ml. All LCLs were routinely grown in RPMI-1640 (Thermo Fisher Scientific)
615 supplemented with 10% FCS, 5% L-glutamine and 5% penicillin-streptomycin. Patient cell lines were
616 validated using Sanger sequencing and immunoblotting. Fibroblast and U-2 OS cell complementation
617 was carried out using the pLVX-IRES-Neo lentiviral vector (Takara Bio) encoding 2xMyc-tagged *SLF2*
618 or untagged *SMC5*.

619 293FT (Thermo Fisher Scientific) were maintained in DMEM supplemented with 10% FBS, 5%
620 L-glutamine and 5% penicillin-streptomycin and U-2-OS cells were cultured in McCoy's 5A medium,
621 supplemented with 10% FBS, and 5% penicillin/streptomycin. 293FT transiently transfected with GFP-
622 BLM or GFP expression vectors using Lipofectamine 2000 (Thermo Fisher Scientific). U-2 OS cells
623 were transiently transfected with *SLF2/SMC5* expression vectors using FuGENE 6 Transfection
624 Reagent (E2692, Promega) or Lipofectamine 3000 Reagent (L3000015, Thermo Fisher Scientific)
625 where indicated. Stable GFP-*SMC5* cell lines were generated by G418 selection and low expressing
626 clones were selected based on GFP expression. All cell lines were routinely tested for mycoplasma.

627

628 **Western blotting**

629 Whole-cell extracts were obtained by sonication in UTB buffer (8 M urea, 50 mM Tris, 150 mM
630 β-mercaptoethanol) and analyzed by SDS-PAGE following standard procedures. Protein samples were
631 run on 6–12% acrylamide gels with SDS-PAGE and transferred onto a nitrocellulose membrane.
632 Immunoblotting was performed using antibodies to: RAD18 (Fortis Life Sciences, A301-340A; 1:1000),
633 *SMC5* (Fortis Life Sciences, A300-236A; 1:500), *SMC6* (Fortis Life Sciences, A300-237A; 1:2000),
634 *SLF2* (generated in house; 1:1000)¹¹, GAPDH (Genetex, GTX100118; 1:1000), Myc (Abcam, ab32;
635 1:1000), GFP (SCBT, sc-9996), HA (SCBT, sc-7392), α-Tubulin (Sigma-Aldrich, T9026), ATR (Fortis
636 Life Sciences, A300-137A; 1:1,000), phospho-ATR (Thr1989) (GeneTex, GTX128145; 1:500),

637 FANCD2 (SCBT, sc-20022; 1:1,000), CHK1 (SCBT, sc-8408; 1:1,000), phospho-CHK1 (Ser345) (Cell
638 Signaling Technology, 2341; 1:100), NBS1 (Genetex, GTX70224; 1:10,000); phospho-NBS1 (Ser343)
639 (Abcam, 47272; 1:500); SMC1 (Fortis Life Sciences, A300-055A; 1:1,000); phospho-SMC1 (Ser966)
640 (Fortis Life Sciences, A300-050A; 1:1,000); HA (Abcam, Ab9110; 1:1000). Loading controls for all blots
641 were derived from re-probing the same membrane, except for the phospho-antibody immunoblots, for
642 which paired gels were run simultaneously and blotted in parallel for phosphorylated and total proteins.

643

644 **Co-immunoprecipitation and GFP-Trap pull-downs**

645 For GFP-Trap pulldown experiments with 293FT cells, cells transfected with plasmids using
646 Lipofectamine 2000, were treated with 2 mM HU for 16 h and harvested. Cells were incubated in lysis
647 buffer (150 mM NaCl, 50 mM Tris HCl pH 7.5, 2 mM MgCl₂, 1% NP40, 90 U/ml Benzonase (Novagen)
648 and EDTA-free protease inhibitor cocktail [Roche]) for 30 min with rotation at 4 °C. Cell lysates were
649 then pre-cleared at 65,000 g at 4 °C for 30 min. For GFP-Trap, 3-5 mg of lysate was incubated with
650 GFP-Trap agarose beads (ChromoTek) for 5 h at 4 °C. The resulting GFP-Trap complexes were
651 washed with wash buffer (150 mM NaCl, 50 mM Tris HCl pH 7.5, 0.5% NP40, and complete protease
652 inhibitor cocktail [Roche]) and analysed by SDS-PAGE.

653 For immunoprecipitations from patient-derived LCLs, 3 mg of lysate (prepared with the same
654 lysis buffer as above) was immunoprecipitated with 5 µg of antibody (RAD18; Fortis Life Sciences,
655 A301-340A or NSMCE2; Fortis Life Sciences, A304-129A) and protein A-sepharose beads (GE
656 Healthcare). Complexes were washed with wash buffer (as described above) and analysed by SDS-
657 PAGE. Experiments were carried out in the presence of Benzonase nuclease to exclude the possibility
658 of interactions being mediated by DNA.

659 For immunoprecipitations from U-2 OS cells, cell lysates were generated using EBC buffer
660 (150mM NaCl; 50mM Tris, pH 7.5; 1mM EDTA; 0.5% IGEPAL CA-630). Lysates were subject to Co-IP
661 using Strep-Tactin Sepharose (IBA GmbH) prior to immunoblot using the following antibodies: GFP (sc-
662 9996, SCBT), HA (sc-7392, SCBT), RAD18 (A301-340A, Fortis Life Sciences), SMC6 (A300-237A,
663 Fortis Life Sciences), SMC5 (Fortis Life Sciences, A300-236A), NSMCE2 (Fortis Life Sciences, A304-
664 129A), α -Tubulin (T9026, Sigma-Aldrich).

665

666 **Laser micro-irradiation**

667 U-2 OS cells were grown on coverslips and sensitized to laser induced DSB formation using 5-
668 Bromo-2-deoxyuridine (B9285-50MG, Sigma-Aldrich) for 24 h. GFP-SLF2 expression vectors were
669 transiently transfected 24 h prior and GFP-SMC5 stable expressing cells were used for micro-
670 irradiation. Laser micro-irradiation induced DSB formation was performed as previously described⁷⁰
671 with 1 h allowed for recovery. Cells were pre-extracted using CSK buffer (100 mM NaCl, 10 mM HEPES,
672 3 mM MgCl₂, 300 mM Sucrose, 0.25% Triton-X100, 1 mM PMSF) prior to fixation in formalin buffer
673 (AMPQ43182, VWR) for 15 mins at room temperature (RT).

674 Fixed coverslips were blocked with 5% Bovine Serum Albumin (A7906, Sigma-Aldrich) for 1 h
675 prior to staining with anti-γ-H2AX (Ser139) (1:1000, 05-636, Merck) and anti-GFP (1:500, PABG1,
676 Chromotek) overnight at 4 °C. After PBS washes cells were stained with Alexa Fluor secondary
677 antibodies and 4',6-Diamidino-2-Phenylindole (DAPI, D1306, Molecular Probes) for 30 mins at RT. After
678 further washing, coverslips were dried completely and mounted for imaging using Mowiol (81381,
679 Sigma-Aldrich).

680

681 **Zebrafish husbandry and embryo maintenance.**

682 All zebrafish experiments were performed according to protocols approved by the Duke
683 University and Northwestern University institutional animal care and use committees (IACUC). Wild
684 type (WT: ZDR or NIH) adults or transgenic *-1.4col1a1:egfp*²⁵ adults were maintained on an AB
685 background and subjected to natural matings to generate embryos for microinjection and/or
686 phenotyping. Embryos were grown in egg water (0.3 g/L NaCl, 75 mg/L CaSO₄, 37.5 mg/L NaHCO₃,
687 0.003% methylene blue) at 28 °C until assessment. Zebrafish sex is unknown until animals are ~3
688 months old. Therefore, in the larvae at <5days post fertilization, it is not possible to know how many
689 males and females are present, and there should be no sex-dependent effects at this stage. However,
690 adults that were used to generate embryos were crossed in a 1 male to 1 female ratio.

691

692 **CRISPR-Cas9 genome editing of zebrafish embryos**

693 Reciprocal translated BLAST of human *SLF2* (NP_060591.3) and *SMC5* (NP_055925.2) was
694 performed against the zebrafish genome and found a single ortholog corresponding to either protein
695 (transcripts targeted: *slf2*: ENSDART00000136689.3, *smc5*: ENSDART00000122170.4). To identify
696 CRISPR/Cas9 single guide RNA (sgRNA) targets in both genes, CHOPCHOPv2⁷¹ (and

697 <http://chopchop.cbu.uib.no>) was used. sgRNAs were generated using the GeneArt precision gRNA
698 synthesis kit (Thermo Fisher Scientific) according to the manufacturer's instructions (Supplementary
699 Table S11). 1 nl of cocktail containing 100 pg sgRNA with or without 200 pg of Cas9 protein (PNA Bio)
700 was injected into the cell of single cell staged zebrafish embryos. To estimate the percentage mosaicism
701 of genome-edited cells, genomic DNA from individual embryos was extracted at 2 days post fertilization
702 (dpf; two controls and ten founder [F0] embryos per sgRNA). PCR was used to amplify the sgRNA
703 targeted region using flanking primers and heteroduplex analysis was performed using polyacrylamide
704 gel electrophoresis (PAGE). PCR products were denatured, reannealed slowly, and migrated on a 20%
705 polyacrylamide gel (Thermo Fisher Scientific). PCR products from five embryos per sgRNA were
706 randomly selected from the heteroduplex analysis, cloned into a TOPO-TA vector (Thermo Fisher
707 Scientific) and sequenced using BigDye terminator 3.1 chemistry (Applied Biosystems). To isolate
708 stable *slf2* mutants, F0 animals were crossed to WT ZDR adults and heterozygous F1 mutants bearing
709 the c.515_522del (p.Ser172_Ser174fs191Ter) variant were identified. Mutant F1 adult siblings were
710 inter-crossed to generate homozygous F2 animals for phenotyping. *slf2* mRNA expression level was
711 monitored by qRT-PCR (QuantStudio, Thermo Fisher Scientific) using SYBR Green detection kit
712 (Thermo Fisher Scientific) with normalization to *β-actin*.

713

714 **Transient suppression of *slf2* and *smc5* in zebrafish embryos**

715 Splice blocking morpholinos (MOs) were designed to target the *slf2* exon 11 (e11i11) and *smc5*
716 exon 3 (e3i3) splice donor sites (Gene Tools; Supplementary Table S11)). Each gene was transiently
717 suppressed independently by injecting 1 nl at different doses (3 ng, 6 ng and 9 ng) into one to four cell
718 staged zebrafish embryos. To validate MO efficiency, total RNA was extracted from pools of 2 dpf
719 embryos (25 animals/condition; controls and MO-injected) using Trizol (Thermo Fisher Scientific)
720 according to manufacturer's instructions. cDNA was synthesised with the QuantiTect Reverse
721 Transcription kit (Qiagen), RT-PCR of the MO target locus was performed, and PCR products were
722 separated on a 1% agarose gel. Resulting PCR bands were gel purified with the QIAquick gel extraction
723 kit (Qiagen) and cloned into the TOPO-TA cloning vector (Thermo Fisher Scientific). Purified plasmids
724 from resulting colonies (n=4/PCR product) were sequenced using BigDye 3.1 terminator chemistry
725 according to standard protocols.

726

727 **Molecular cloning and site directed mutagenesis of human *SLF2* and *SMC5* constructs for**
728 **expression of human proteins in zebrafish**

729 Full length Gateway-compatible *SLF2* (NM_018121.4) and *SMC5* (NM_015110.4) open
730 reading frame (ORF) entry vectors were obtained (Horizon). WT ORFs of both genes were inserted into
731 a pCS2+ Gateway destination vector using LR clonase II (Thermo Fisher Scientific). *SMC5* variants
732 identified in either affected individuals (p.His990Asp, p.Arg372del, p.Arg425Ter) or in gnomAD (dbSNP
733 ID: rs59648118, p.(Arg733Gln); 16 homozygotes of 140,814 individuals, negative control) were inserted
734 using site directed mutagenesis as described (Supplementary Table S11)⁷². After full ORF sequence
735 confirmation of all WT and mutant plasmids, each construct was linearised with NotI and in vitro
736 transcription was performed with the mMessage mMachine SP6 Transcription kit (Thermo Fisher
737 Scientific) according to manufacturer's instructions. 150 pg *SLF2* mRNA with 6 ng *slf2* MO and 150 pg
738 *SMC5* mRNA with 9 ng *smc5* MO was used for in vivo complementation assays.

739

740 **Live imaging of zebrafish larvae**

741 Images of tricaine-anesthetized larvae at 3 dpf were captured using the Vertebrate Automated
742 Screening Technology (VAST) Bioimager (Union Biometrica) mounted to an AXIO Imager.M2m
743 microscope (Zeiss) with a 10x objective lens. Larvae were passed sequentially through a 600 µm
744 capillary on the detection platform. Each larva was detected by software on the computer screen and
745 oriented automatically for lateral and ventral side images with a pre-provided template setting in the
746 software. VAST software (version 1.2.6.7) operated in automatic imaging mode with a 70% minimum
747 similarity threshold, as described⁷³. Bright field lateral images were captured with the VAST onboard
748 camera and a fluorescent signal from ventrally positioned larvae with an Axiocam 503 monochrome
749 camera (Zeiss) and ZenPro software (Zeiss).

750

751 **TUNEL assay and phospho-histone H3 (pHH3) immunostaining in zebrafish larvae**

752 Terminal deoxynucleotidyl transferase biotin-dUTP nick end labeling (TUNEL) assays or pHH3
753 immunostaining on whole mount embryos were performed as described^{27,74,75}. Embryos were
754 dechorionated at 2 dpf (*slf2* and *smc5*) or 3 dpf (*smc5*) and fixed overnight in 4% paraformaldehyde
755 (PFA) at 4 °C. Embryos were then dehydrated in methanol at -20 °C for 2 h and gradually rehydrated
756 in methanol in PBS and 0.1% Tween (PBST) in the following percent volume/volume ratios: 75/25;

757 50/50; 25/75 for 10 min each at RT. Embryos were bleached for 12 min in a solution of 9 ml PBST + 1
758 ml H₂O₂ + 0.05 g KOH before proteinase K treatment and fixation in 4% PFA for 20 min at RT. For
759 TUNEL, embryos were then incubated in equilibration buffer for 1 h and treated overnight with TdT
760 enzyme at 37 °C in a humidified incubator. Following treatment with digoxigenin (ApopTag red in situ
761 apoptosis detection kit, Sigma-Aldrich) for 2 h, embryos were washed 3x with PBST (10 min each) and
762 processed for imaging. For pHH3 staining, embryos were washed 3x (10 min each) with PBST and
763 incubated in blocking solution (IF buffer [1% BSA in PBST] +10% FBS) for 1 h. Embryos were then
764 treated with primary antibody diluted in 1% BSA overnight: anti-pHH3 (SCBT, sc-374669: 1:500) at 4
765 °C. Following staining with a secondary antibody: Alexa Fluor 488 goat anti-rabbit IgG (Thermo Fisher
766 Scientific, A11008: 1:500) diluted in 1% BSA for 2 h at RT, embryos were washed 2x (10 min each)
767 with IF buffer and processed for imaging. For both TUNEL and pHH3 stained embryos, a z-stacked
768 fluorescent signal of the dorsal aspect was captured with a Nikon AZ100 microscope facilitated by a
769 Nikon camera controlled by Nikon NIS Elements Software.

770

771 **Zebrafish image analysis**

772 ImageJ (NIH) was used to measure lateral head size, ceratohyal angle and count cells (TUNEL
773 or pHH3) in the specified head region. Raw images were exported as TIF files and contrast and
774 brightness were adjusted using identical settings for all images across the experiments. To measure
775 head size, a straight line was drawn from the posterior otolith to the tip of the mouth (line a), the dorsal
776 head area outlined (line b), and the arbitrary shape closed with a line perpendicular to line a (line c).
777 Ceratohyal angle was measured with the angle tool. To count TUNEL or pHH3 positive cells, the image-
778 based tool for counting nuclei (ICTN) plugin for ImageJ was used. A consistent region between the two
779 eyes was selected that spanned the most anterior region of the head to the most anterior region of the
780 yolk.

781

782 **Immunofluorescence in human cells**

783 Patient-derived fibroblasts or U-2 OS CRISPR HM cells were seeded onto coverslips at least
784 48 h before extraction and fixation. Cells were pre-extracted for 5 min on ice with ice-cold extraction
785 buffer (25 mM HEPES [pH 7.4], 50 mM NaCl, 1 mM EDTA, 3 mM MgCl₂, 300 mM sucrose, and 0.5%
786 Triton X-100) and then fixed with 4% paraformaldehyde (PFA) for 10 min. For immunofluorescence

787 involving patient-derived LCLs, cells were seeded onto Poly-L-Lysine coated coverslips 20 min before
788 fixation with ice-cold methanol for 20 min. For immunofluorescence using cells treated with exogenous
789 DNA damage, patient-derived fibroblasts or LCLs cells were incubated with 500 nM APH, 50 ng/ml
790 MMC or 250 μ M CX5461 (Selleck Chemicals, S2684), as indicated in the figure legends, 24 h before
791 fixation.

792 Fixed cells were then stained with primary antibodies specific to γ H2AX (Sigma-Aldrich, 05-
793 636; 1:1,000), CENPA (Abcam, Ab13939; 1:750), 53BP1 (Novus Biologicals, NB100-304; 1:1,000),
794 CENPF/Mitosin (Abcam, Ab5; 1:500 and BD Transduction Laboratories, 610768; 1:500), α -Tubulin
795 (Sigma-Aldrich, B-5-1-2; 1:4000), PCNT (Abcam, Ab4448; 1:100), and RAD51 (Merck, PC130; 1:500),
796 and with secondary antibodies: anti-rabbit IgG Alexa Fluor 488 (Thermo Fisher Scientific, A11070;
797 1:1000) and anti-mouse IgG Alexa Fluor 594 (Thermo Fisher Scientific, A11032; 1:1000). Cells were
798 then stained with DAPI and visualized with a 100x oil-immersion objective lens on a Nikon Eclipse Ni
799 microscope.

800 To visualize DNA replication, cells were incubated in medium containing 10 μ M EdU for 30-45
801 min before harvesting. EdU immunolabeling was performed using the Click-iT EdU Imaging Kit (Thermo
802 Fisher Scientific, C10337) according to the manufacturer's protocol.

803

804 **DNA fibre spreading assay**

805 Patient-derived fibroblasts or U-2 OS cells were seeded at least 48 h prior to harvesting. Cells
806 were incubated with 25 mM CldU for 30 min, washed with media containing 250 mM IdU (with or without
807 250 μ M CX5461), incubated with 250 mM IdU (with or without 250 μ M CX5461) for 30 min, and
808 harvested by trypsinization. For patient-derived LCLs, untreated cells were incubated with 25 mM CldU
809 for 20 min, washed with media containing 250 mM IdU, before being incubated with 250 mM IdU for 20
810 min and harvested. LCLs were incubated with 50 ng/ml MMC for 24 h prior to pulse labelling with 25
811 mM CldU for 20 min and then 250 mM IdU for 20 min. For all incubation or washing steps, 50 ng/ml
812 MMC was present in the media. For cells treated with HU, after being incubated with 25 mM CldU for
813 20 min, LCLs were incubated with media containing 2 mM HU for 2 h, before being washed in media
814 containing 250 mM IdU, then incubated with 250 mM IdU for 20 min and harvested.

815 Following harvesting, cells were washed with PBS and resuspended to a concentration of
816 500,000 cells/ml in PBS, and then lysed in lysis buffer (200 mM Tris-HCl [pH 7.5], 50 mM EDTA, 0.5%

817 SDS) directly on glass microscope slides. DNA fibres were spread down the slide by gravity, fixed in
818 methanol/acetic acid (3:1) and denatured with 2.5 M HCl. The thymidine analogues, CldU and IdU,
819 were detected via rat anti-BrdU antibody (clone BU1/75, ICR1; Abcam, ab6326; 1:500) and mouse anti-
820 BrdU antibody (clone B44; BD Biosciences, 347583; 1:500) respectively, and secondary antibodies
821 conjugated to Alexa Fluor 594 or Alexa Fluor 488 (Thermo Fisher Scientific). Labelled DNA fibres were
822 visualized with a Nikon Eclipse Ni microscope with 100x oil-immersion objective lenses, and images
823 were acquired with NIS-Elements software (Nikon Instruments). Replication fork structures and CldU
824 and IdU track lengths were then quantified with ImageJ software (US NIH).

825

826 **Metaphase spreads**

827 Giemsa-stained metaphase spreads from patient-derived cell lines or U-2 OS CRISPR SLF2
828 HM cells were prepared by adding of 0.2 mg/ml colcemid (KaryoMAX, Life Technologies) and
829 incubating for 3 h. The cells were then harvested by trypsinization, subjected to hypotonic shock for 30
830 min at 37 °C in hypotonic buffer (10 mM KCl, 15% FCS), and fixed in ethanol/acetic acid solution (3:1).
831 The cells were dropped onto microscope slides, stained for 15 min in Giemsa-modified solution (Sigma-
832 Aldrich; 5% vol/vol in water), and washed in water for 5 min. For analysis of cohesion fatigue in SLF2
833 patient LCLs, the metaphase spread protocol was followed as above. However, instead of adding
834 colcemid, 25µM MG132 (Sigma-Aldrich, M7449) was added 4 h before harvesting.

835 To prepare Giemsa-stained metaphase spreads from peripheral blood, whole blood was diluted
836 in RPMI1640 and 180 µg/ml PHA (Thermo Fisher Scientific) was added for 48-72 h at 37 °C. 4 h prior
837 to harvesting 0.2 mg/ml colcemid was added. The cells were pelleted and then subjected to hypotonic
838 shock for 10 min at 37 °C in hypotonic buffer (0.075M KCl). Finally, the cells were then fixed in
839 methanol/acetic acid solution (3:1) and processed as described above.

840

841 **Fluorescence in situ hybridization**

842 For Fluorescence In Situ Hybridization (FISH) was carried out on peripheral blood lymphocytes
843 metaphases using a peptide nucleic acid (PNA) pan-centromere FISH probe conjugated to Alexa Fluor
844 488 (5'-ATTCGTTGGAAACGGGA-3', PNA Bio, F3004 CENPB-Alexa488). Briefly, the PNA FISH
845 probes was made up as per the manufacturer's instructions. Metaphase spreads were harvested from
846 patient blood samples as above, and metaphases were dropped onto acetic-acid humidified microscope

847 slides. 24 h later, the slides were re-hydrated in PBS, dehydrated in an ethanol series (70%, 95%,
848 100%) and air dried. The slides were pre-warmed to 37 °C and before being incubated with hybridization
849 buffer (20 mM Tris, pH7.4, 60% formamide, 0.5% blocking reagent [Roche Blocking Reagent,
850 11096176001], 1% v/v PNA probe) for 10 min at 85 °C. The slides were then incubated in a dark,
851 humidified chamber at RT for 2 h, before being washed in wash buffer (70% formamide, 10mM Tris)
852 and dehydrated in an ethanol series (70%, 95%, 100%). The slides were then air dried and fixed with
853 prolong gold DAPI mounting medium (ProLong Gold Antifade Mountant with DAPI, P36935).

854

855 **Sister chromatid exchange analysis**

856 For sister chromatid exchange analysis, LCLs were incubated with 10 µM BrdU for 48 h before
857 incubating with 0.2 µg/ml demecolcine for 3 h. Cells were then resuspended in 0.075M KCl and
858 incubated at 37 °C for 1 h, fixed in methanol/acetic acid (3:1) and dropped onto microscope slides. The
859 slides were then incubated in 10 µg/ml Hoescht for 20 min and exposed to UVA light for 1 h in 2× SSC
860 buffer. Slides were incubated in 2× SSC buffer for 1 h at 60 °C and stained with 5% Giemsa. For
861 metaphase spread analysis of cells treated with exogenous DNA damage, patient-derived LCLs cells
862 were incubated with 500 nM APH or 50 ng/ml MMC 24 h before harvesting.

863 For analyses of telomere sister chromatid exchange, LCLs were cultured in the presence of
864 BrdU:BrdC (final concentration of 7.5 mM BrdU [MP Biomedicals, 100166] and 2.5 mM BrdC [Sigma-
865 Aldrich, B5002]) for 10 hr prior to harvesting. KaryoMAX colcemid (Gibco, 15212-012) was added at a
866 concentration of 0.1 µg/mL during the last 2 h. Cells were collected and washed in 75 mM KCl. Cells
867 were then fixed 3x in methanol:acetic acid (3:1) by adding fixative solution dropwise with constant gentle
868 agitation by vortex. Following fixation, cells were dropped onto microscope slides and metaphase
869 spreads were allowed to dry overnight. Next, slides were rehydrated in 1x PBS and then treated with
870 0.5 mg/ml RNase A (Sigma-Aldrich, R5125) for 30 min at 37 °C. Next, slides were treated with 0.5 µg/ml
871 Hoescht 33258 (Sigma-Aldrich, 861405) in 2x SSC for 15 min at RT, UV-irradiated, and digested with
872 ExoIII (NEB M0206L) for at least 30 min at 37 °C. Slides were then washed once in 1x PBS and
873 dehydrated in an ethanol series (70%, 90%, 100%) and air dried. FISH was performed using a TelC-
874 Alexa488-conjugated PNA probe (PNA Bio, F1004; 1:1,000) followed by a TelG-Cy3-conjugated PNA
875 probe (PNA Bio, F1006; 1:1,000) diluted in hybridization solution (10 mM Tris-HCl pH 7.2; 70%
876 formamide; 0.5% blocking reagent (Roche, 11096176001)) each for 2 h at RT. Next, slides were

877 washed at RT twice for 30 min in PNA wash A (70% formamide, 0.1% BSA, 10 mM Tris pH 7.2) and 3x
878 for 5 min in PNA wash B (100 mM Tris pH 7.2, 150 mM NaCl, 0.1% Tween-20). The second PNA wash
879 B contained DAPI (Life Technologies, D1306) at a 1:1000 concentration. Slides were then dehydrated
880 and dried as described above prior to mounting with Vectashield (Vectalabs, H1000). Slides were
881 imaged using a Zeiss Spinning Disk confocal microscope. Image analyses were blinded and used FIJI
882 version 2.1.0/153.c. Statistical analysis was performed using GraphPad Prism version 9.4.1.

883

884 **LCL proliferation assays**

885 LCL proliferation assays were carried out as previously reported⁴⁹. Briefly, LCLs were seeded at a
886 concentration of 0.25×10^6 cells per ml in 25 cm² flasks and incubated with an increasing concentration
887 of CX5461. The treated cells were counted when the untreated cells had reached a concentration of
888 2.0×10^6 cells per ml (approximately three population doubling times). The viability of the cells was
889 expressed as a percentage of the untreated cell count.

890

891 **Plasmids, mutagenesis and sequencing primers**

892 Total RNA was extracted from cell lines using RNeasy Mini kit (Qiagen) according to the
893 manufacturer's instructions. DNA was removed by treatment with DNase I (Qiagen), and cDNA was
894 generated using Superscript II and primed with oligo-dT (Thermo Fisher Scientific). PCR was carried
895 out using Phusion Hot Start II (Thermo Fisher Scientific). 2xMyc-SLF2 or untagged SMC5 lentiviral
896 expression constructs were generated by cloning a PCR-generated cDNA into the NotI site of pLVX-
897 IRES-neo (Takara Bio). The SLF2 and SMC5 ORFs were verified by sequencing using the primers in
898 Supplementary Table S12.

899 Full length SLF2 cDNA was also cloned into pcDNA4/TO (Thermo Fisher Scientific) and
900 deletion constructs were generated using KOD Hot Start DNA polymerase (Merck) according to
901 manufacturer's instructions. The following primer sets in Supplementary Table S13 were used to
902 generate the SLF2 deletion constructs and SLF2 'minimal binding region' (MBR) constructs. GFP-SLF2
903 is previously described¹¹. Full length SMC5 cDNA was amplified and cloned into pEGFP-C1 (Takara
904 Bio) using KpnI/BamHI. SLF2/SMC5 mutagenesis was achieved using the Q5 Site-Directed
905 Mutagenesis Kit (E0554S, NEB) according to manufacturer's instructions. The following primer sets in

906 Supplementary Table S13 were used to generate mutant expression vectors. SLF2 p.Gln1162His
907 variant was generated using gene synthesis (Thermo Fisher Scientific).

908 Lentiviral plasmids encoding the bacterial Holliday junction resolvase RusA were a kind gift
909 from Agata Smorgorzewska⁴⁰.

910

911 **RT-PCR analysis of patient cells**

912 RT-PCR of SLF2 was performed using transcript specific primers (Supplementary Table S14)
913 to assess the mRNA levels of the two longest annotated *SLF2* transcripts (NM_018121.4 and
914 NM_001136123.2) in patient whole blood RNA (Paxgene) or commercially-obtained human cDNA
915 panels: Human Universal QUICK-Clone II (Clontech), which is pool of cDNA obtained from 35 different
916 healthy adult or fetal tissues; and Human multiple tissue cDNA (MTC) panel I (Clontech). PCR product
917 was migrated on a 1% agarose gel for 40 minutes at 100V.

918

919 **CRISPR-Cas9 genome editing of U-2 OS cells**

920 Pairs of SLF2 targeting guide RNAs (sgRNA 1, 5'-AGTTTCATCACTCGGTTCCCT-3'; sgRNA 2,
921 5'-GGCTTGGCACCTTCAAATTC-3') were designed using the CHOPCHOP web tool (version 2)^{71,76}
922 and hybridised and ligated into the purpose built AIO-GFP All-in-One Cas9D10A nickase vector at
923 unique BbsI and BsaI sites. These constructs were transfected into U-2 OS cells using FuGENE
924 transfection reagent according to manufacturer's instructions (3:1 ratio of FuGENE to DNA). Cells were
925 sorted for high GFP expression by fluorescence-activated cell sorting (FACS) into 96-well dishes and
926 recovered in McCoy's 5A media supplemented with 20% FBS and 5% penicillin-streptomycin. After
927 three weeks, 25 colonies were chosen to be propagated and screened for successful gene editing. After
928 propagating, potential clones were lysed in lysis buffer (100 mM Tris/HCl pH 8.5, 5 mM EDTA, 0.2%
929 SDS, 200 mM NaCl, 100 µg Proteinase K/ml) and the DNA was precipitated with isopropanol and
930 resuspended in 10 mM Tris/HCl, 0.1 mM EDTA, pH 7.5. Screening of genomic DNA from clones was
931 achieved by sequencing a region of SLF2 surrounding the Cas9 nickase cut sites (Reverse primer, 5'-
932 AGTTCCGATAATCCACCCCTT-3'; Forward primer, 5'-TTTCTGCAACCAGGTAGTCCT-3'). Following
933 secondary screening of five clones by Western blotting, two SLF2 CRISPR HM clones were chosen
934 (renamed as cl.1 and cl.2) and were characterised further by inserting the amplified region of SLF2
935 described above into TOPO-TA vectors. 20 TOPO-TA vector clones were then sequenced for both cl.1

936 and cl.2 to identify all SLF2 mutant alleles and ensure no WT allele was present. The HM clones cl.1
937 and cl.2 were then complemented by 2xMyc tagged SLF2 cloned into pLVX-IRES-neo (Takara Bio).

938

939 **Statistical Analysis**

940 Statistical analyses were performed as indicated in the figure legends. A p-value of less than
941 0.05 indicates significance. The number of independent experimental replicates is denoted in the figure
942 legends. In all cases, independent experiments represent distinct samples, and not the same sample
943 measured repeatedly.

944

945

946

947 **Data Availability**

948 The datasets generated during WES are not publicly available due to reasons of sensitivity, e.g. human
949 data, but may be available from the corresponding author upon request subject to parental consent.
950 Gene variant frequency was obtained from the gnomAD database (<https://gnomad.broadinstitute.org/>).
951 Accession codes for genes/proteins analysed within this study are: Human SLF2 (NM_018121.4
952 [https://www.ncbi.nlm.nih.gov/nuccore/NM_018121.4], NM_001136123.2
953 [https://www.ncbi.nlm.nih.gov/nuccore/NM_001136123.2], NP_060591.3
954 [https://www.ncbi.nlm.nih.gov/protein/NP_060591.3]), Human SMC5 (NM_015110.4
955 [https://www.ncbi.nlm.nih.gov/nuccore/NM_015110.4], NP_055925.2
956 [https://www.ncbi.nlm.nih.gov/protein/NP_055925.2]), zebrafish slf2 (XM_002664123.6
957 [https://www.ncbi.nlm.nih.gov/nuccore/XM_002664123.6], XP_002664169.3
958 [https://www.ncbi.nlm.nih.gov/protein/XP_002664169.3]), zebrafish smc5 (NM_001193541.1
959 [https://www.ncbi.nlm.nih.gov/nuccore/NM_001193541.1], NP_001180470.1
960 [https://www.ncbi.nlm.nih.gov/protein/NP_001180470.1]). Plasmids obtained from Addgene
961 (<https://www.addgene.org/>) used in this study: pLV-hTERT-IRES-hygro (Addgene #85140), psPax2
962 (Addgene #12260) and pMD2.G (Addgene #12259). PDB files used within this study to model the
963 structural impact of SMC5 patient variants: *Saccharomyces cerevisiae* Smc5 (PDB: 3HTK), *Pyrococcus*
964 *furiosus* RAD50 (PDB: 1F2T and 1FTU). AlphaFold models used to facilitate structural predictions:
965 human SMC5 (AF-Q8IY18-F1). Source data and uncropped and unprocessed scans of the
966 immunoblotting experiments are provided with this paper.
967

968 **References**

- 969 1. Alcantara, D. & O'Driscoll, M. Congenital microcephaly. *Am J Med Genet C Semin Med Genet*
970 **166C**, 124-39 (2014).
- 971 2. O'Driscoll, M. The pathological consequences of impaired genome integrity in humans;
972 disorders of the DNA replication machinery. *J Pathol* **241**, 192-207 (2017).
- 973 3. Grand, R.J.A. & Reynolds, J.J. (eds.). *DNA Repair and Replication: Mechanisms and Clinical*
974 *Significance*, 348 (Garland Science, Boca Raton, 2018).
- 975 4. Schmit, M. & Bielinsky, A.K. Congenital Diseases of DNA Replication: Clinical Phenotypes and
976 Molecular Mechanisms. *Int J Mol Sci* **22**(2021).
- 977 5. Klingseisen, A. & Jackson, A.P. Mechanisms and pathways of growth failure in primordial
978 dwarfism. *Genes Dev* **25**, 2011-24 (2011).
- 979 6. Hanks, S. et al. Constitutional aneuploidy and cancer predisposition caused by biallelic
980 mutations in BUB1B. *Nat Genet* **36**, 1159-61 (2004).
- 981 7. Snape, K. et al. Mutations in CEP57 cause mosaic variegated aneuploidy syndrome. *Nat Genet*
982 **43**, 527-9 (2011).
- 983 8. Yost, S. et al. Biallelic TRIP13 mutations predispose to Wilms tumor and chromosome
984 missegregation. *Nat Genet* **49**, 1148-1151 (2017).
- 985 9. Pisani, F.M. Spotlight on Warsaw Breakage Syndrome. *Appl Clin Genet* **12**, 239-248 (2019).
- 986 10. Avagliano, L. et al. Chromatinopathies: A focus on Cornelia de Lange syndrome. *Clin Genet*
987 **97**, 3-11 (2020).
- 988 11. Raschle, M. et al. DNA repair. Proteomics reveals dynamic assembly of repair complexes
989 during bypass of DNA cross-links. *Science* **348**, 1253671 (2015).
- 990 12. Aragon, L. The Smc5/6 Complex: New and Old Functions of the Enigmatic Long-Distance
991 Relative. *Annu Rev Genet* **52**, 89-107 (2018).
- 992 13. Sole-Soler, R. & Torres-Rosell, J. Smc5/6, an atypical SMC complex with two RING-type
993 subunits. *Biochem Soc Trans* **48**, 2159-2171 (2020).
- 994 14. Palecek, J.J. SMC5/6: Multifunctional Player in Replication. *Genes (Basel)* **10**(2018).
- 995 15. Schuster, K. et al. A neural crest origin for cohesinopathy heart defects. *Hum Mol Genet* **24**,
996 7005-7016 (2015).
- 997

- 998 16. Piché, J., Piet Van Vliet, P., Pucéat, M. & Andelfinger G. The expanding phenotypes of
999 cohesinopathies: one ring to rule them all! *Cell Cycle* **18**, 2828-2848 (2019).
- 1000 17. Rossi, F. et al. SMC5/6 acts jointly with Fanconi anemia factors to support DNA repair and
1001 genome instability. *EMBO Rep* **21**, e48222 (2020).
- 1002 18. van der Crabben, S.N. et al. Destabilized SMC5/6 complex leads to chromosome breakage
1003 syndrome with severe lung disease. *J Clin Invest* **126**, 2881-92 (2016).
- 1004 19. Willemse, B.W.M. et al. New insights in phenotype and treatment of lung disease immuno-
1005 deficiency and chromosome breakage syndrome (LICS). *Orphanet J Rare Dis* **16**, 137 (2021).
- 1006 20. Payne, F. et al. Hypomorphism in human NSMCE2 linked to primordial dwarfism and insulin
1007 resistance. *J Clin Invest* **124**, 4028-38 (2014).
- 1008 21. Pryzhkova, M.V. & Jordan, P.W. Conditional mutation of Smc5 in mouse embryonic stem cells
1009 perturbs condensin localization and mitotic progression. *J Cell Sci* **129**, 1619-34 (2016).
- 1010 22. Hassler, M. et al. Towards a unified model of SMC complex function. *Curr Biol* **28**, R1266-
1011 R1281 (2018).
- 1012 23. Hopfner, K.P. et al. Structural biology of Rad50 ATPase: ATPdriven conformational control in
1013 DNA double strand break repair and the ABC-ATPase superfamily. *Cell* **101**, 789-800 (2000).
- 1014 24. Etheridge, T.J. et al. Live-cell single-molecule tracking highlights requirements for stable
1015 Smc5/6 chromatin association in vivo. *Elife* **10**, e68579.
- 1016 25. Kague, E. et al. Skeletogenic fate of zebrafish cranial and trunk neural crest. *PLoS One* **7**,
1017 e47394 (2012).
- 1018 26. Atkins, A. et al. SMC5/6 is required for replication fork stability and faithful chromosome
1019 segregation during neurogenesis. *Elife* **9**(2020).
- 1020 27. Ansar, M. et al. Bi-allelic Variants in DYNC112 Cause Syndromic Microcephaly with Intellectual
1021 Disability, Cerebral Malformations, and Dysmorphic Facial Features. *Am J Hum Genet* **104**,
1022 1073-1087 (2019).
- 1023 28. Khan, T.N. et al. Mutations in NCAPG2 Cause a Severe Neurodevelopmental Syndrome that
1024 Expands the Phenotypic Spectrum of Condensinopathies. *Am J Hum Genet* **104**, 94-111
1025 (2019).

- 1026 29. Venegas, A.B., Natsume, T., Kanemaki, M. & Hickson, I.D. Inducible degradation of the human
1027 SMC5/6 complex reveals an essential role only during interphase. *Cell Reports* **31**, 107533
1028 (2020).
- 1029 30. Ogi, T. et al. Identification of the first ATRIP-deficient patient and novel mutations in ATR define
1030 a clinical spectrum for ATR-ATRIP Seckel Syndrome. *PLoS Genet* **8**, e1002945 (2012).
- 1031 31. Reynolds, J.J. et al. Mutations in DONSON disrupt replication fork stability and cause
1032 microcephalic dwarfism. *Nat Genet* **49**, 537-549 (2017).
- 1033 32. Copsey, A. et al. Smc5/6 coordinates formation and resolution of joint molecules with
1034 chromosome morphology to ensure meiotic divisions. *PLoS Genet* **9**, e1004071 (2013).
- 1035 33. Behlke-Steinert, S., Touat-Todeschini, L., Skoufias, D.A. & Margolis, R.L. SMC5 and MMS21
1036 are required for chromosome cohesion and mitotic progression. *Cell Cycle* **8**, 2211-2218
1037 (2009).
- 1038 34. Stephan, A.K. et al. Roles of vertebrate Smc5 in sister chromatid cohesion and homologous
1039 recombination. *Mol Cell Biol* **31**, 1369-1381 (2011).
- 1040 35. Lin, S.-J. et al. An acetyltransferase-independent function of Eso1 regulates centromere
1041 cohesion. *Mol Cell Biol* **27**, 4002-4010 (2016).
- 1042 36. Daum, J.R. et al. Cohesion fatigue induces chromatid separation in cells delayed at metaphase.
1043 *Curr Biol* **21**, 1018-24 (2011).
- 1044 37. Loffler, H., Fechter, A., Liu, F.Y., Poppelreuther, S. & Kramer, A. DNA damage-induced
1045 centrosome amplification occurs via excessive formation of centriolar satellites. *Oncogene* **32**,
1046 2963-72 (2013).
- 1047 38. Marthiens, V. et al. Centrosome amplification causes microcephaly. *Nat Cell Biol* **15**, 731-40
1048 (2013).
- 1049 39. Sarbajna, S., Davies, D. & West, S.C. Roles of SLX1-SLX4, MUS81-EME1, and GEN1 in
1050 avoiding genome instability and mitotic catastrophe. *Genes Dev* **28**, 1124-36 (2014).
- 1051 40. Garner, E., Kim, Y., Lach, F.P., Kottemann, M.C. & Smogorzewska, A. Human GEN1 and the
1052 SLX4-associated nucleases MUS81 and SLX1 are essential for the resolution of replication-
1053 induced Holliday junctions. *Cell Rep* **5**, 207-15 (2013).
- 1054 41. Agashe, S. et al. Smc5/6 functions with Sgs1-Top3-Rmi1 to complete chromosome replication
1055 at natural pause sites. *Nature Comms* **12**, 2111 (2021).

1056

1057 42. Branzei, D. et al. Ubc9- and mms21-mediated sumoylation counteracts recombinogenic events
1058 at damaged replication forks. *Cell* **127**, 509-522 (2006).

1059 43. Menolfi, D. et al. Essential roles of the Smc5/6 complex in replication through natural pausing
1060 sites and endogenous DNA damage tolerance. *Mol Cell* **60**, 835-846 (2015).

1061 44. Torres-Rosell, J. et al. SMC5 and SMC6 genes are required for the segregation of repetitive
1062 chromosome regions. *Nat Cell Biol* **7**, 412-419 (2005).

1063 45. Bermudez-Lopez, M. et al. Sgs1's roles in DNA end resection, HJ dissolution, and crossover
1064 suppression require a two-step SUMO regulation dependent on Smc5/6. *Genes Dev* **30**, 1339-
1065 56 (2016).

1066 46. Bonner, J.N. et al. Smc5/6 Mediated Sumoylation of the Sgs1-Top3-Rmi1 Complex Promotes
1067 Removal of Recombination Intermediates. *Cell Rep* **16**, 368-378 (2016).

1068 47. Masud, T. et al. Ubiquitin-mediated DNA damage response is synthetic lethal with G-
1069 quadruplex stabilizer CX-5461. *Sci Rep* **11**, 9812 (2021).

1070 48. Xu, H. et al. CX-5461 is a DNA G-quadruplex stabilizer with selective lethality in BRCA1/2
1071 deficient tumours. *Nat Commun* **8**, 14432 (2017).

1072 49. van Schie, J.J.M. et al. Warsaw Breakage Syndrome associated DDX11 helicase resolves G-
1073 quadruplex structures to support sister chromatid cohesion. *Nat Commun* **11**, 4287 (2020).

1074 50. Jegadesan, N.K. & Branzei, D. DDX11 loss causes replication stress and pharmacologically
1075 exploitable DNA repair defects. *Proc Natl Acad Sci USA* **118**, e2024258118 (2021).

1076 51. Lerner, L.K. et al. Timeless couples G-quadruplex detection with processing by DDX11 helicase
1077 during DNA replication. *EMBO J* **39**, e104185 (2020).

1078 52. Bruno, P.M. et al. The primary mechanism of cytotoxicity of the chemotherapeutic agent CX-
1079 5461 is topoisomerase II poisoning. *Proc Natl Acad Sci USA* **117**, 4053-4060 (2020).

1080 53. Pan, M. et al. The chemotherapeutic CX-5461 primarily targets TOP2B and exhibits selective
1081 activity in high-risk neuroblastoma. *Nat Commun* **12**, 6468 (2021).

1082 54. Fernandez-Casanas, M. & Chan, K.L. The Unresolved Problem of DNA Bridging. *Genes*
1083 (*Basel*) **9** (2018).

1084 55. Wilhelm, T. et al. Mild replication stress causes chromosome mis-segregation via premature
1085 centriole disengagement. *Nat Commun* **10**, 3585 (2019).

- 1086 56. Gutierrez-Escribano, P. et al. Purified Smc5/6 Complex Exhibits DNA Substrate Recognition
1087 and Compaction. *Mol Cell* **80**, 1039-1054 e6 (2020).
- 1088 57. Serrano, D. et al. The Smc5/6 Core Complex Is a Structure-Specific DNA Binding and
1089 Compacting Machine. *Mol Cell* **80**, 1025-1038 e5 (2020).
- 1090 58. Adamus, M. et al. Molecular Insights into the Architecture of the Human SMC5/6 Complex. *J*
1091 *Mol Biol* **432**, 3820-3837 (2020).
- 1092 59. Hallett, S.T. et al. Nse5/6 is a negative regulator of the ATPase activity of the Smc5/6 complex.
1093 *Nucleic Acids Res* **49**, 4534-4549 (2021).
- 1094 60. Taschner, M. et al. Nse5/6 inhibits the Smc5/6 ATPase and modulates DNA substrate binding.
1095 *EMBO J* **40**, e107807 (2021).
- 1096 61. Spiegel, J., Adhikari, S. & Balasubramanian, S. The Structure and Function of DNA G-
1097 Quadruplexes. *Trends Chem* **2**, 123-136 (2020).
- 1098 62. Inoue, A. et al. Loss of ChlR1 helicase in mouse causes lethality due to the accumulation of
1099 aneuploid cells generated by cohesion defects and placental malformation. *Cell Cycle* **6**, 1646-
1100 54 (2007).
- 1101 63. Peng, X.P. et al. Acute Smc5/6 depletion reveals its primary role in rDNA replication by
1102 restraining recombination at fork pausing sites. *PLoS Genet* **14**, e1007129 (2018).
- 1103 64. Wechsler, T., Newman, S. & West, S.C. Aberrant chromosome morphology in human cells
1104 defective for Holliday junction resolution. *Nature* **471**, 642-6 (2011).
- 1105 65. Jacome, A. et al. NSMCE2 suppresses cancer and aging in mice independently of its SUMO
1106 ligase activity. *EMBO J* **34**, 2604-19 (2015).
- 1107 66. Sobreira, N., Schiettecatte, F., Valle, D. & Hamosh, A. GeneMatcher: a matching tool for
1108 connecting investigators with an interest in the same gene. *Hum Mutat* **36**, 928-30 (2015).
- 1109 67. Logan, C.V. et al. DNA Polymerase Epsilon Deficiency Causes IMAGE Syndrome with Variable
1110 Immunodeficiency. *Am J Hum Genet* **103**, 1038-1044 (2018).
- 1111 68. Strauss, K.A. et al. Genomic diagnostics within a medically underserved population: efficacy
1112 and implications. *Genet Med* **20**, 31-41 (2018).
- 1113 69. Murray, J.E. et al. Mutations in the NHEJ component XRCC4 cause primordial dwarfism. *Am J*
1114 *Hum Genet* **96**, 412-24 (2015).

- 1115 70. Poulsen, M., Lukas, C., Lukas, J., Bekker-Jensen, S. & Mailand, N. Human RNF169 is a
1116 negative regulator of the ubiquitin-dependent response to DNA double-strand breaks. *J Cell*
1117 *Biol* **197**, 189-99 (2012).
- 1118 71. Labun, K., Montague, T.G., Gagnon, J.A., Thyme, S.B. & Valen, E. CHOPCHOP v2: a web tool
1119 for the next generation of CRISPR genome engineering. *Nucleic Acids Res* **44**, W272-6 (2016).
- 1120 72. Niederriter, A.R. et al. In vivo modeling of the morbid human genome using *Danio rerio*. *J Vis*
1121 *Exp*, e50338 (2013).
- 1122 73. Isrie, M. et al. Mutations in Either TUBB or MAPRE2 Cause Circumferential Skin Creases
1123 Kunze Type. *Am J Hum Genet* **97**, 790-800 (2015).
- 1124 74. Frosk, P. et al. A truncating mutation in CEP55 is the likely cause of MARCH, a novel syndrome
1125 affecting neuronal mitosis. *J Med Genet* **54**, 490-501 (2017).
- 1126 75. Stankiewicz, P. et al. Haploinsufficiency of the Chromatin Remodeler BPTF Causes Syndromic
1127 Developmental and Speech Delay, Postnatal Microcephaly, and Dysmorphic Features. *Am J*
1128 *Hum Genet* **101**, 503-515 (2017).
- 1129 76. Labun, K. et al. CHOPCHOP v3: expanding the CRISPR web toolbox beyond genome editing.
1130 *Nucleic Acids Res* **47**, W171-W174 (2019).
- 1131

1132 **Acknowledgments**

1133 We would like to thank the parents and affected individuals from the Atelís Syndrome families for taking
1134 part in this study and generously donating tissue samples. We would also like to thank Agata
1135 Smorgorzewska, Kasper Fugger and Stephen West for providing plasmids expressing RusA, Gen1,
1136 Mus81 and Eme1. GSS, RH, GSN, SLC, AG are funded by a CR-UK Programme Grant
1137 (C17183/A23303). LJG is supported by a joint funded University of Birmingham and CR-UK Ph.D
1138 studentship (C17422/A25154). JJR and AMRT are supported by the University of Birmingham. SSJ is
1139 supported by a project grant funded by the Great Ormond Street Hospital Charity and Sparks (V5019).
1140 RFS and NM are supported by Novo Nordisk Foundation (NNF14CC0001) and Independent Research
1141 Fund Denmark (9040-00038B). DP and APJ are supported by a European Union Horizon 2020
1142 research and innovation program European Research Council (ERC) Advanced Grant (grant
1143 agreement 788093) and by a Medical Research Council (MRC) Unit core grant (U127580972). NM is
1144 supported by AMED (JP21ek0109486, JP21ek0109549, and JP21ek0109493). YU is supported by
1145 JSPS KAKENHI (JP21K15907). AKB and RMB are supported by grants from the National Institutes of
1146 Health (R01 GM134681 and R35 GM141805). FU is funded by the Higher Education Commission of
1147 Pakistan under the International research support initiative program (IRSIP). EED is supported by US
1148 National Institutes of Health grant R01 MH106826 and is the Ann Marie and Francis Klocke MD
1149 Research Scholar.

1150

1151 **Author contributions**

1152 L.J.G, J.J.R, R.F.S, R.M.B, R.H, G.S.M, S.L.C, M.R.H, N.M, A-K.B and G.S.S designed and performed
1153 the cell biology experiments. F.U, X.L, T.K, and E.E.D generated, performed, and supervised analysis
1154 on the *slf2* and *smc5* knockdown and knockout zebrafish. L.J.G, A.G and S.S.J designed and generated
1155 the *SLF2* CRISPR knockout constructs and U-2 OS cell lines. A.W.O carried out structural modelling of
1156 patient-associated mutations in SMC5. T.N. and N.Matsumoto, designed and generated aid-tagged
1157 *SLF2* degron cell lines. B.I, G.A.M-M, S.C, C.G.M, D.P, M.A.S, N.N, Z.Y, M.D, A.K, P.V, A-M.J, S.A.S,
1158 C.G-J, K.W.B, A.P.A.S, M.K, D.J, Y.U, Y.O, A.M, H.O, Z.A, J.A, C.T.R.M.S, A.M.R.T, A.P.J and C.Le
1159 C provided patient samples, performed next-generation sequencing, carried out bioinformatic analysis
1160 of next-generation sequencing data and performed other molecular genetic experiments. J.J.R,

1161 A.M.R.T, N.M, A-K.B, A.P.J, E.E.D. and G.S.S wrote the manuscript. G.S.S. planned and supervised
1162 the study.

1163

1164 **Competing Financial Interests**

1165 The authors declare no competing financial interests.

1166

1167 **Figure Legends**

1168

1169 **Figure 1: *SLF2* and *SMC5* variants cause severe microcephaly and short stature**

1170 **a** Table listing biallelic *SLF2* and *SMC5* variants in 11 individuals. ss, splice site created or destroyed
1171 by variant. '-' denotes that the allele variant was not present in the gnomAD database. Scores predicting
1172 the pathogenicity of the identified missense variants in *SLF2* and *SMC5* were generated using
1173 Polyphen-2 (<http://genetics.bwh.harvard.edu/pph2/>). NA; Not applicable. **b** Length and head
1174 circumference (occipital frontal circumference; OFC) at birth and at the age of last exam as z-scores
1175 (s.d. from population mean for age and sex; SD). Dashed line at -3 SD indicates cut-off for normal
1176 population distribution. Orange values indicate *SMC5* patients and blue values indicate *SLF2* patients.
1177 **c** Schematic of full length WT *SLF2* protein and *SLF2* patient variants. APIM, atypical PCNA binding
1178 motif. SMC, *SMC5/6* binding region. SLF1, *SLF1* binding region. **d** Schematic of full length WT *SMC5*
1179 protein and *SMC5* patient variants. CC, coiled-coil region.

1180

1181 **Figure 2: Impact of patient associated variants on the stability of *SLF2* and *SMC5* protein and**
1182 **the integrity of the *SMC5/6* complex**

1183 **a** Representative immunoblot analysis of cell extracts from lymphoblastoid (LCL) cell lines derived from
1184 patients with variants in *SLF2*. WT-AH and WT-LQ (WT; wild type) indicate unrelated healthy individuals.
1185 **b** Representative immunoblot analysis of cell extracts from lymphoblastoid (LCL) cell lines derived from
1186 patients with variants in *SMC5*. WT-SW and WT-WCS indicate unrelated healthy individuals. **c & d**
1187 Whole cell extracts prepared from WT cell lines, *SLF2* patient LCLs (c) or *SMC5* patient LCLs (d) were
1188 subjected to immunoprecipitation with the indicated antibodies, and inputs and immunoprecipitates (IP)
1189 were analysed by immunoblotting (IB). **e** U-2 OS cells expressing Flag-*SLF2* were transfected with WT
1190 or mutant GFP-*SMC5*. GFP-*SMC5* was precipitated from cell extracts using GFP-Trap beads and co-
1191 precipitated proteins were detected using immunoblotting with the indicated antibodies. * represents a
1192 cross-reaction of the NSMCE2 antibody to GFP. **f** Whole cell extracts prepared from WT cell lines or
1193 *SMC5* patient LCLs were subjected to immunoprecipitation with the indicated antibody, and inputs and
1194 immunoprecipitates were analysed by immunoblotting. Immunoblotting and immunoprecipitation
1195 experiments in panels a, b, c, d, and f are representative of two independent experiments with similar
1196 results. Panel e is representative of three independent experiments with similar results.

1197

1198 **Figure 3: Loss of *slf2* and *smc5* in zebrafish give rise to microcephaly and aberrant craniofacial**
1199 **patterning**

1200 **a** Top: Representative lateral bright field images acquired at 3 days post-fertilization (dpf); white dashed
1201 shape depicts head size measured. Bottom: Representative ventral images of GFP signal from the
1202 anterior region of *-1.4col1a1:egfp* transgenic reporter larvae at 3 dpf. The white dashed lines show the
1203 ceratohyal angle. **b** Quantification of lateral head size measurements. Larvae were injected with two
1204 independent sgRNAs targeting *slf2* with or without Cas9; n=3 independent experiments (left to right;
1205 56, 37, 37, 36, 36 larvae/batch). **c** Quantification of the ceratohyal angle. Larvae were injected with two
1206 independent *slf2* sgRNAs: n=3 independent experiments (left to right; 39, 42, 30, 20, 44 larvae/batch).
1207 **d** Top: Representative lateral bright field images at 3 dpf. Bottom: Representative ventral images of
1208 GFP signal in the anterior region of *-1.4col1a1:egfp smc5* sgRNA1 transgenic larvae at 3 dpf. **e**
1209 Quantification of lateral head size measurements in 3 dpf larvae (as shown in panel A); n=3 independent
1210 experiments (left to right; 50, 50, 52, 46, 53, 38 larvae/batch). The chart shows two independent
1211 experiments for sgRNA1 and sgRNA2 with a vertical line grouping independent controls with test
1212 conditions. **f** Quantification of the ceratohyal angle. Larvae were injected with two independent *smc5*
1213 sgRNAs: n=3 independent experiments (left to right; 34, 53, 37, 62, 28, 48 larvae/batch). The chart
1214 shows two independent experiments for sgRNA1 and sgRNA2 with a vertical line grouping independent
1215 controls with test conditions. **g** Left: Representative lateral bright field images of WT control and *slf2*^{-/-}
1216 mutants at 3 dpf. Right: Quantification of lateral head size measurements in 3 dpf WT control and *slf2*^{-/-}
1217 mutant larvae (as shown in panel a); n=3 independent experiments (left to right; 10, 12, 12
1218 larvae/batch). In (a & b): (top left) white dashed shape depicts head size measured; (bottom left) white
1219 dashed lines show the ceratohyal angle measured. Abbreviations: MK, Meckel's cartilage; CH,
1220 ceratohyal cartilage (indicated with arrowheads, respectively); and CB, ceratobranchial arches
1221 (asterisks). Scale bars represent 300 μm, with equivalent sizing across panels. Error bars represent
1222 standard deviation of the mean. Statistical differences were determined with an unpaired Student's t-
1223 test (two sided).

1224

1225 **Figure 4: Loss of *slf2* and *smc5* induces apoptosis and altered cell cycle progression in**
1226 **zebrafish larvae**

1227 **a** Representative dorsal inverted fluorescent images showing TUNEL positive cells in control and *slf2*
1228 F0 mutants at 2 dpf (left two panels), and control and *smc5* F0 mutants at 3 dpf (right two panels). The
1229 blue dashed line indicates the region of interest (ROI) quantified. Embryos of the same developmental
1230 stage and similar magnification were evaluated for all *slf2* and *smc5* conditions. **b** Left: Quantification
1231 of TUNEL positive cells in the ROI of control and *slf2* F0 mutants at 2 dpf shown in panel a (left to right;
1232 27, 23, 19, 29, 30 embryos/condition were analysed from 3 independent experiments). Right:
1233 Quantification of TUNEL positive cells in control and *smc5* F0 mutants at 3 dpf in the ROI as shown in
1234 panel a (left to right; 37, 27, 22, 25, 23, 23 embryos/condition were analysed from 3 independent
1235 experiments). The chart shows two independent experiments for sgRNA1 and sgRNA2 with a vertical
1236 line grouping independent controls with test conditions. **c** Representative dorsal inverted fluorescent
1237 images showing phospho-histone H3 (pHH3) positive cells in control and *slf2* F0 mutants at 2 dpf (left
1238 two panels), and control and *slf2* F0 mutants at 3 dpf (right two panels). Embryos of the same
1239 developmental stage and similar magnification were evaluated for all *slf2* and *smc5* conditions. **d** Left:
1240 Quantification of pHH3 positive cells of control and *slf2* F0 mutants at 2 dpf in the ROI as shown in
1241 panel a (left to right; 21, 24, 22, 24, 26 embryos/condition were analysed from 3 independent
1242 experiments). Right: Quantification of pHH3 positive cells in the ROI in control and *smc5* F0 mutants at
1243 3 dpf as shown in panel a (left to right; 25, 23, 26 embryos/condition were analysed from 3 independent
1244 experiments). For all panels: Statistical differences were determined with an unpaired Student's t-test
1245 (two sided). Error bars represent standard deviation of the mean. Scale bars, 30 μ m with equivalent
1246 sizing across panels.

1247

1248 **Figure 5: Patient-derived cell lines from individuals with bi-allelic *SLF2* or *SMC5* variants exhibit**
1249 **increased levels of spontaneous replication fork instability**

1250 **a** Top: Schematic representation for DNA fibre analysis in untreated cells. The indicated cell lines were
1251 pulse-labelled with CldU for 20 min, then pulse-labelled with IdU for 20 min. Bottom: DNA fibre analysis
1252 of *SLF2* patient-derived LCLs or LCLs from a WT individual. The percentage of ongoing forks (left) or
1253 stalled forks (right) was quantified. n=4 independent experiments. A minimum of 1,500 fork structures
1254 were counted. **b** DNA fibre analysis of *SMC5* patient-derived LCLs or WT LCLs. Quantification of the
1255 levels of ongoing forks (left) or stalled forks (right). n=4 independent experiments. A minimum of 750
1256 fork structures were counted. **c & d** Quantification of replication fork asymmetry of WT, *SLF2* patient

1257 (c) or SMC5 patient LCLs (d). n=4 independent experiments. A minimum of 75 fork structures were
1258 counted. Red lines denote median values. A Mann-Whitney rank sum test was performed for statistical
1259 analysis. Replication fork asymmetry represents the ratio of the left to right fork-track lengths of
1260 bidirectional replication forks. **e & f** DNA fibre analysis of SLF2 (e) and SMC5 (f) mutant fibroblast cell
1261 lines infected with lentiviruses encoding WT SLF2, WT SMC5, or an empty vector. The percentage of
1262 ongoing forks (left) or stalled forks (right) in untreated cells was quantified. A minimum of 350 fork
1263 structures in total were counted over 3 independent experiments. **g** DNA fibre analysis of U-2-OS SLF2
1264 CRISPR hypomorphic (HM) cells infected with lentiviruses encoding WT SLF2 or an empty vector. The
1265 percentage of stalled forks in untreated cells was quantified. A minimum of 1,000 fork structures in total
1266 were counted over 3 independent experiments. For panels a, b, e, f and g; a Student's t-test (two-sided,
1267 equal variance) was performed for statistical analysis and error bars denote SEM.

1268

1269 **Figure 6: SLF2 and SMC5 patient cells exhibit S-phase associated DNA damage**

1270 **a** Percentage of cells positive for EdU staining with >10 53BP1 foci in SLF2 and SMC5 mutant fibroblast
1271 cell lines infected with lentiviruses encoding WT SLF2, WT SMC5, or an empty vector. A minimum of
1272 900 EdU positive cells across 3 independent experiments were counted. **b** SLF2 and SMC5 patient
1273 fibroblast cell lines were pulsed with 10 μ M EdU for 45 min, fixed, and mitotic DNA synthesis was
1274 visualised by mitotic EdU incorporation following labelling with click chemistry. The percentage of mitotic
1275 cells with EdU foci was quantified. A minimum of 300 mitotic cells were counted. n=3 independent
1276 experiments. **c** Immunofluorescent microscopy analysis to quantify the percentage of G1-phase cells
1277 (CENPF negative cells) with >3 53BP1 bodies in WT SLF2, WT SMC5, or an empty vector expressing
1278 SLF2 and SMC5 patient fibroblasts. n=3 independent experiments. A minimum of 750 G1-phase cells
1279 were counted. **d** Levels of micronuclei in cells from (c). n=3 independent experiments. A minimum of
1280 2,500 cells were counted. **e** Levels of micronuclei in U-2 OS SLF2 CRISPR HM cells infected with
1281 lentiviruses encoding WT SLF2 or an empty vector. n=3 independent experiments. A minimum of 1,700
1282 cells were counted. **f & g** Quantification of the average number of chromosomal aberrations per
1283 metaphase (which includes chromatid/chromosome gaps, breaks, fragments and chromosomes
1284 radials) in WT, SLF2 patient (f), or SMC5 patient LCLs (g). n=3 independent experiments. A minimum
1285 of 140 metaphases were counted. **h** Average number of chromosomal aberrations per metaphase
1286 (chromatid/chromosome gaps, breaks, fragments and chromosome radials) in SLF2 and SMC5 mutant

1287 fibroblast cell lines infected with lentiviruses encoding WT SLF2, WT SMC5, or an empty vector was
1288 quantified. n=3 independent experiments. A minimum of 90 metaphases were counted. **i** Average
1289 number of chromosomal aberrations (chromatid/chromosome gaps, breaks, fragments and
1290 chromosome radials) per metaphase in U-2 OS SLF2 CRISPR HM cell lines expressing either WT SLF2
1291 or an empty vector. n=3 independent experiments. A minimum of 100 metaphases were counted. In all
1292 cases, a Student's t-test (two-sided, equal variance) was performed for statistical analysis and error
1293 bars denote SEM.

1294

1295 **Figure 7: SLF2 and SMC5 patient cells exhibit mosaic variegated hyperploidy, mitotic**
1296 **abnormalities and sister chromatid cohesion defects**

1297 **a** Quantification of the numbers of chromosomes per metaphase in peripheral blood lymphocytes from
1298 SLF2 or SMC5 patients, or an unrelated WT individual. 200 metaphases were counted in total from 2
1299 independent blood samples. **b** Average number of mitotic cells with mis-segregated lagging
1300 chromosomes in SLF2 and SMC5 mutant fibroblast cell lines infected with lentiviruses encoding WT
1301 SLF2, WT SMC5, or an empty vector. n=3 independent experiments for SLF2-P1, SMC5-P7 and SMC5-
1302 P8, and n=4 independent experiments for SLF2-P2. A minimum of 250 mitotic cells were counted. **c**
1303 Representative images of mitotic cells from (b) with lagging chromosomes (scale bar: 10 μ M). **d**
1304 Average number of mitotic cells with mis-segregated lagging chromosomes in U-2 OS SLF2 CRISPR
1305 HM cells infected with lentiviruses encoding WT SLF2 or an empty vector. n=3 independent
1306 experiments. A minimum of 190 mitotic cells were counted. **e** Left: percentage of metaphases with rail
1307 road chromosomes in peripheral blood lymphocytes from SLF2 or SMC5 patients, or an unrelated WT
1308 individual. A minimum of 380 metaphases were counted in total from 2 independent blood samples.
1309 Right: Representative images of metaphases (scale bar: 10 μ M). **f** Percentage of metaphases with
1310 premature chromatid separation following 4 h treatment with 25 μ M MG132 in SLF2 and SMC5 patient
1311 LCLs. n=4 independent experiments. 200 total metaphases were counted. **g** Percentage of S/G2 cells
1312 (CENPF positive cells) with >2 centrosomes with or without 24 h exposure to 250 nM APH. n=3
1313 independent experiments. A minimum of 900 CENPF positive cells were counted. **h** Percentage of
1314 mitotic cells in SLF2 and SMC5 mutant LCLs with multi-polar spindles in untreated cells and cells
1315 exposed to 250 nM APH for 24 h. A minimum of 300 mitotic cells were counted over 3 independent
1316 experiments. **i** The percentage of G1-phase cells (CENPF negative cells) with >5 53BP1 bodies in SLF2

1317 and SMC5 mutant fibroblast cell lines, with or without 24 h exposure to 500nM APH. n=4 independent
1318 experiments. A minimum of 390 G1-phase cells were counted. In all cases, a Student's t-test (two-
1319 sided, equal variance) statistical test was performed and error bars denote SEM.

1320

1321 **Figure 8: Variants in the RAD18-SLF1/2-SMC5/6 complex compromise the ability of cells to**
1322 **replicate in the presence of stabilised G4 quadruplex structures.**

1323 **a** Left: Average number of segmented chromosomes per metaphase in peripheral blood lymphocytes
1324 (PBLs) from SLF2 or SMC5 patients, or an unrelated WT individual. 250 total metaphases were counted
1325 from 2 independent blood samples. Middle: Representative images of 'type 1' and 'type 2' segmented
1326 chromosomes. Right: Representative image of a metaphase exhibiting segmented chromosomes from
1327 SLF2-P3 PBLs (scale bar: 10 μ M). **b** Representative image of FISH with a centromere-specific probe
1328 showing di-centric chromosomes in a metaphase prepared from SLF2-P3 PBLs (scale bar: 10 μ M). **c**
1329 Average number of sister chromatid exchanges in metaphase spreads from SLF2 and SMC5 patient-
1330 derived LCLs. n=3 independent experiments. A minimum of 100 metaphases were counted. **d**
1331 Quantification of the IdU:CldU track length ratio in untreated and CX451-treated SLF2 and SMC5
1332 patient fibroblast cells. Cell lines were pulse-labelled first with CldU for 30 min, followed by IdU, with or
1333 without 250 nM CX5461, for 30 min. n=3 independent experiments. A minimum of 250 ongoing fork
1334 structures were counted. **e** Average number of chromosomal aberrations (chromatid/chromosome
1335 gaps, breaks, fragments and chromosome radials) per metaphase in SLF2 and SMC5 patient-derived
1336 LCLs with and without 24 h exposure to 250 nM CX5461. n=5 independent experiments. A minimum of
1337 350 metaphases were counted. Student's t-test (two-sided, equal variance) was performed. Error bars
1338 denote SEM. **f** LCL proliferation assay. WT and SLF2 and SMC5 patient-derived LCLs were cultured in
1339 increasing concentrations of CX5461 for the time untreated cells took to undergo three population
1340 doublings. Cell viability following CX5461 treatment was calculated as a percentage of the number of
1341 untreated cells. n=4 independent experiments. Error bars denote SEM. A two-way ANOVA statistical
1342 test was performed. **g** Quantification of IdU:CldU track length ratio in untreated, pyridostatin-, etoposide-
1343 and BMH21-treated SLF2 and SMC5 mutant fibroblast cells. Cell lines were pulse-labelled first with
1344 CldU for 30 min, followed by IdU with or without 1 μ M pyridostatin, 50nM etoposide or 1 μ M BMH21, for
1345 30 min. n=3 independent experiments. A minimum of 150 ongoing forks were counted. For panels c, d
1346 and g, red lines denote median values, and a Mann-Whitney rank sum statistical test was performed.

Figure 1**a**

| Individual | Ancestry | Gene | Mutation 1 | Allele Frequency | Polyphen-2 score | Mutation 2 | Allele Frequency | Polyphen-2 score |
|------------|--------------|-------------|-----------------------------------------|------------------|------------------|------------------------------------------|------------------|------------------|
| P1 | UK | <i>SLF2</i> | c.1006dup; p.(Arg336LysfsTer27) | - | NA | c.1006dup; p.(Arg336LysfsTer27) | - | NA |
| P2 | France | <i>SLF2</i> | c.2444C>G; p.(Ser815Ter) | - | NA | c.3486G>C (ss); p.(Gln1162His) | - | 0.999 |
| P3 | Netherlands | <i>SLF2</i> | c.3330G>A (ss) p.(Arg1110ArgΔexon17) | - | NA | c.3330G>A (ss); p.(Arg1110ArgΔexon17) | - | NA |
| P4-1 | Japan | <i>SLF2</i> | c.2582A>T; p.(Asn861Ile) | 3.98e-6 | 0.996 | c.2719dup; p.(Ser907PhefsTer5) | - | NA |
| P4-2 | Japan | <i>SLF2</i> | c.2582A>T; p.(Asn861Ile) | 3.98e-6 | 0.966 | c.2719dup; p.(Ser907PhefsTer5) | - | NA |
| P5 | Saudi Arabia | <i>SLF2</i> | c.2347_2348del; p.(Asp783SerfsTer53) | - | NA | c.2347_2348del; p.(Asp783SerfsTer53) | - | NA |
| P6 | German | <i>SLF2</i> | c.568C>T; p.(Arg190Ter) | 3.19e-5 | NA | c.568C>T; p.(Arg190Ter) | 3.19e-5 | NA |
| P7 | Spain | <i>SMC5</i> | c.1110_1112del; p.(Arg372del) | - | NA | c.1273C>T; p.(Arg425Ter) | 3.99e-6 | NA |
| P8 | US | <i>SMC5</i> | c.2970C>G; p.(His990Asp) | - | 1.000 | c.2970C>G; p.(His990Asp) | - | 1.000 |
| P9-1 | US | <i>SMC5</i> | c.2970C>G; p.(His990Asp) | - | 1.000 | c.2970C>G; p.(His990Asp) | - | 1.000 |
| P9-2 | US | <i>SMC5</i> | c.2970C>G; p.(His990Asp) | - | 1.000 | c.2970C>G; p.(His990Asp) | - | 1.000 |

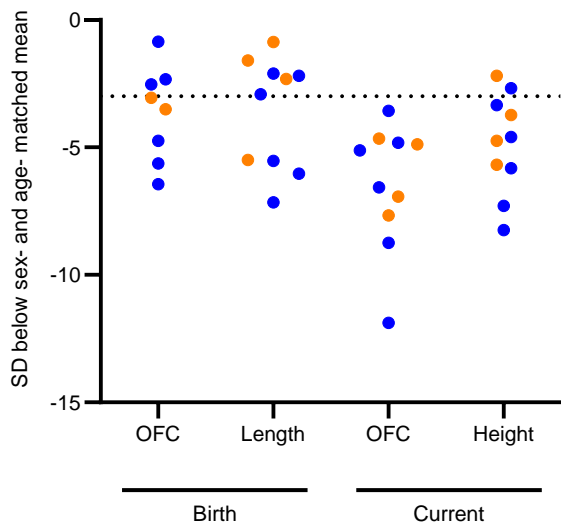
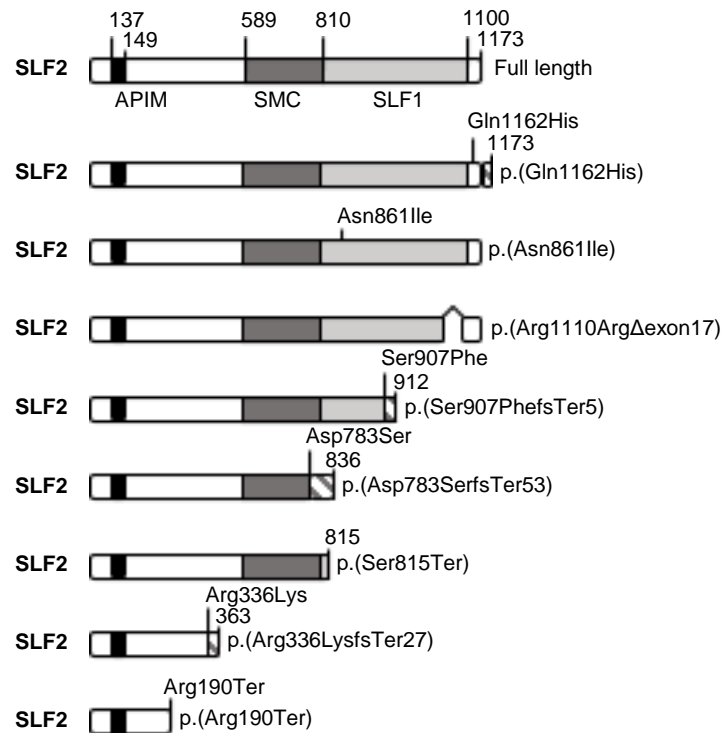
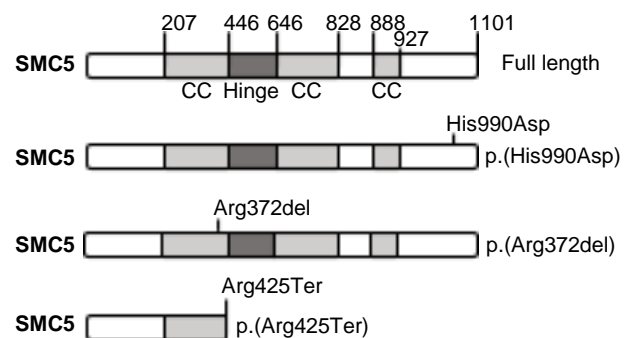
b**c****d**

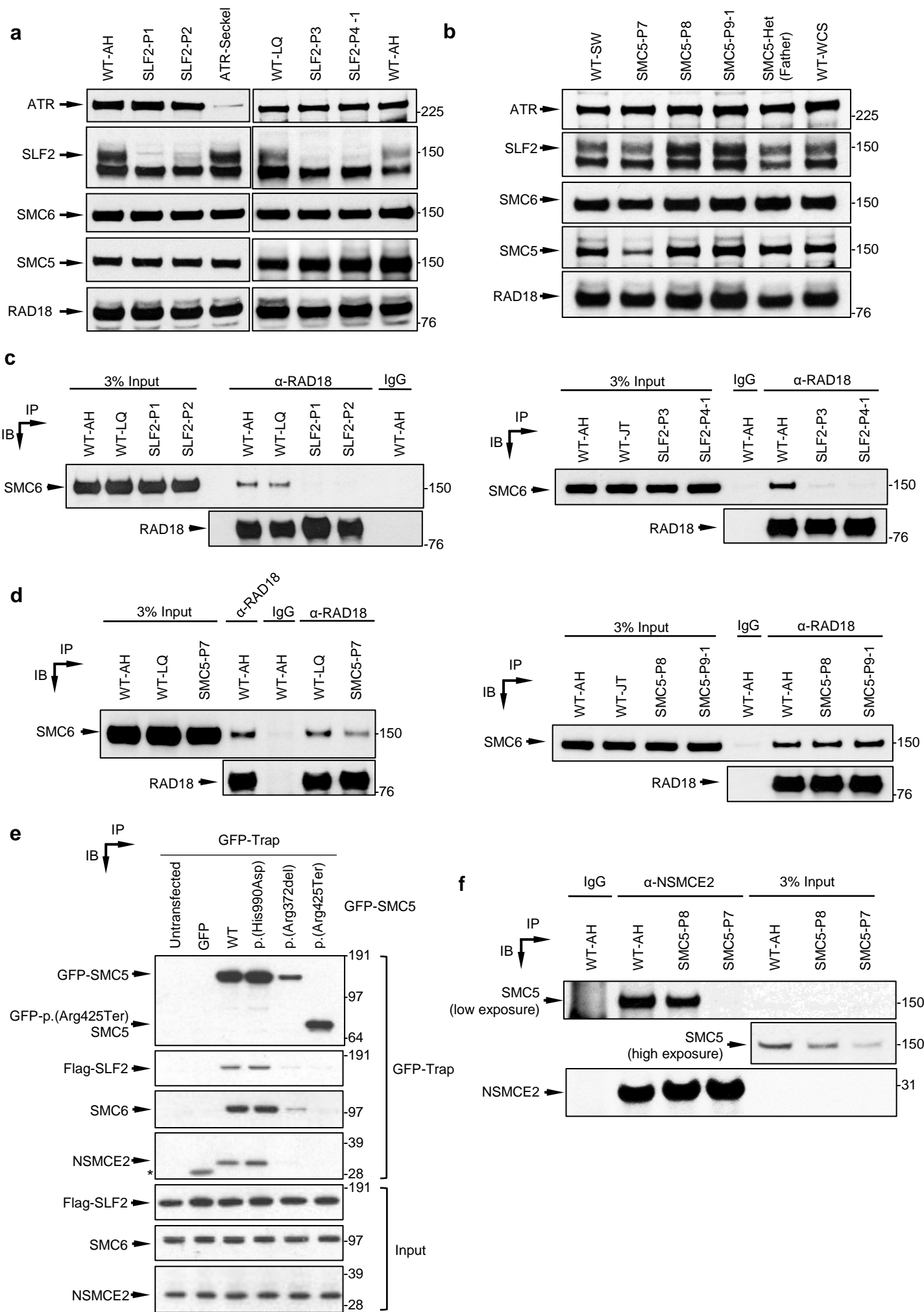
Figure 2

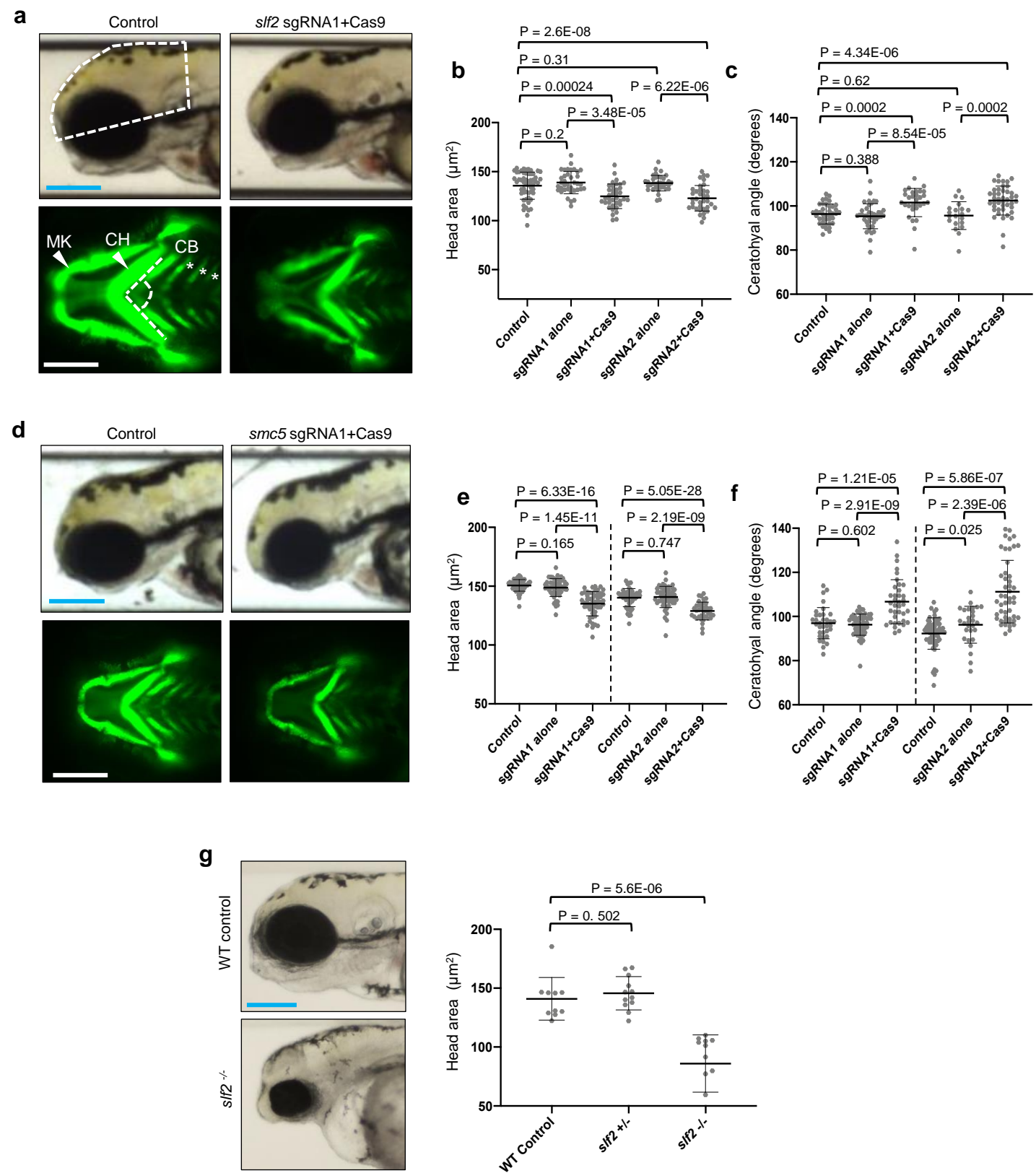
Figure 3

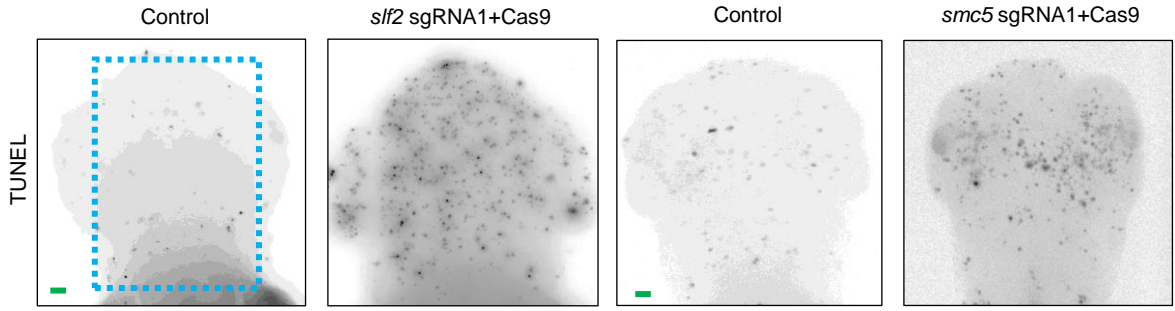
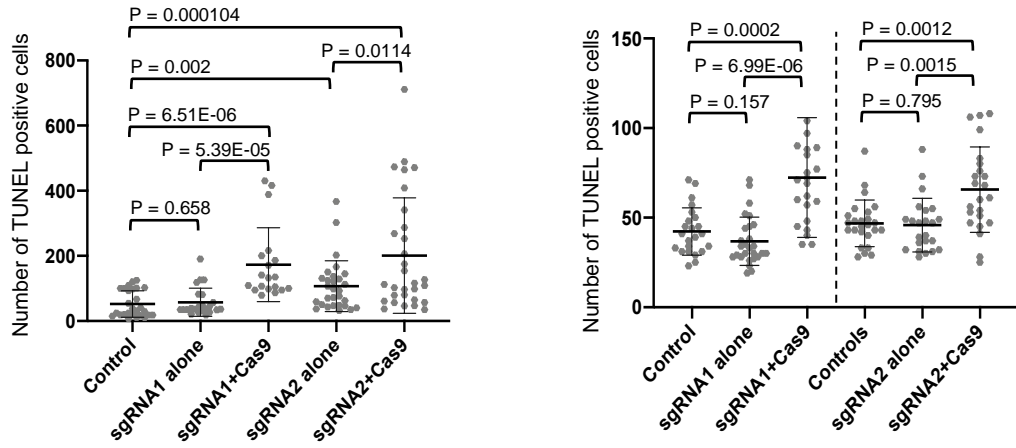
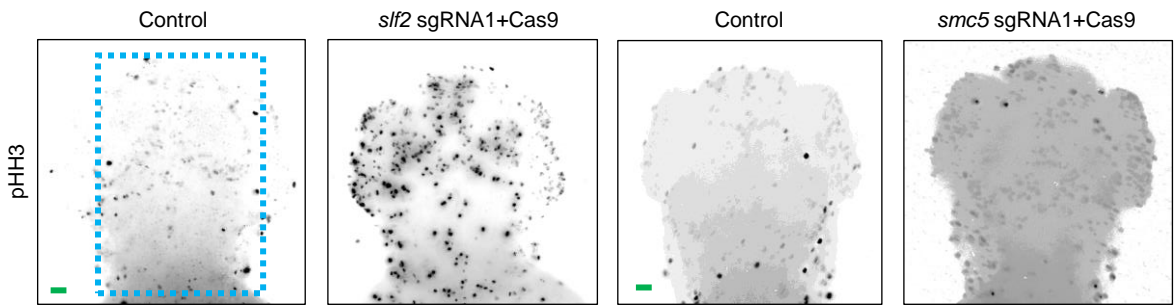
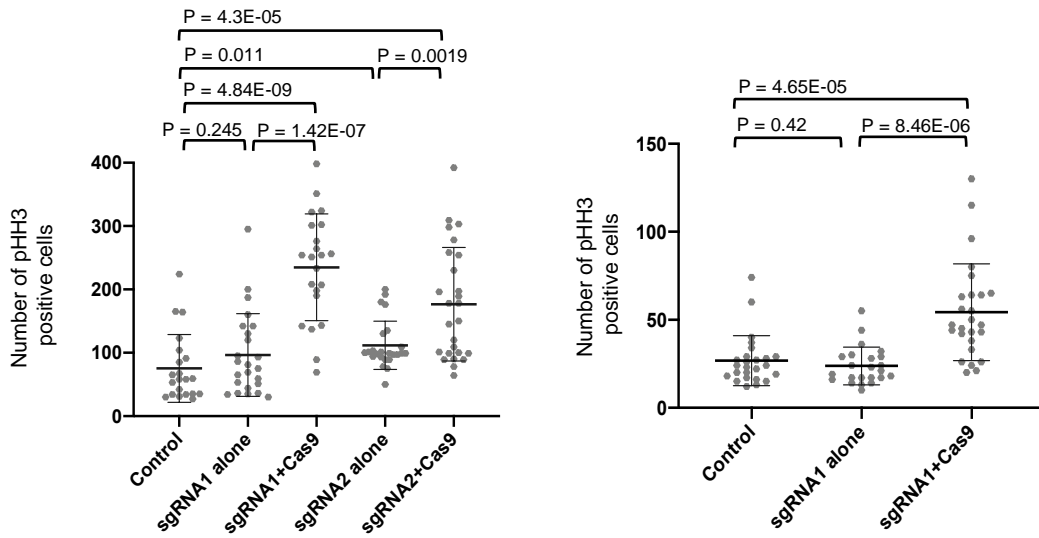
Figure 4**a****b****c****d**

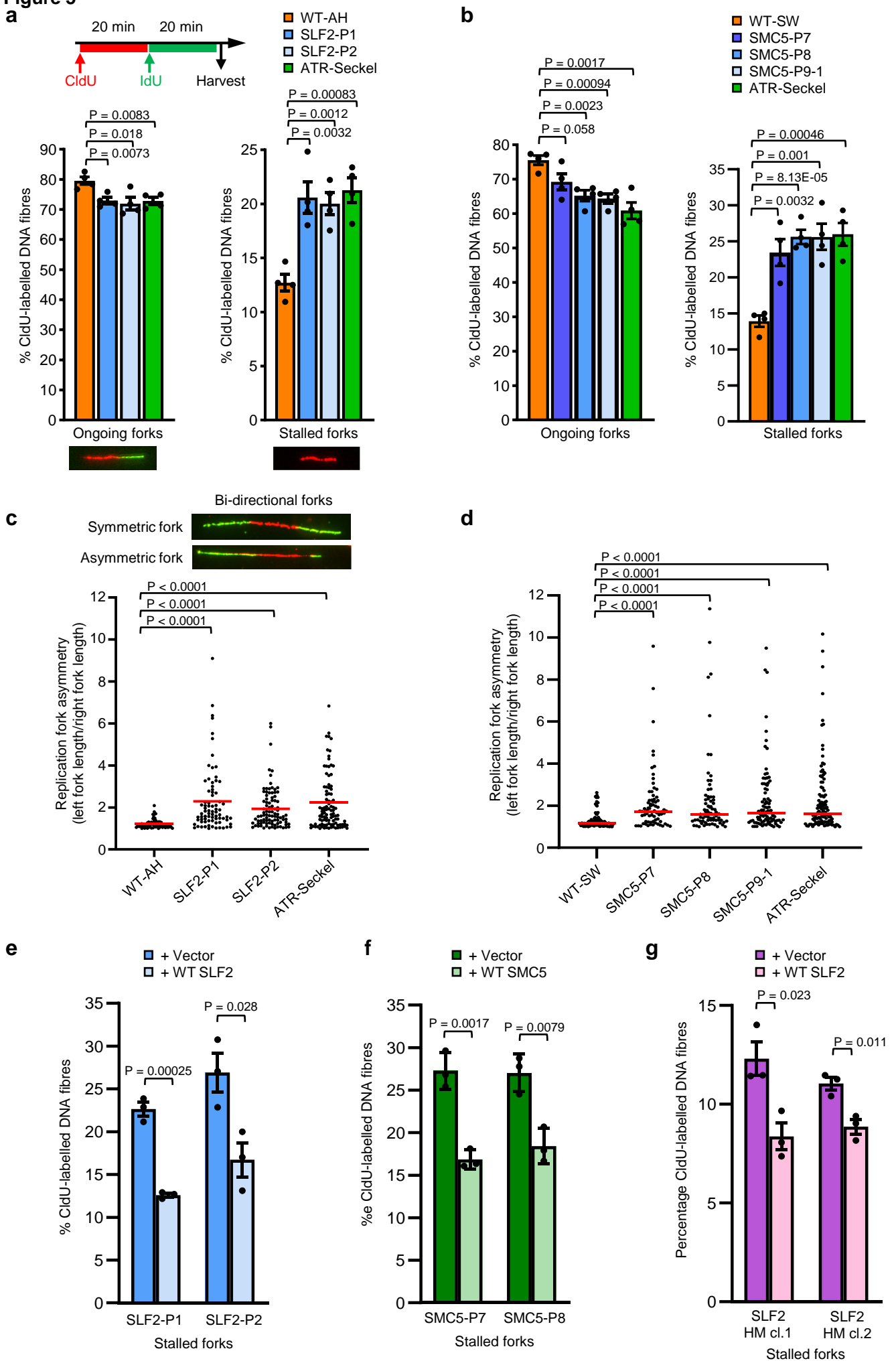
Figure 5

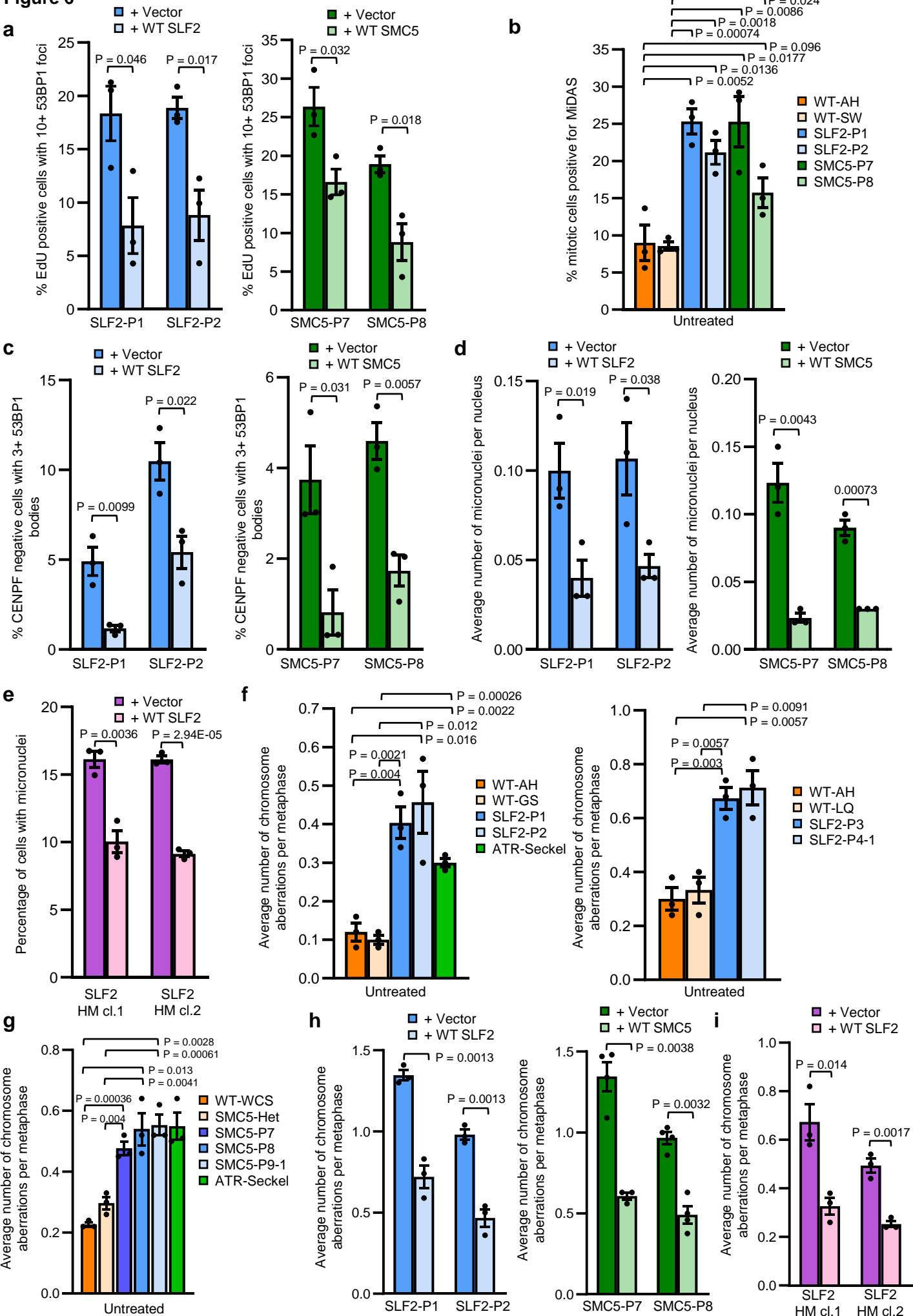
Figure 6

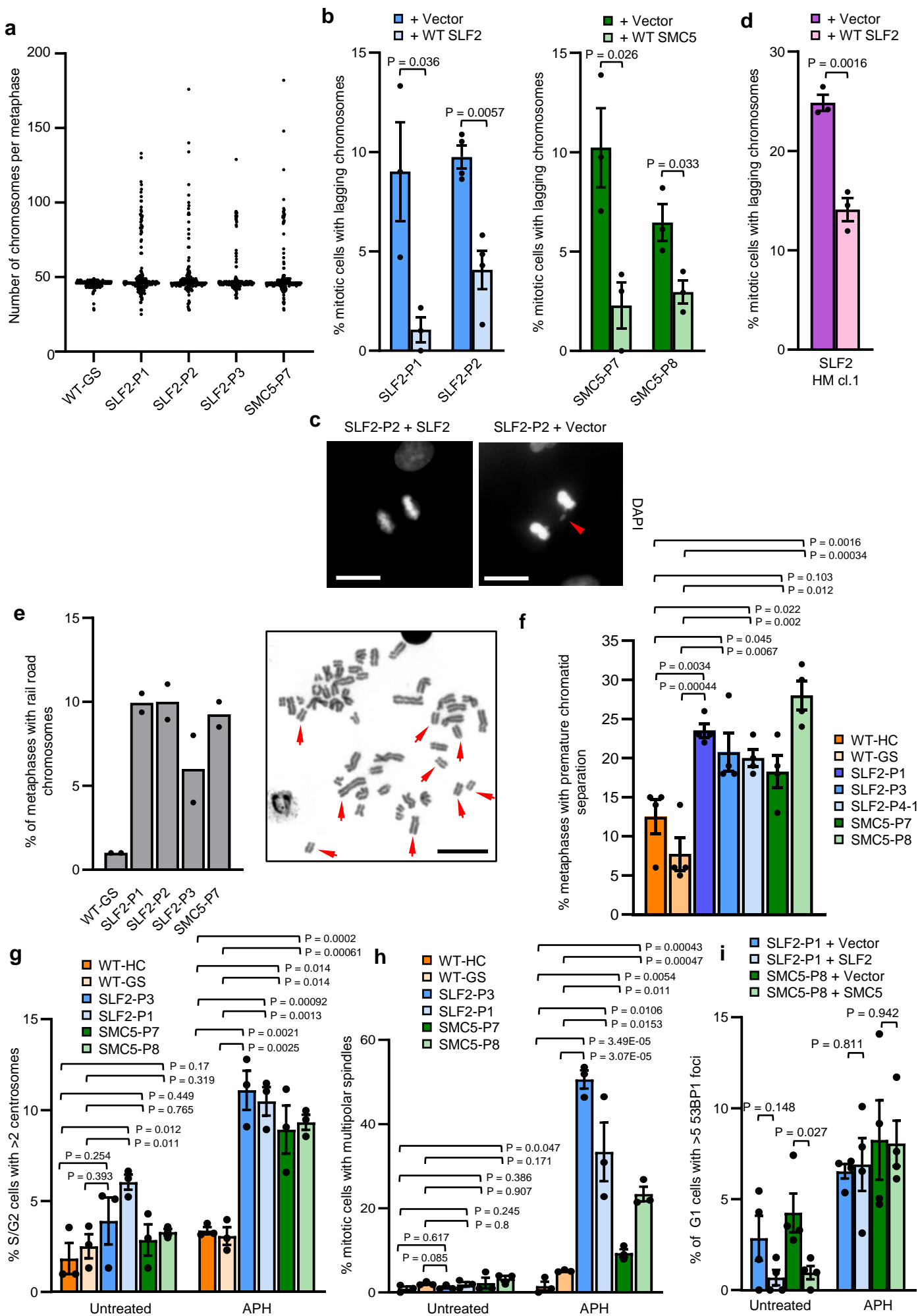
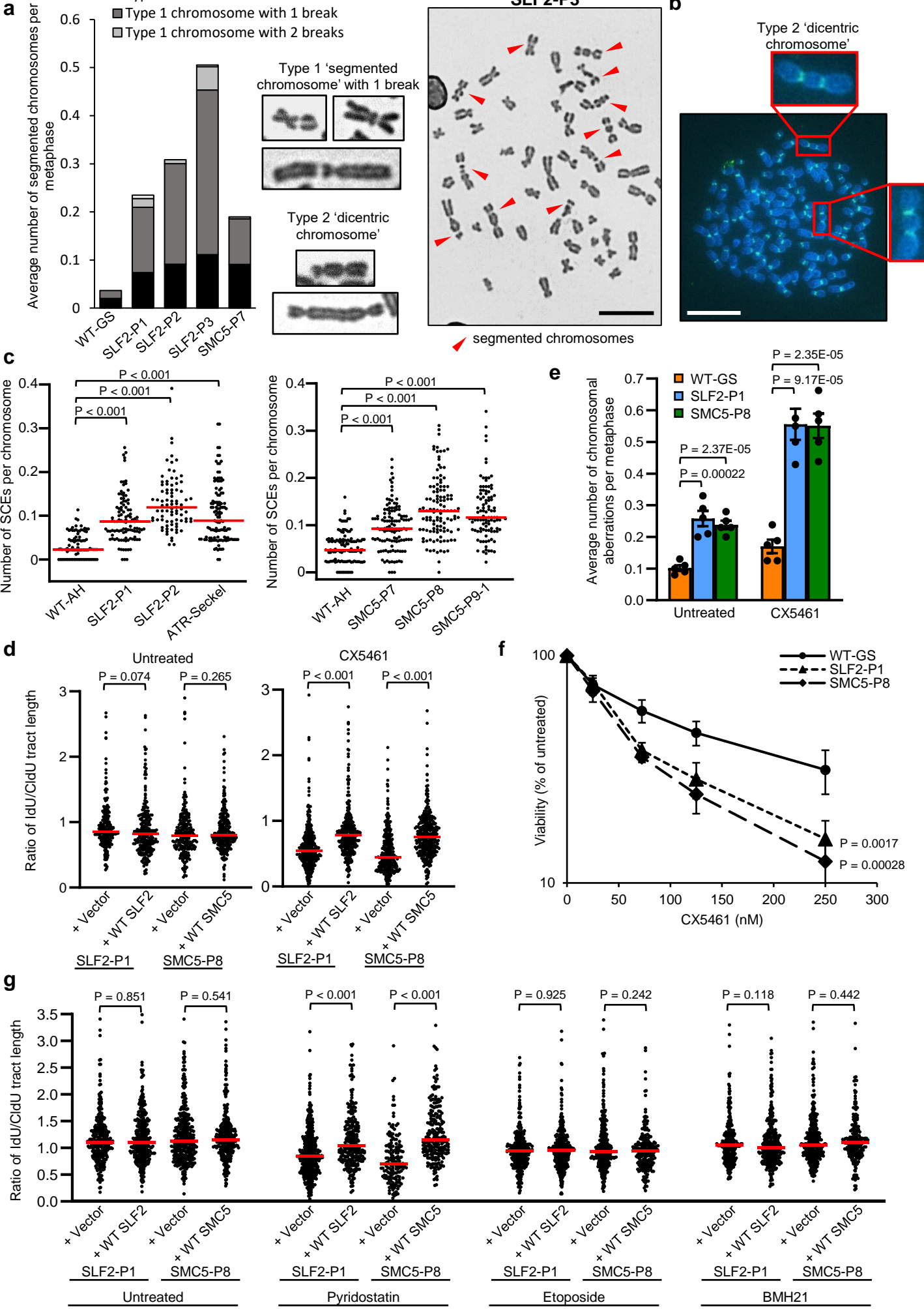
Figure 7

Figure 8

Supplementary Figure 1

a

SLF2

p. (Ans861Ile)

| | | |
|------------|---------------------------|-----|
| Human | SLSDVAAVFFNMGIDFRSLFPLEN | 908 |
| Chimpanzee | SLSDVAAVFFNMGIDFRSLFPLEN | 908 |
| Dog | SLSDIAAVFFNMGIDFRSLFPLEN | 905 |
| Mouse | SLSDIAAVFFNMGVGFGLFPLET | 898 |
| Chicken | SLADVTTVLVNMGIRLRSFLFPLOH | 924 |
| Zebrafish | SIRDITQVFLNMGASFTSLFPPLDV | 708 |

p. (Gln1162His)

| | | |
|------------|--------------------------|------|
| Human | GKWQELIQNCRPTGGQLHDFWVPD | 1173 |
| Chimpanzee | GKWQELIQNCRPTGGQLHDFWVPD | 1173 |
| Dog | GKWQELIQNCRPTGGQLHDFWVPD | 1170 |
| Mouse | GKWQELIQNCRPTGGQLHDFWVPD | 1163 |
| Chicken | GRWQDLIQNSRLTGGQLHDFWVPD | 1189 |
| Zebrafish | TKWQVLLTRTRPQEGMLYDYWKPP | 999 |

b

SMC5

p. (His990Asp)

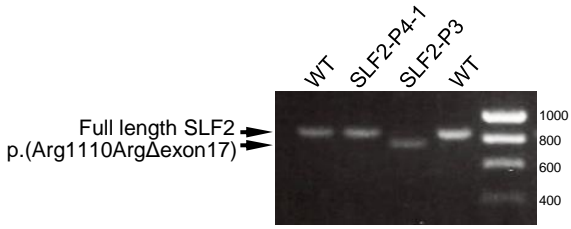
| | | |
|--------------|--------------------------------------------------------------|------|
| Human | SSMQCAGEVDLHTENEEDYDKYGRIRVRFERSSTQLHELTPPHQSGGERSVSTMIYLMAL | 1007 |
| Chimpanzee | SSMQCAGEVDLHTENEEDYDKYGRIRVRFERSSTQLHELTPPHQSGGERSVSTMIYLMAL | 1007 |
| Dog | SSMQCAGEVDLHTENEEDYDKYGRIRVRFERSSTQLHELTPPHQSGGERSVSTMIYLMAL | 1011 |
| Mouse | SSMQCAGEVDLHTENEEDYDKYGRIRVRFERSSTQLHELTPPHQSGGERSVSTMIYLMAL | 1007 |
| Chicken | SSMESVGEVDLHVNEEEYDKYGRIRVRFHNFDTLHELTPYHQSGGERSVSTMIYLMAL | 971 |
| Zebrafish | QSMQCAGEVDLHSENEEEYDKYGRIQVCFRRNTRMHELTPPHQSGGERSVSTMIYLMAL | 982 |
| Drosophila | ESIEYVGEVWLSKTDKYDFDSYGTQIMVCFRRGLQLPDKFIQSGGERAVSIATYSLSL | 955 |
| S.Cerevisiae | NNVGSAGAVRLEKP--KDYAEWKTEIMVRFERDAPLKKLDSHTQSGGERAVSTVLYMIAL | 1002 |
| S.Pombe | SGMGYAGEVRLGKS--DDYDKWYTDLLVCFREEEGLQKLTGQRQSGGERSVSTMIYLLSL | 982 |

p. (Arg372del)

| | | |
|--------------|--------------------------------------------------------------|-----|
| Human | IERKD--KHIEELQQALIVKQNEEL-D--RQRRI-GNTRKMIEDLQNELKTEN----- | 392 |
| Chimpanzee | IERKD--KHIEELQQALIVKQNEEL-D--RQRRI-GNTRKMIEDLQNELKTEN----- | 392 |
| Dog | IERKD--KQIEELQQALTIVKQNEEH-D--RQRRI-SNTRKMIEDLQNELKTEN----- | 396 |
| Mouse | IERKD--RQIKELQQALTIVKQNEEL-D--RQRRI-SNTRKMIEDLQSELKTAEN----- | 392 |
| Chicken | LEMKD--KQISEINQALRMKKDEEV-D--RKKKI-LSAYKMIDEWNNELNTVTD----- | 371 |
| Zebrafish | LELKN--KEVDDIKQDMSLQTEEA-D--RQRRI-GHTQLMIRDQLKELQNMGT----- | 381 |
| Drosophila | -AAID--GKMDSLKQGIYQKK-----YEQNIKKSRRTATE----- | 336 |
| S.Cerevisiae | -----IFEKLNTRDEVIKKKNQNEYRGRTKKLQATIISTKEDFLRSQEILAQT--HLP | 393 |
| S.Pombe | LRARASFSNFMENEKKLYEKVN-----TNRTLRRNANLTLNEAQQSVKSLTERQGPRP | 362 |

Supplementary Figure 2

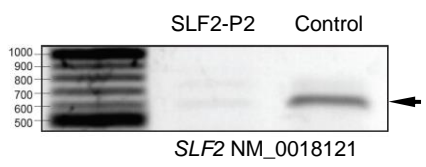
a



b

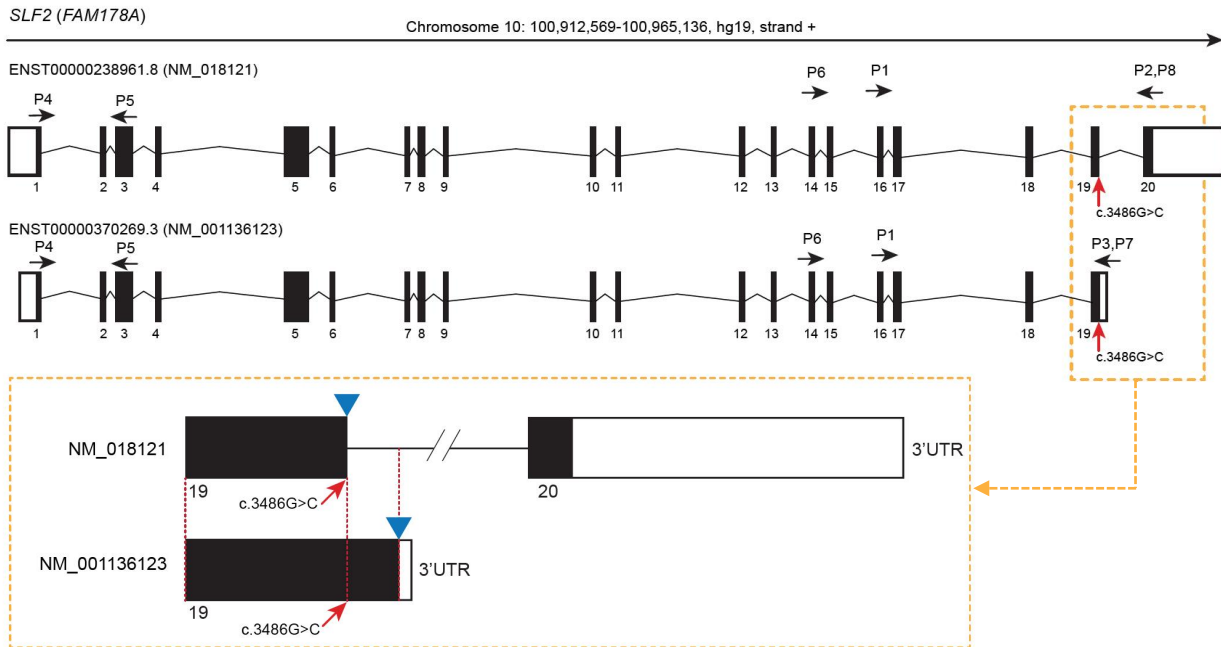


c

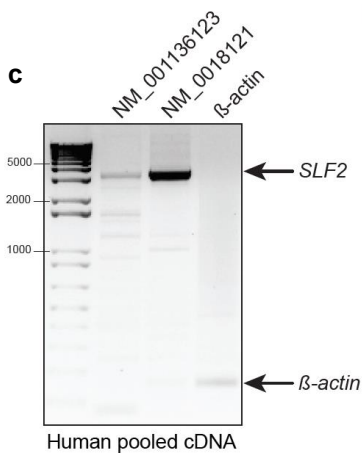


Supplementary Figure 3

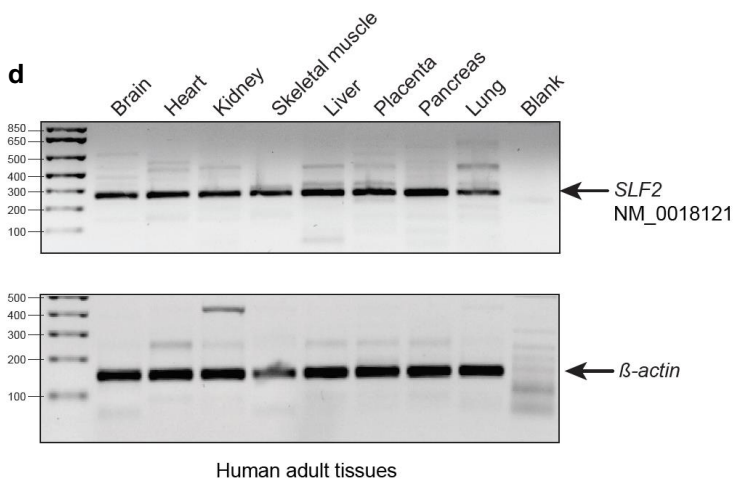
a



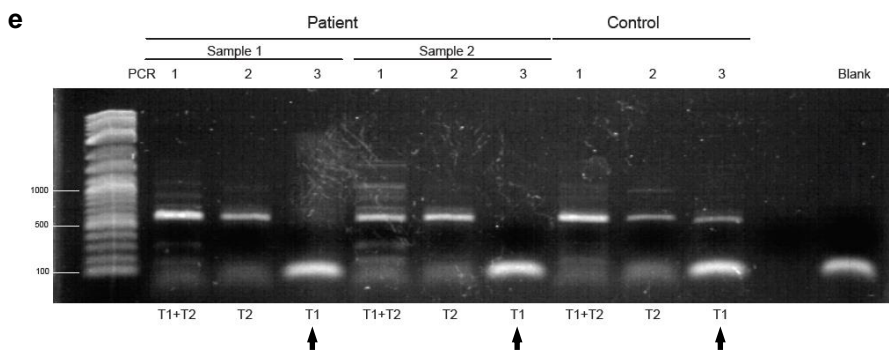
c



d

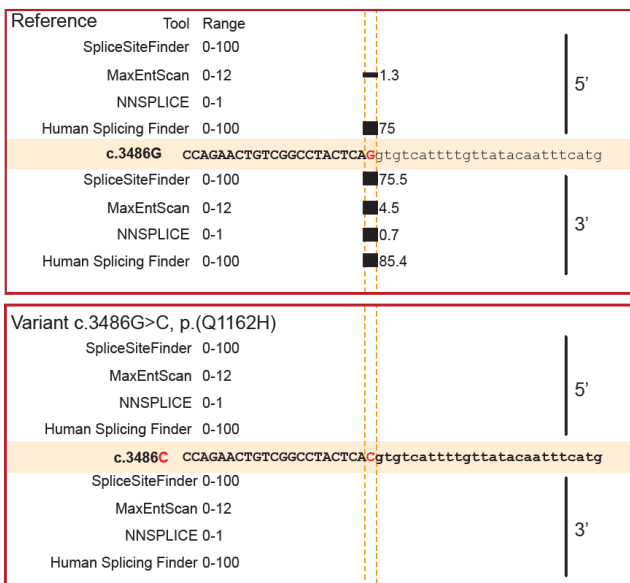


e

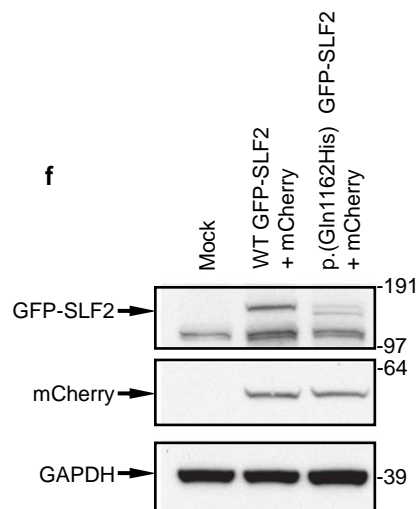


b

SLF2
NM_0018121

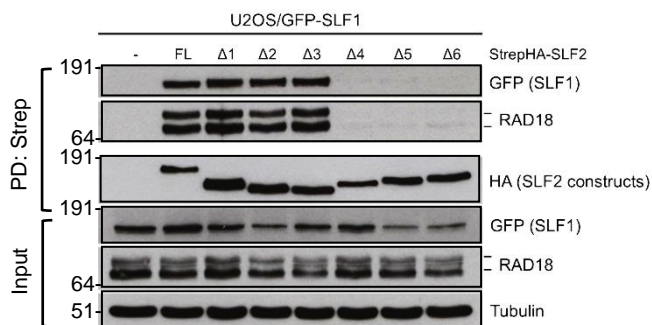
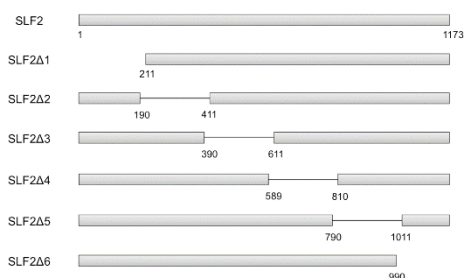


f

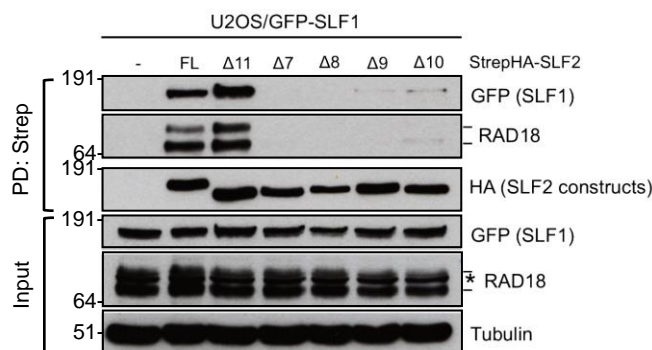
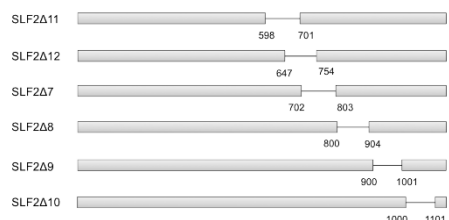


Supplementary Figure 4

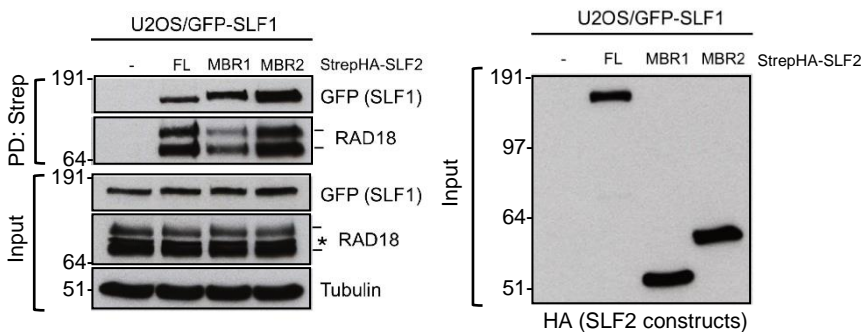
a



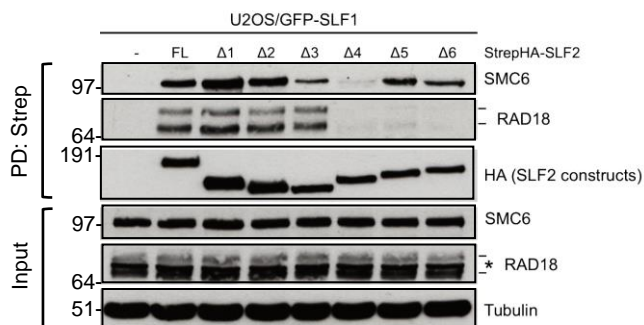
b



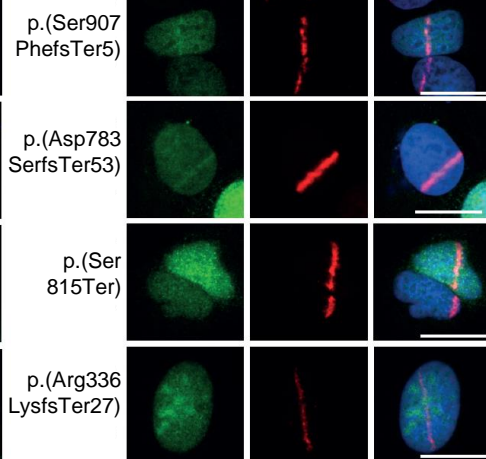
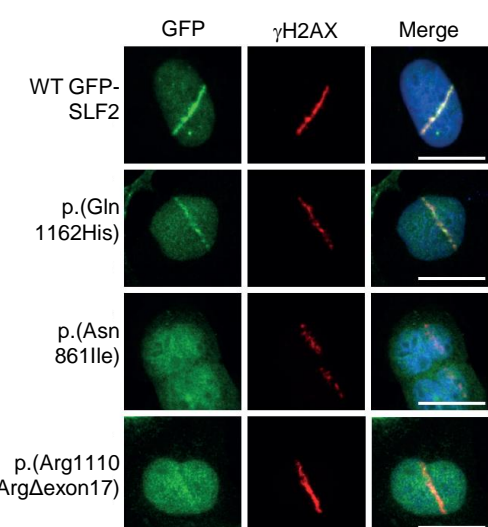
c



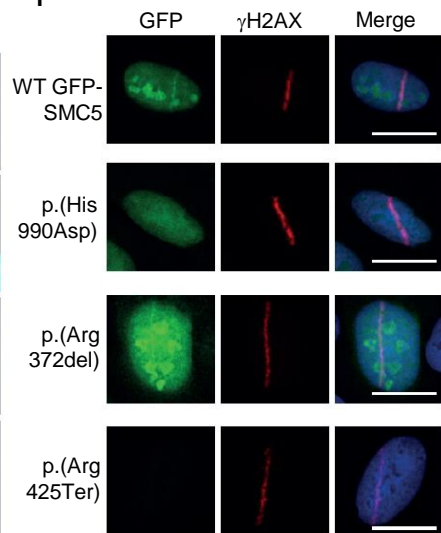
d



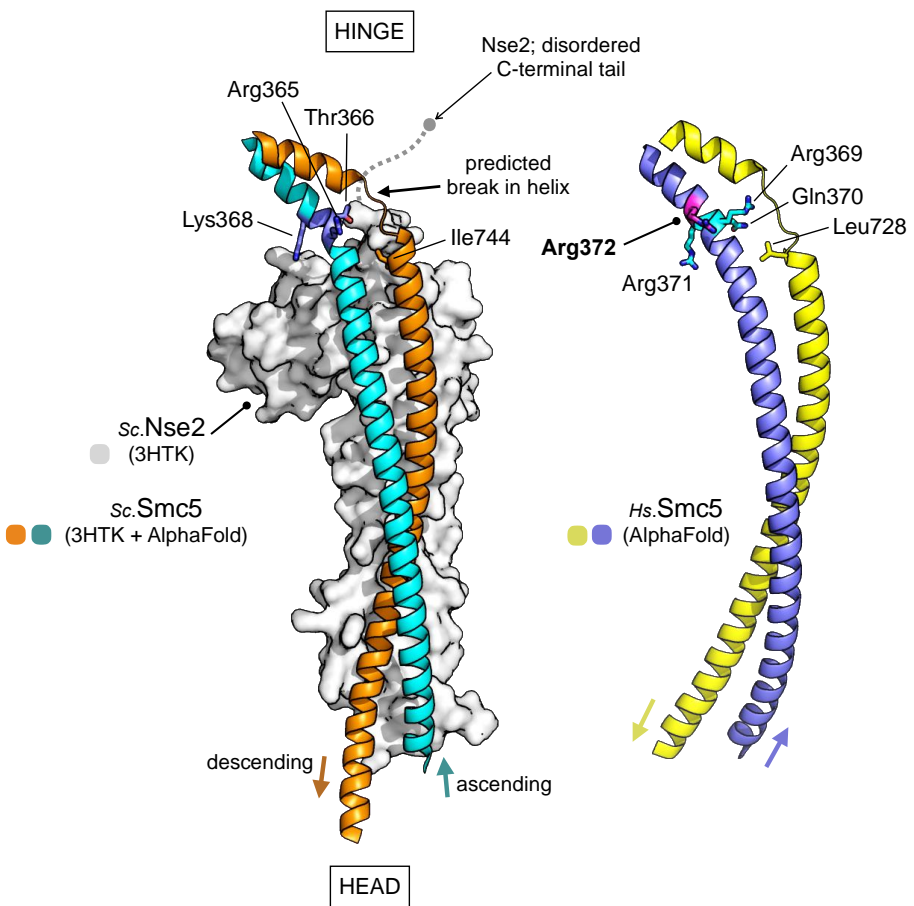
e



f

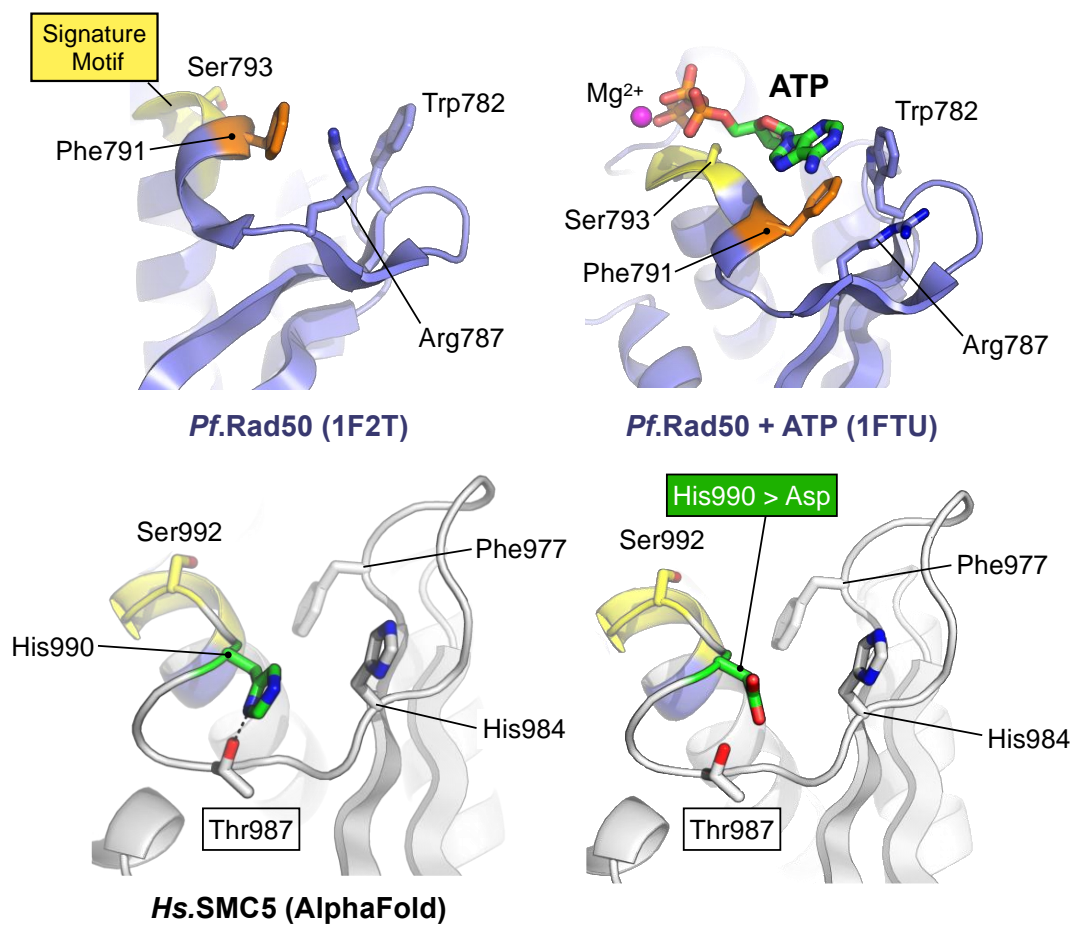


Supplementary Figure 5



Supplementary Figure 6

a

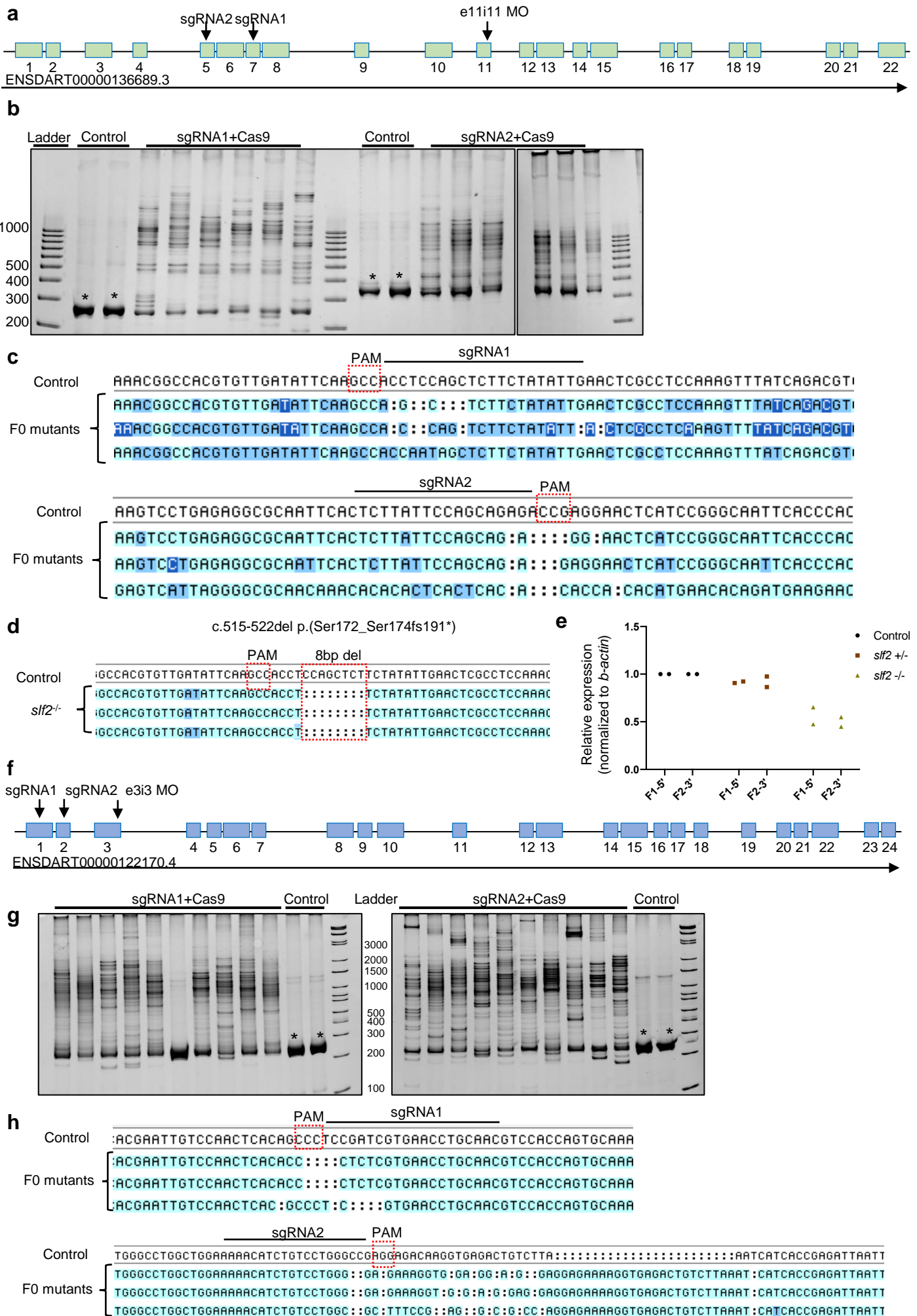


b

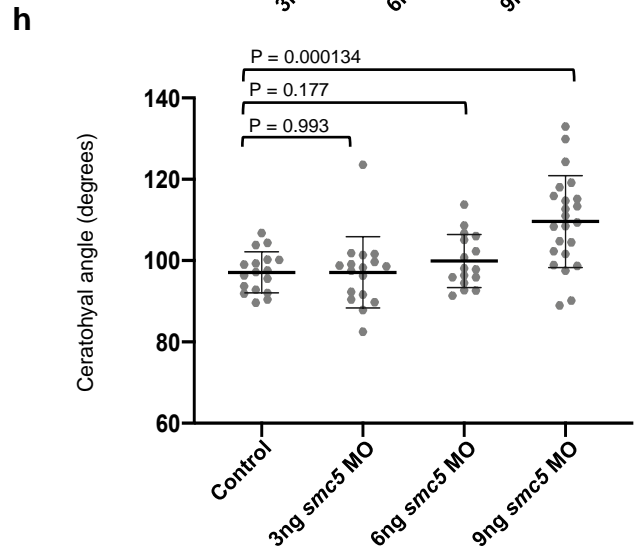
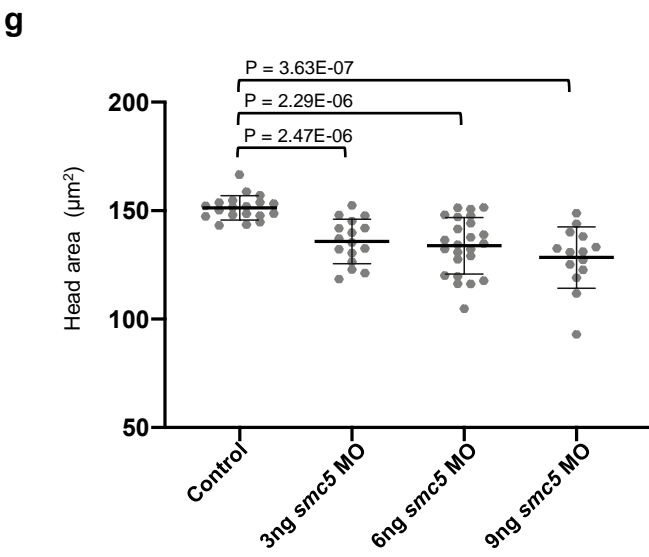
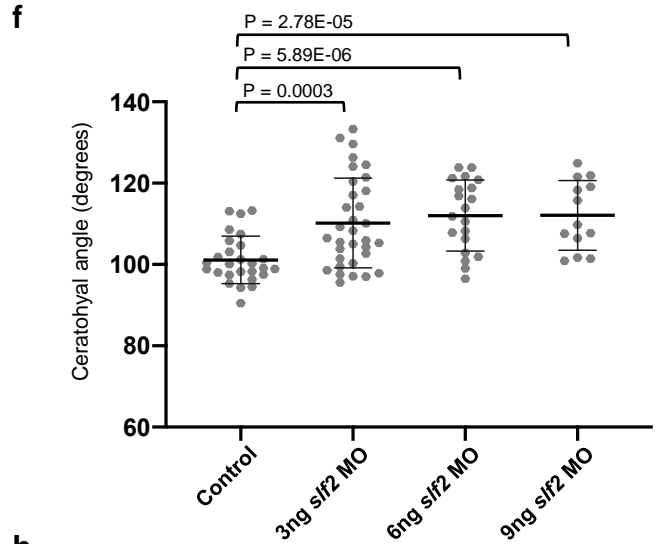
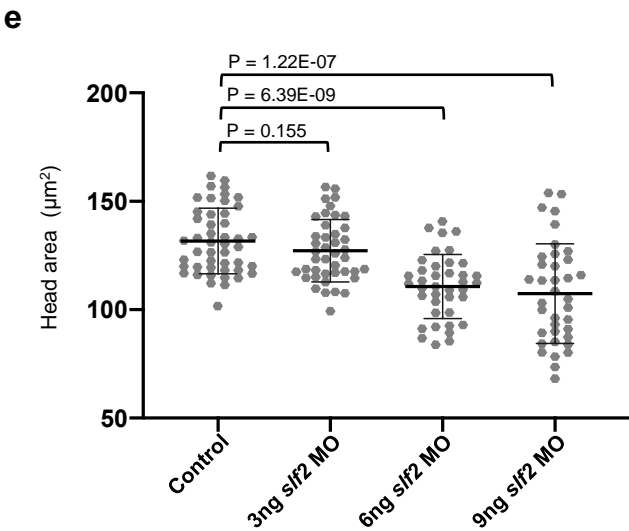
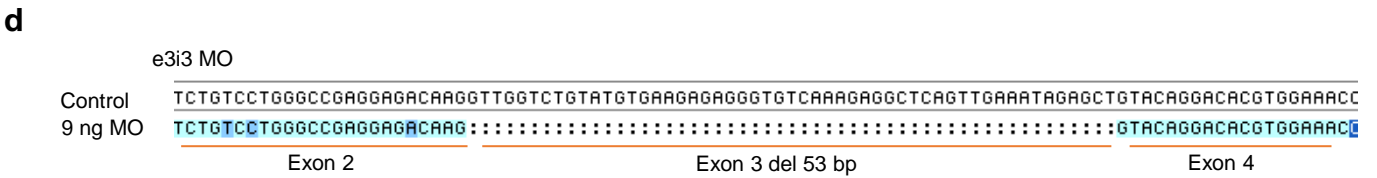
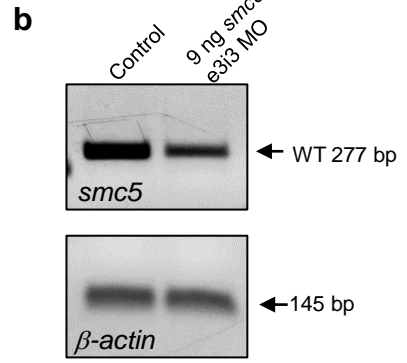
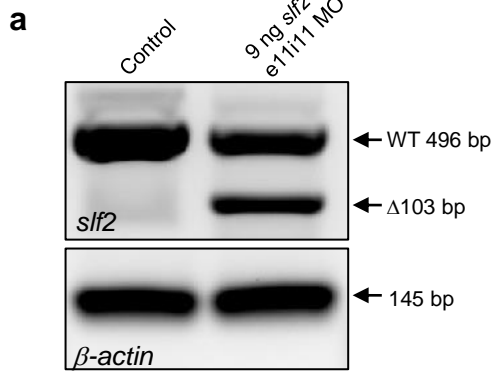
| Analysis Program* | $\Delta\Delta G$ (kcal.mol ⁻¹) | Predicted Effect |
|-------------------|----------------------------------------------------------------|----------------------------------|
| DynaMut | 0.587 | Stabilising |
| mCSM | 0.342 | Stabilising |
| DUET | 0.368 | Stabilising |
| SDM | -0.200 | Destabilising |
| EnCOM | 0.164 | Destabilising |
| | | |
| Analysis Program | $\Delta\Delta SVib$ (kcal.mol ⁻¹ .K ⁻¹) | Predicted Effect |
| ENCoM | -2.05 | Decrease of molecule flexibility |

* all values obtained from DynaMut webserver

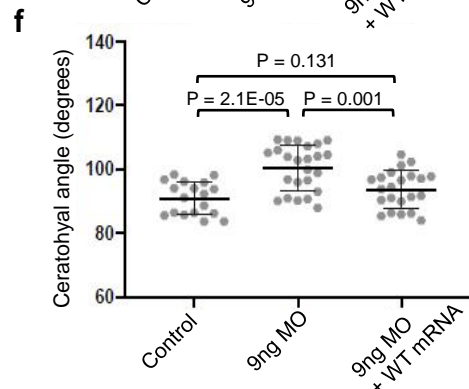
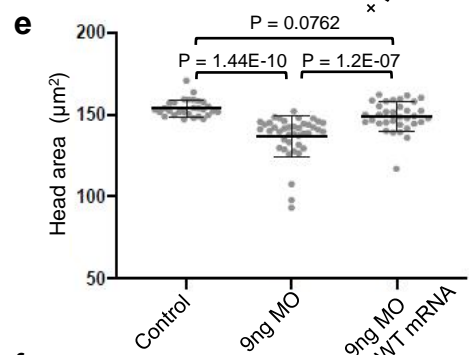
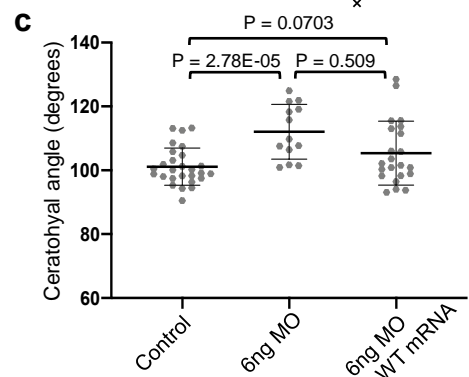
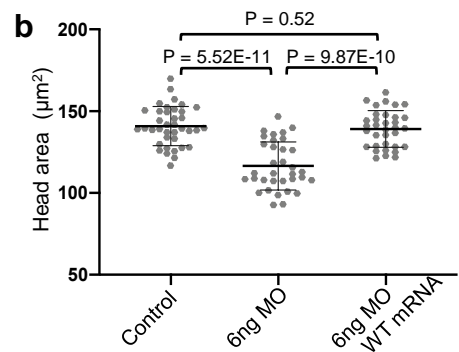
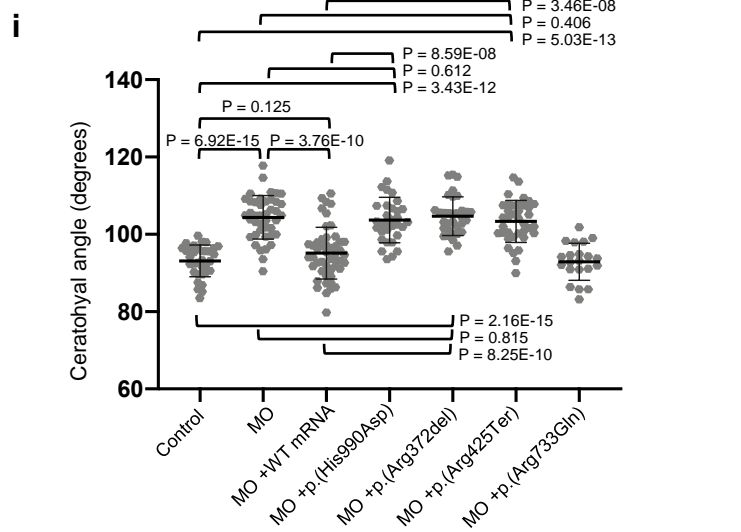
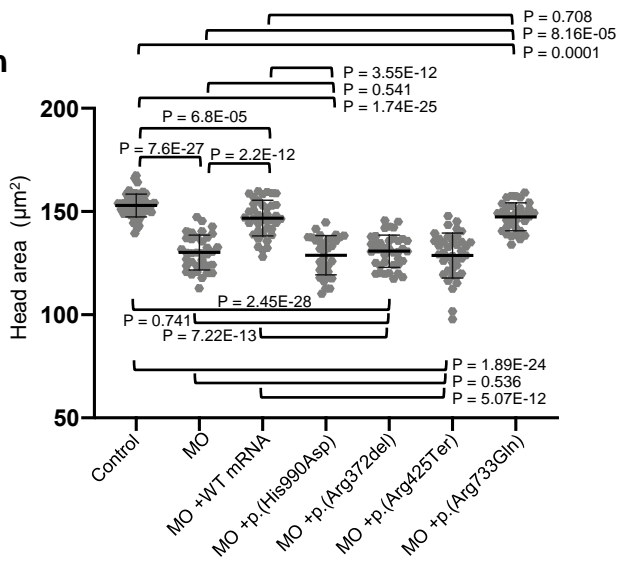
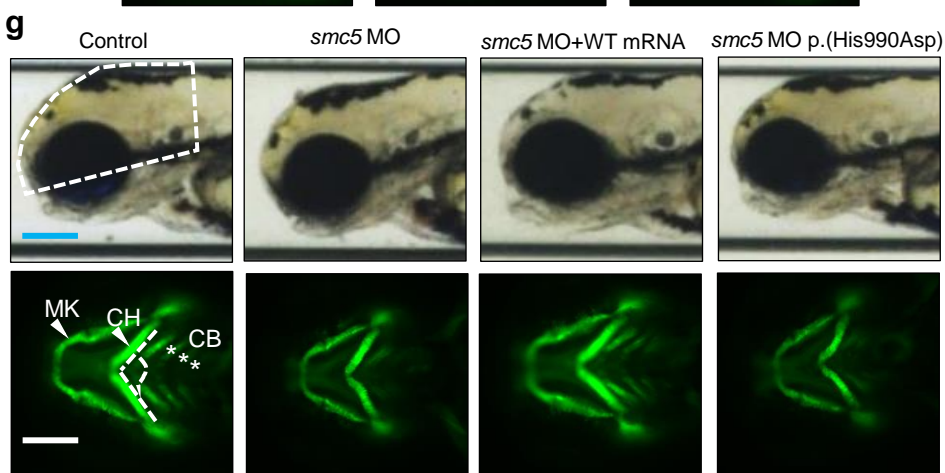
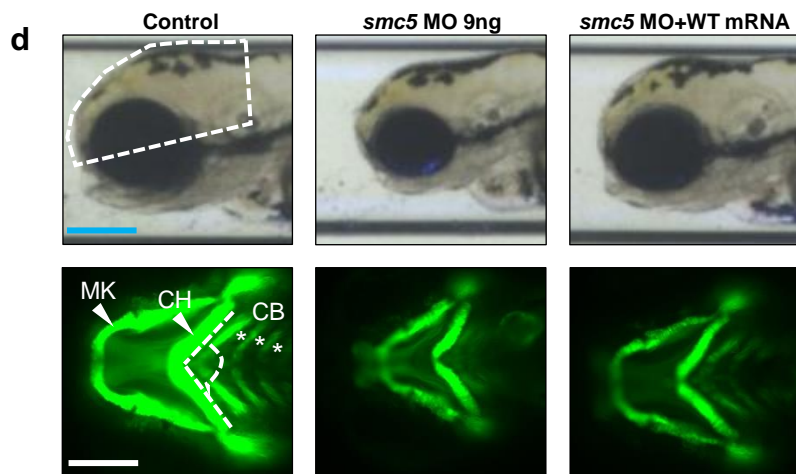
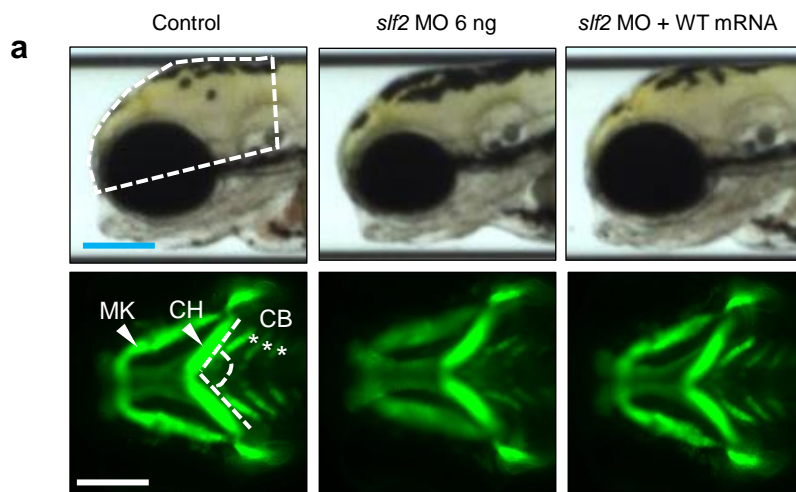
Supplementary Figure 7



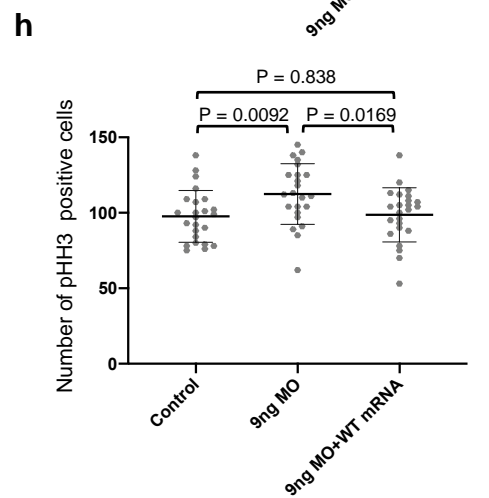
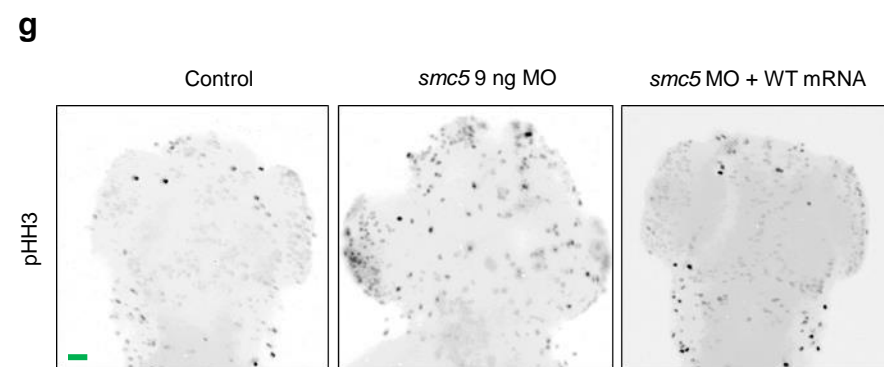
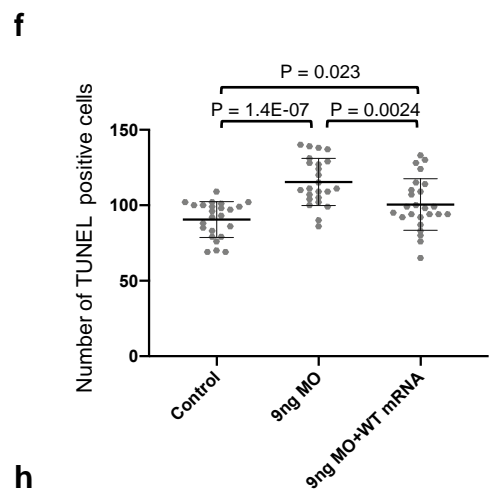
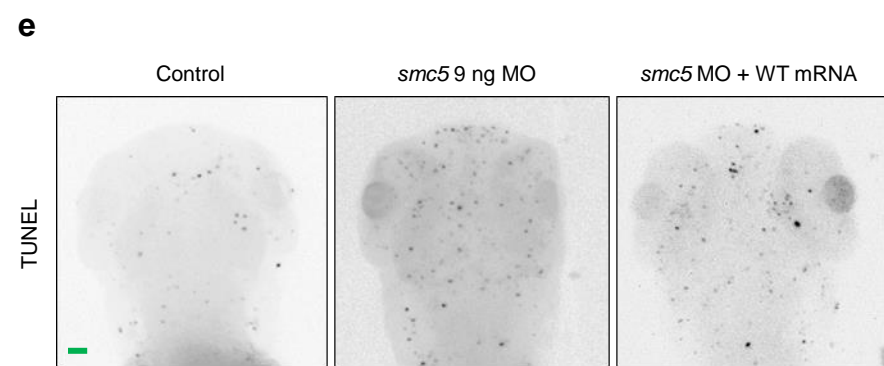
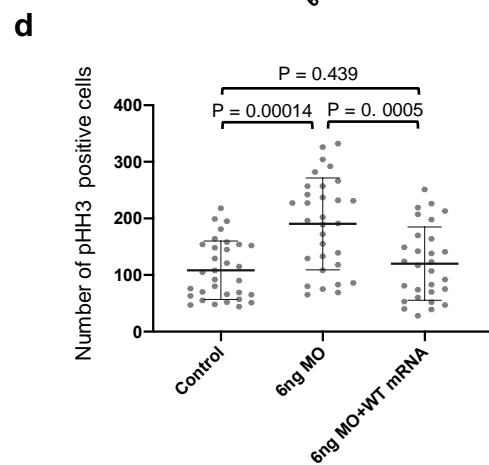
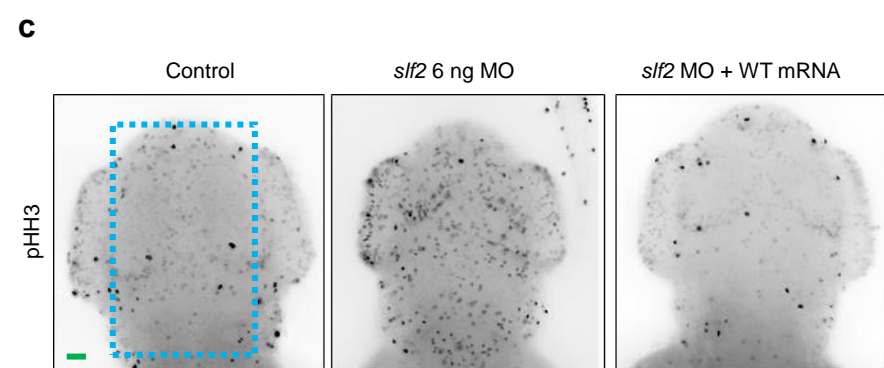
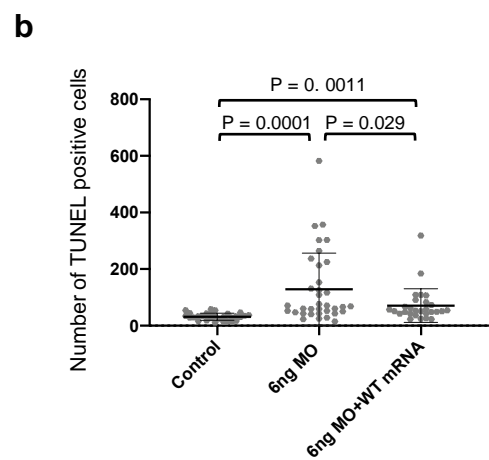
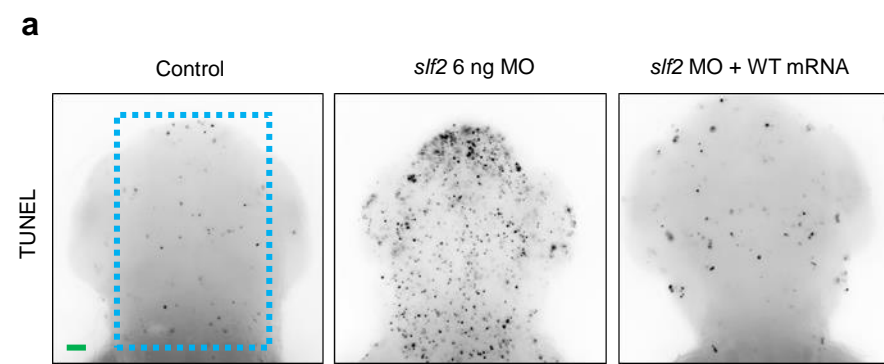
Supplementary Figure 8



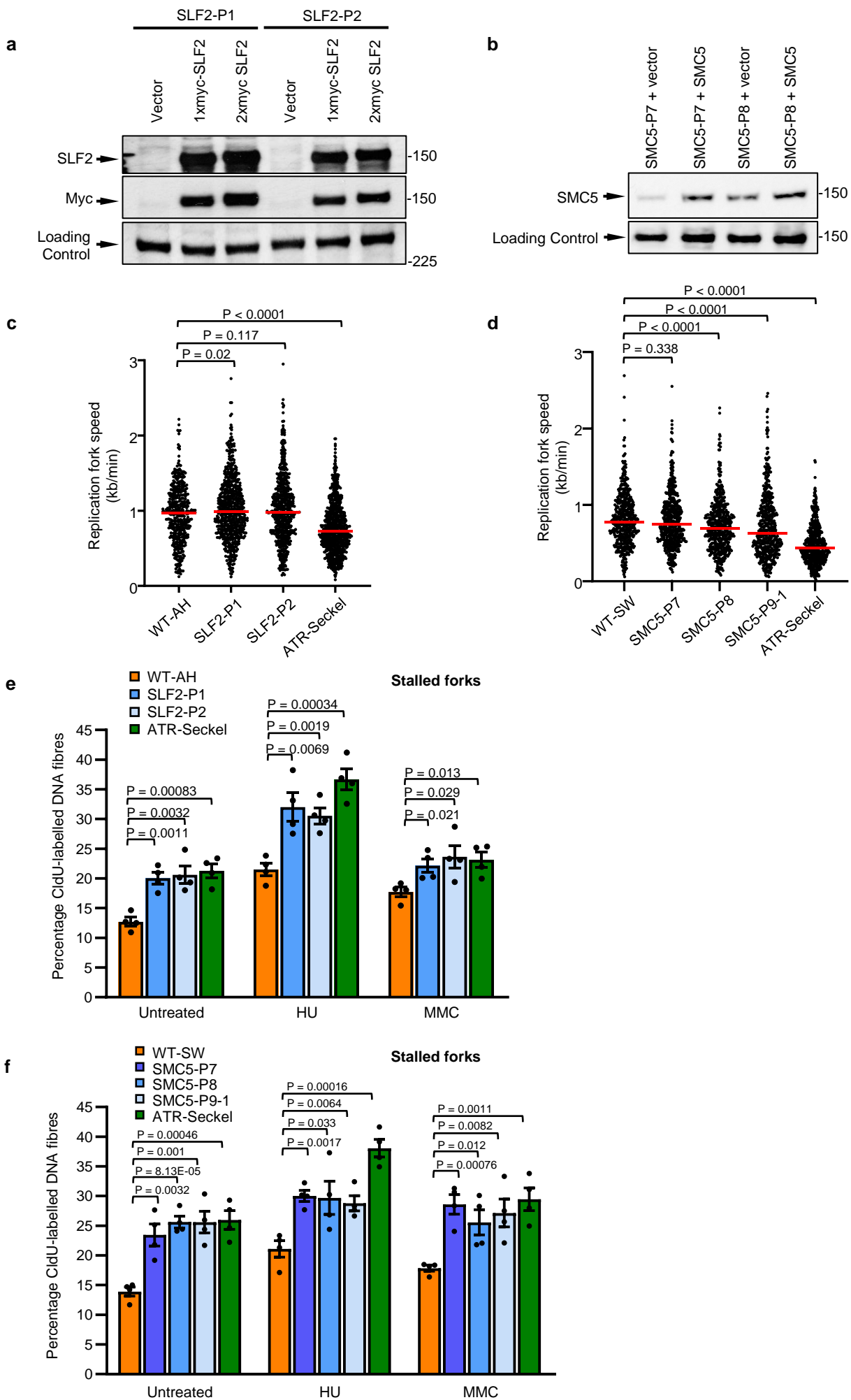
Supplementary Figure 9



Supplementary Figure 10

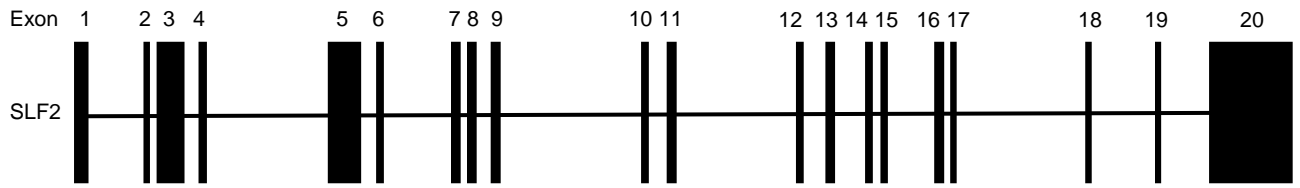


Supplementary Figure 11



Supplementary Figure 12

a

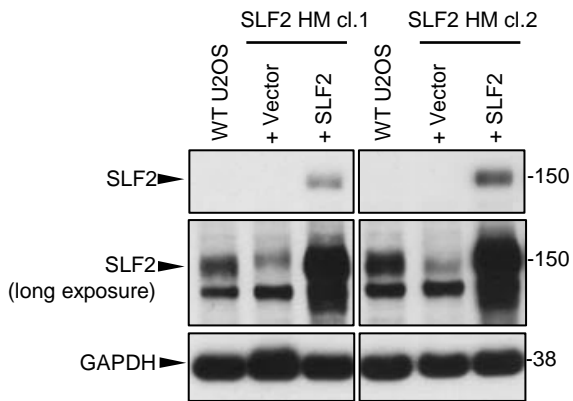


sgRNA 2
 GAAGATATATCCAAGGAACCGAGTGATGAACTGATGGCTCTTCTGCA**GGCTTGGCACCTTCAAATTC**TGGCAATTCTGG
 CTTCTATATAG**GTTCCTTGGCTCACTACTTTG**ACTACCGAGAAGACGTC**CGAACCGT**GGAAGTTTAAGACCGTTAAGACC
 sgRNA 1

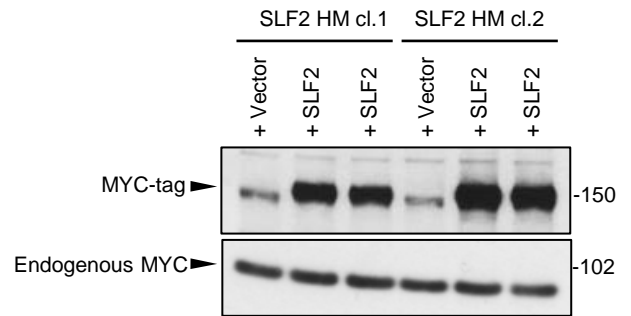
b

| Clone # | Mutation |
|---------|----------------------------------------------------------------------------------------------------------|
| Cl. 1 | c. 1192_1210dupGATGAACTGATGGCTCTT, p.(Ser403Ter) |
| | c. 1184_1232dupAACCGAGTGATGAACTGATGGCTCTTCTGCAGGCTTGGCACCTTCAAAA, p.(Asn411Lysfs3Ter) |
| | c. 1185_1232dupACCGAGTGATGAACTGATGGCTCTTCTGCAGGCTTGGCACCTTCAAAA, p.(Ser410_Asn411insKPSDETDGSSAGLAPS) |
| Cl. 2 | c. 1207_1223delTCTTCTGCAGGCTTGGC, p.(Ser403Thrfs14Ter) |
| | c. 1188_1208delGAGTGATGAACTGATGGCTC, p.(Asp398_Ser404del) |

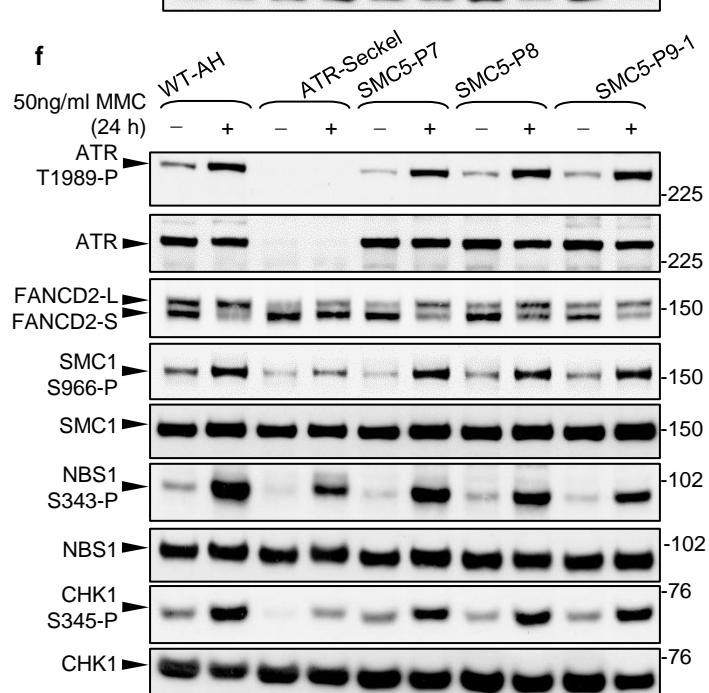
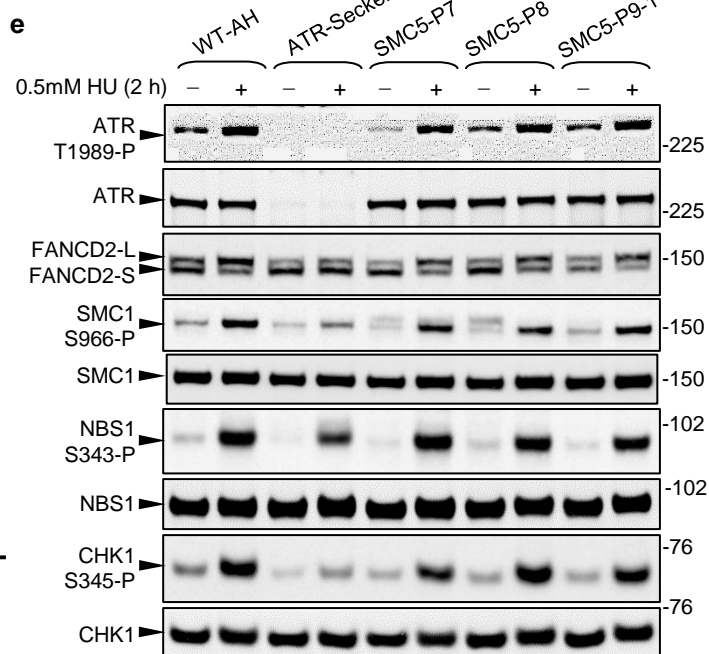
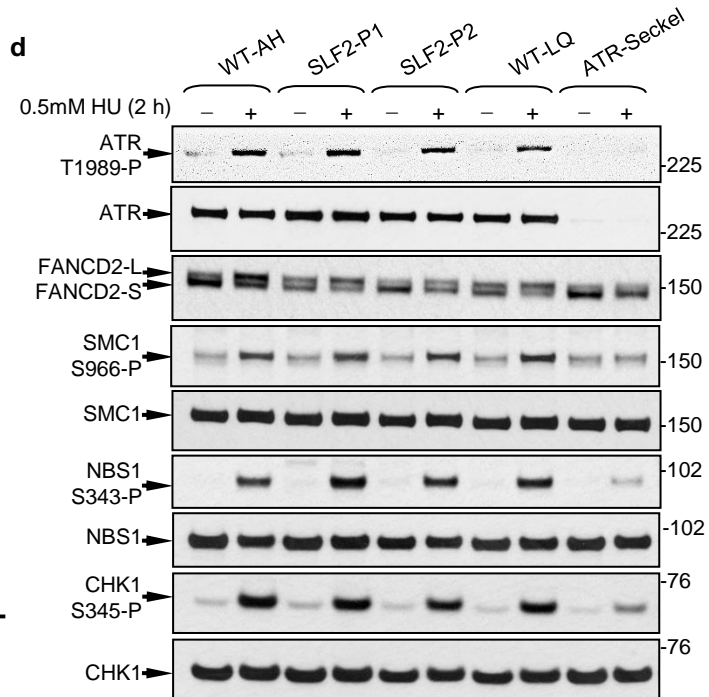
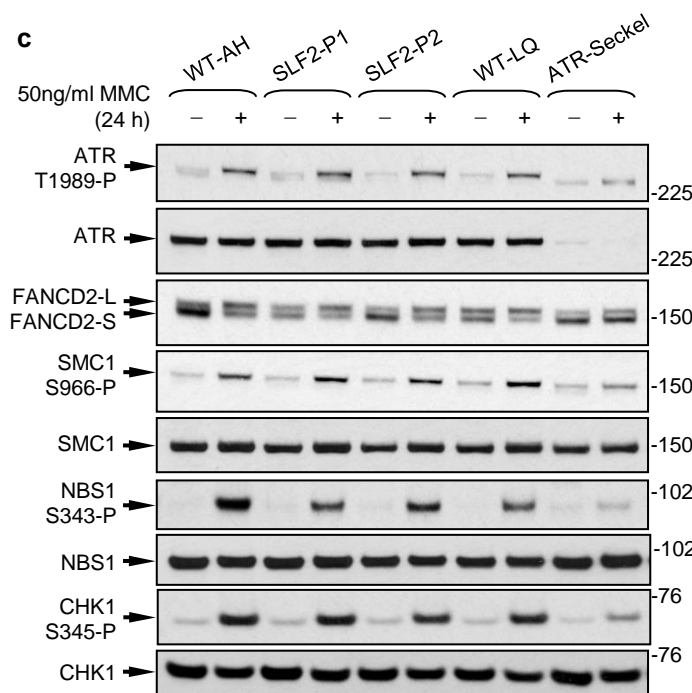
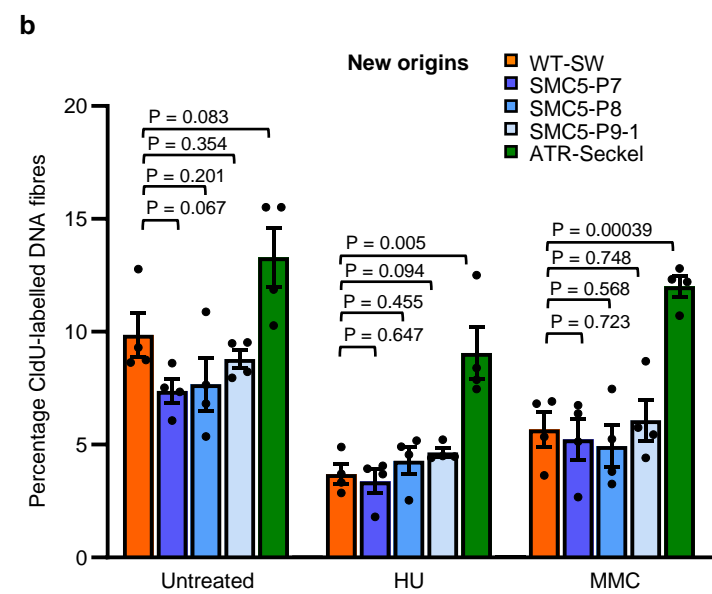
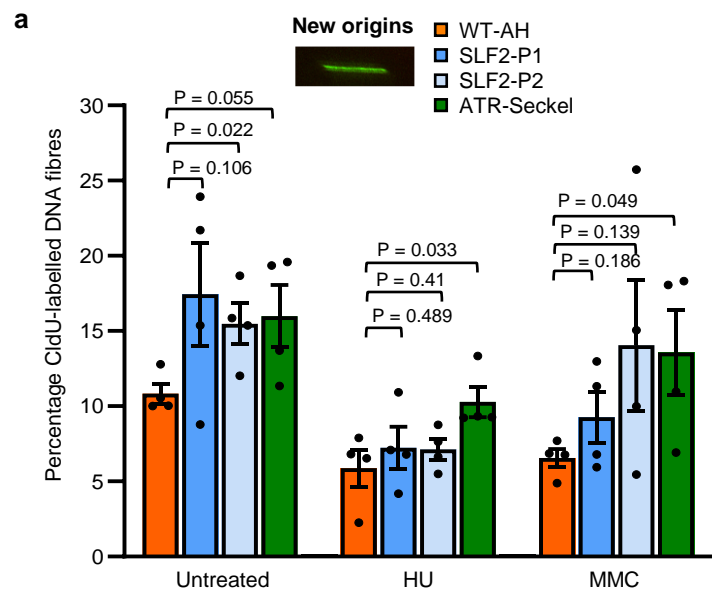
c



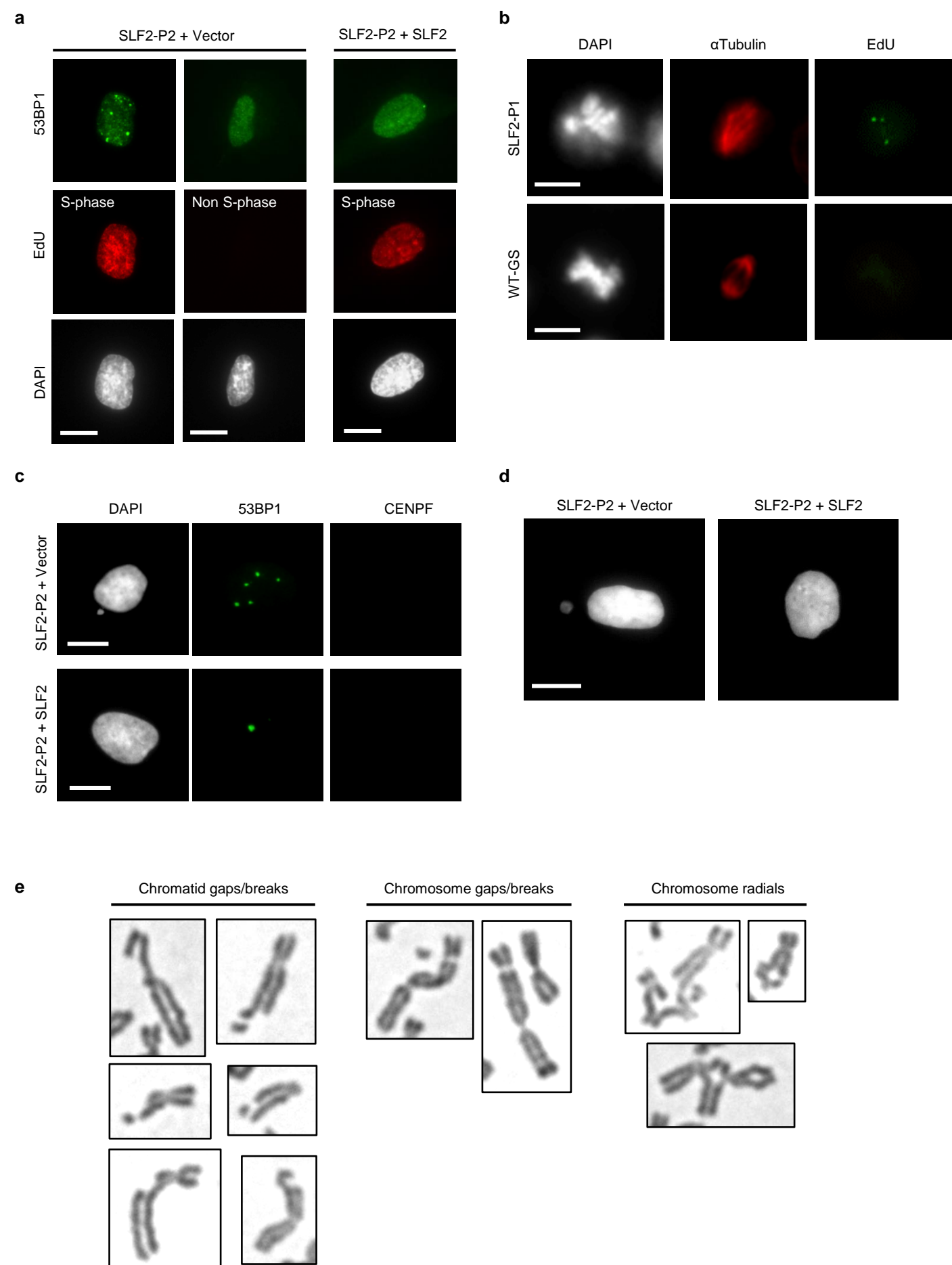
d



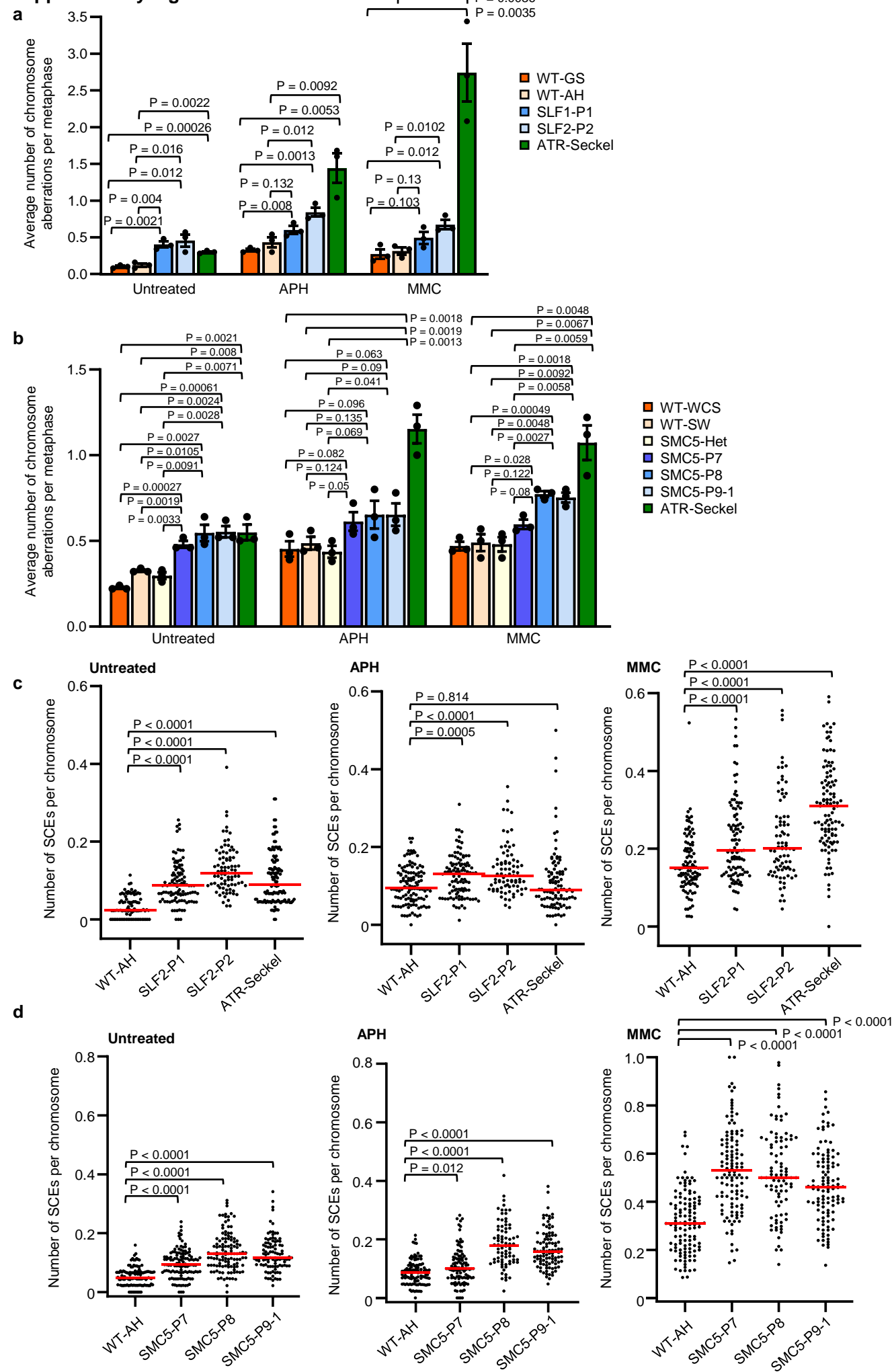
Supplementary Figure 13



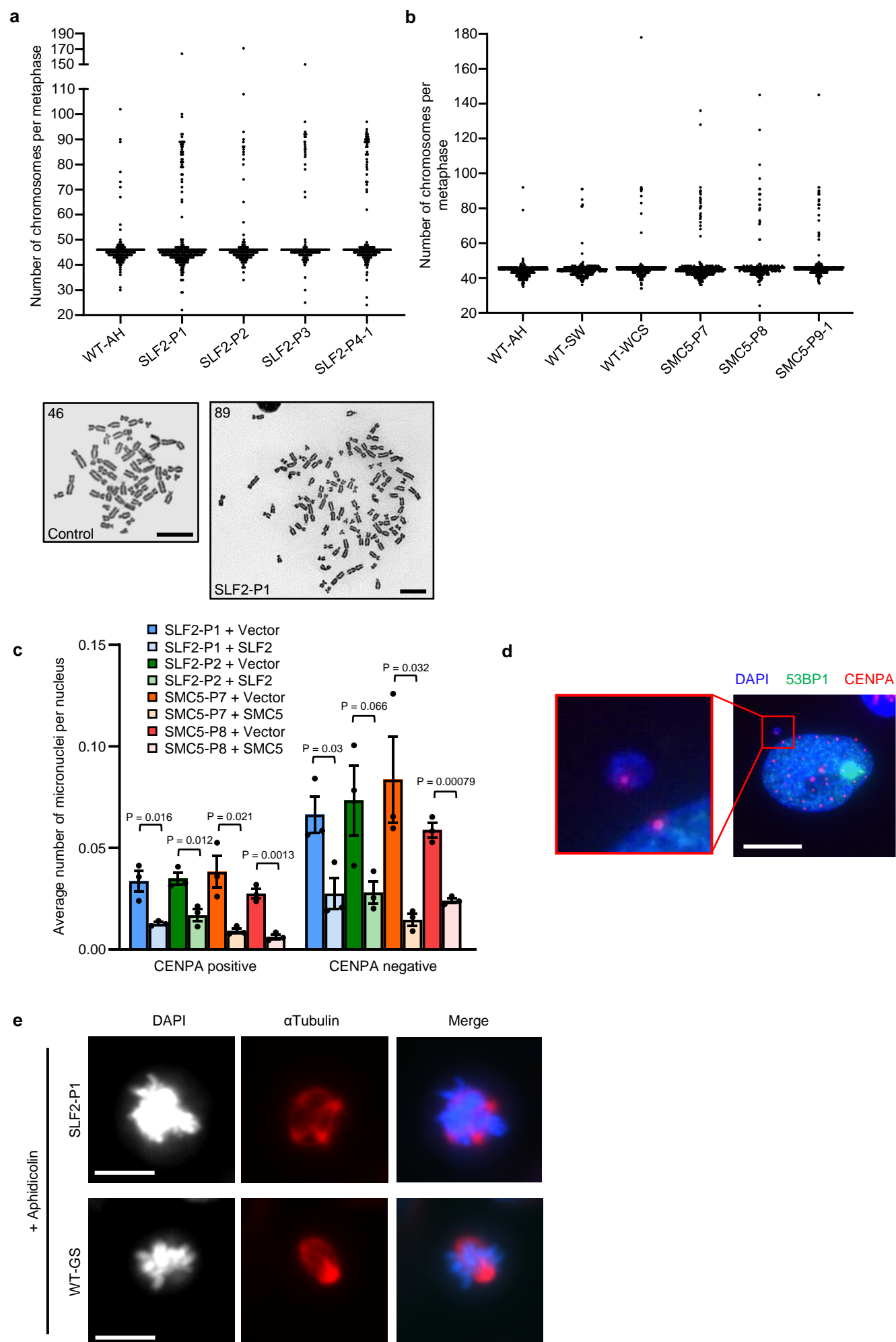
Supplementary Figure 14



Supplementary Figure 15



Supplementary Figure 16

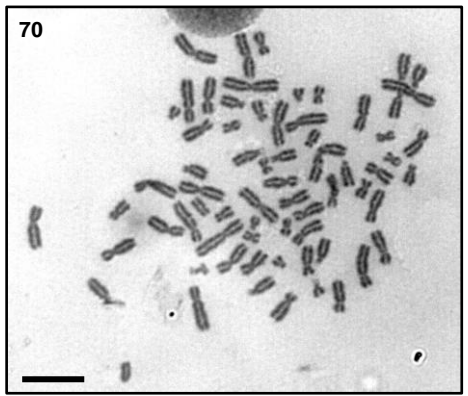
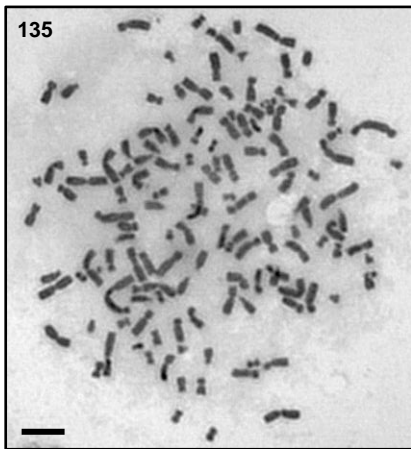
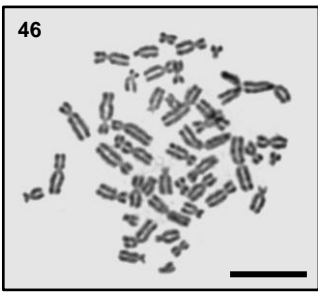
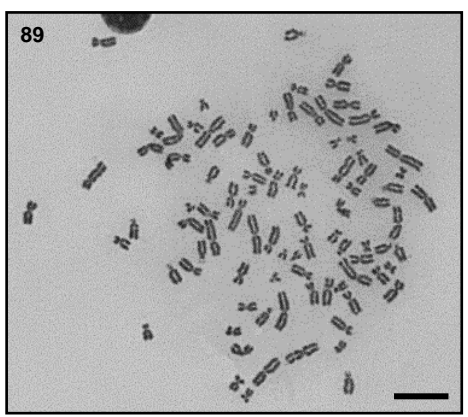
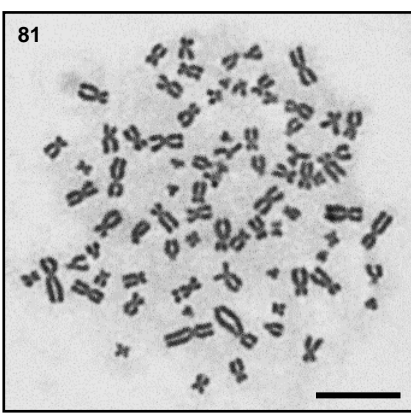
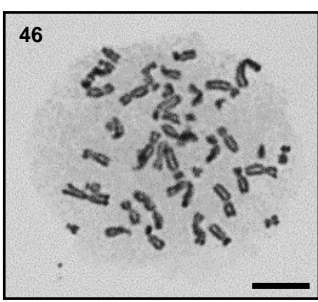


Supplementary Figure 17

a

Control

SLF2 patients

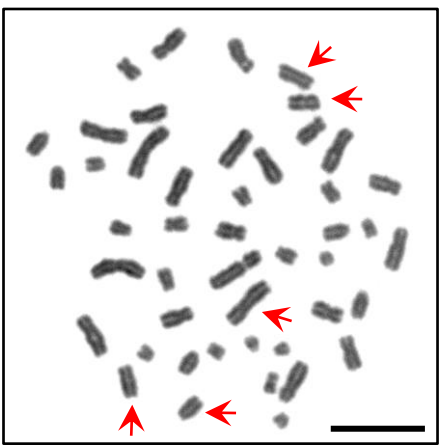
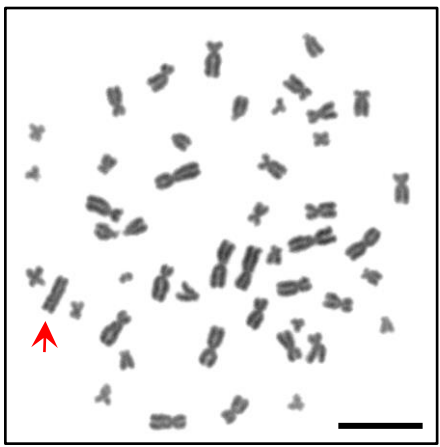
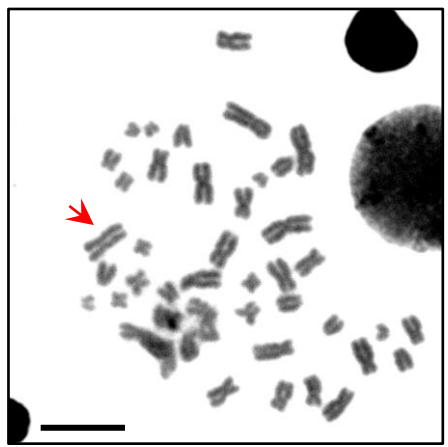


b

SLF2-P3

SLF2-P3

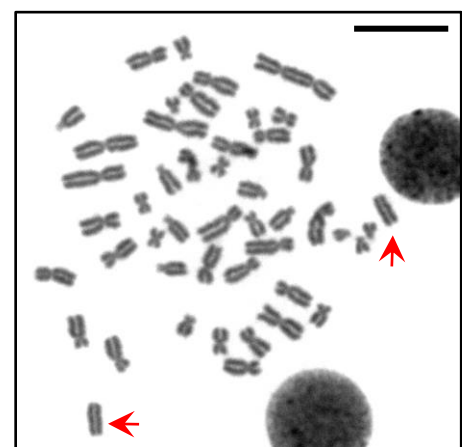
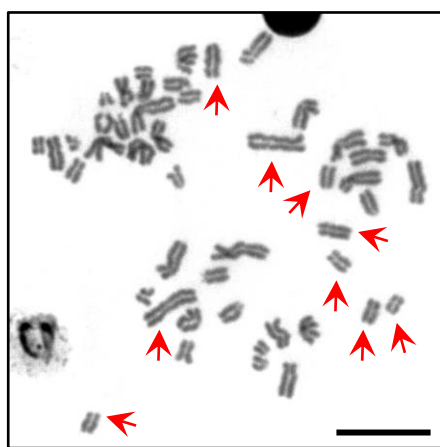
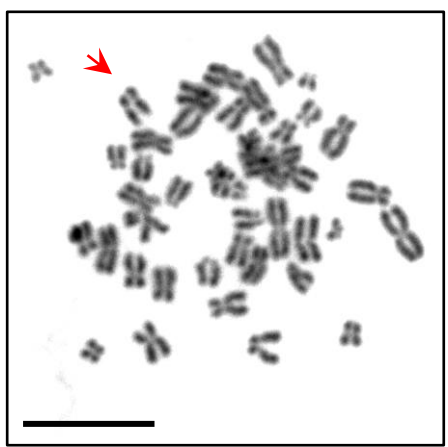
SLF2-P3



SLF2-P1

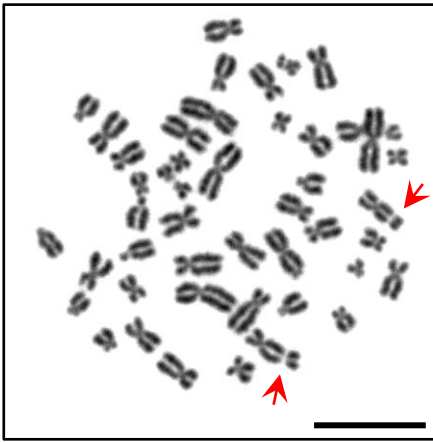
SMC5-P7

SMC5-P7

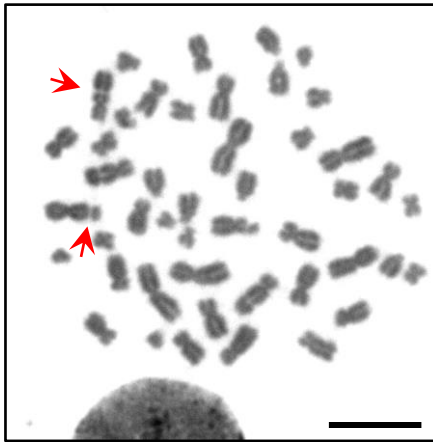


Supplementary Figure 18

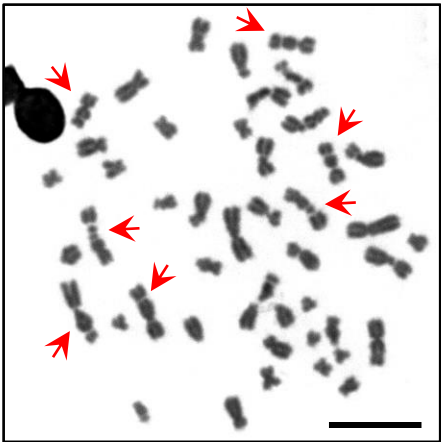
SMC5-P7



SLF2-P3



SLF2-P3



SLF2-P1



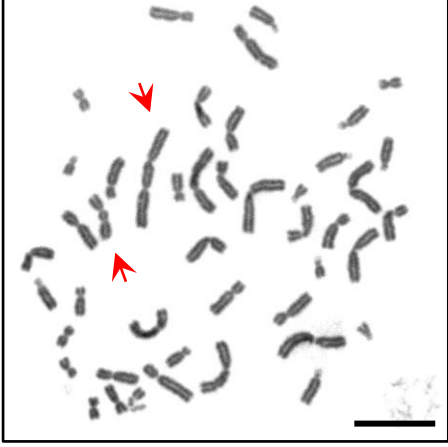
SLF2-P2



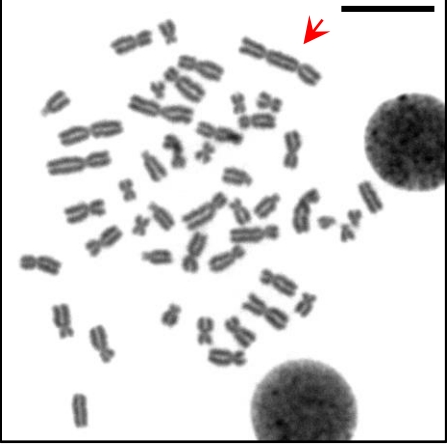
SLF2-P2



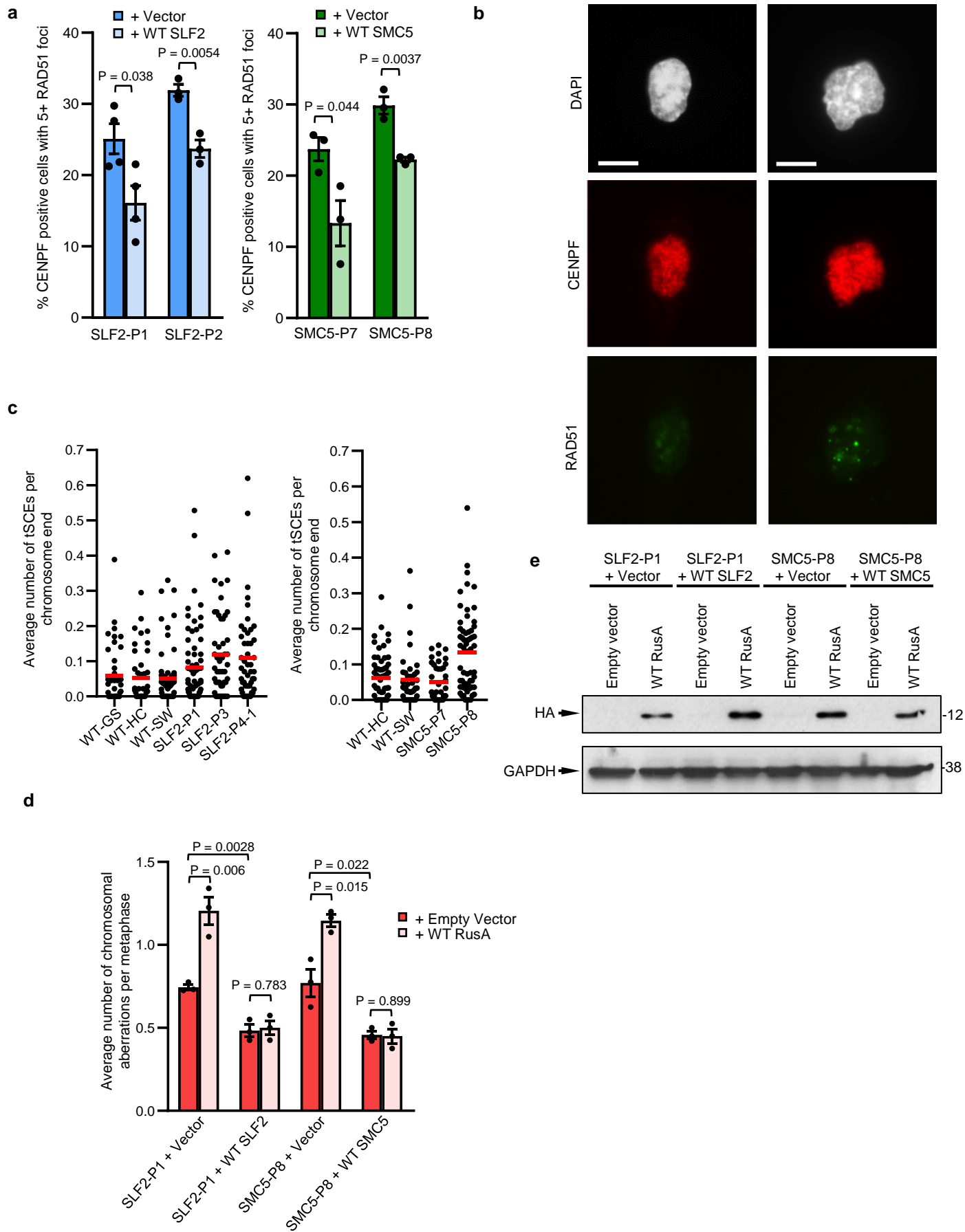
SMC5-P7



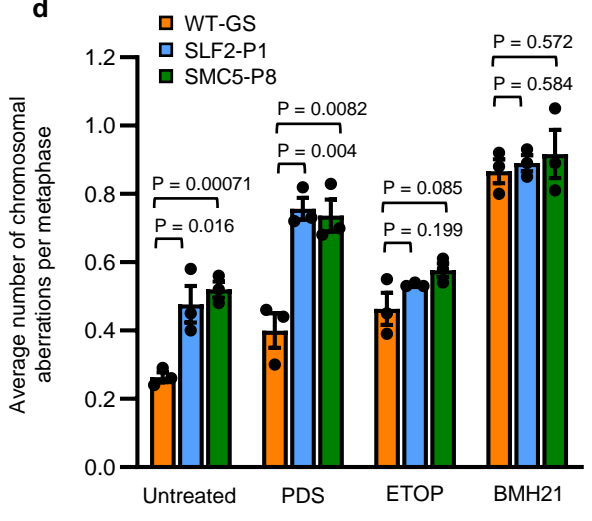
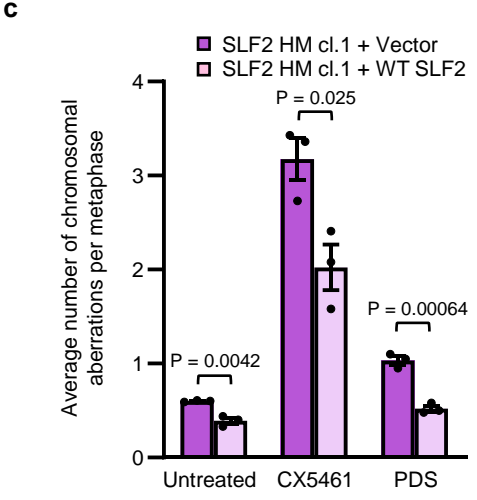
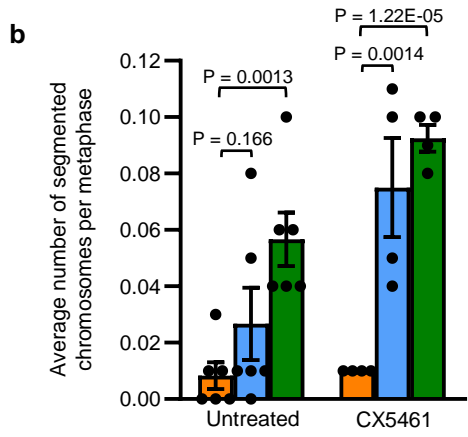
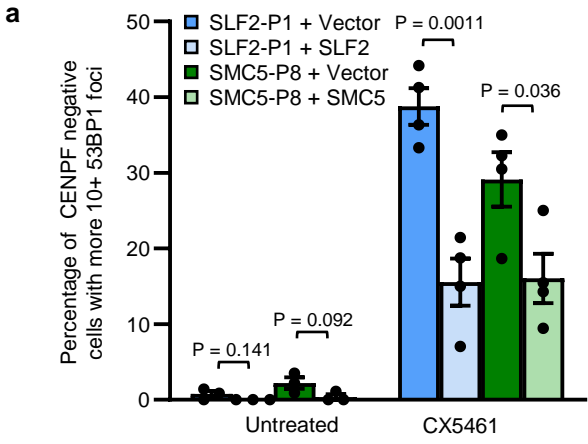
SMC5-P7



Supplementary Figure 19



Supplementary Figure 20



Supplementary Figure Legends

Supplementary Figure 1: Conservation of *SLF2* and *SMC5* amino acids mutated in patients

a Amino acid alignment of *SLF2* protein from different species showing the degree of evolutionary conservation of disease causing *SLF2* point variants, generated using Clustal Omega. Blue arrows indicate the missense variants present in *SLF2*-P2 (p.Gln1162His) and *SLF2*-P4-1 and *SLF2*-P4-2 (p.Asn861Ile). **b** Amino acid alignment of *SMC5* protein from different species, generated using Clustal Omega, showing the degree of evolutionary conservation of the disease causing *SMC5* point variants p.(Arg372del), present in *SMC5*-P7, and p.(His990Asp), present in *SMC5*-P8, *SMC5*-P9-1 and *SMC5*-P9-2. Blue arrows indicate location of the variants.

Supplementary Figure 2: Analysis of *SLF2* mRNA in *SLF2*-P2, *SLF2*-P3 and *SLF2*-P4-1

a PCR amplification of *SLF2* from cDNA derived from healthy normal WT individuals or *SLF2* patients *SLF2*-P4-1 and *SLF2*-P3. **b** Chromatograms showing the skipping of exon 17 in the p.(Arg1110Arg Δ exon17) variant from patient *SLF2*-P3. **c** A fragment of *SLF2* transcript (NM_018121.4) was amplified by RT-PCR from whole blood-derived mRNA from *SLF2* patient *SLF2*-P2, as well as an age and sex matched control sample.

Supplementary Figure 3: Analysis of *SLF2* mRNA in *SLF2*-P2

a Top: Schematic of the two longest annotated *SLF2* transcripts, NM_018121.4 and NM_001136123.2 containing 20 and 19 exons, respectively. Black arrows indicate position of primers used for amplification of *SLF2*. Variant c.3486G>C, (p.Gln1162His; red arrow) affects the last nucleotide of NM_018121 exon 19 (splice donor). Bottom: Enlarged view of the 3' terminal regions of the NM_018121 and NM_001136123 transcripts. Variant c.3486G>C, (p.Gln1162His) is indicated as a red arrow. Blue arrowhead shows stop codon used by either NM_018121 or NM_001136123 transcripts. Red dashed lines indicate identical sequences between NM_018121 and NM_001136123 transcripts. **b** Bioinformatic predictions indicate disrupted splicing at the exon 19 donor site (NM_018121) by the c.3486G>C, (p.Gln1162His) variant. MaxEntScan, NNSPLICE, Human Splicing Finder have been used with Alamut software to examine the probability of splicing through a donor (top, delineated by red box, labelled 5') or acceptor paradigm (bottom, labelled 3'). Range of possible values is indicated. Values obtained with each tool are indicated as black boxes. Variant c.3486G>C, p.(Gln1162His), is indicated

in red. **c** RT-PCR on pooled cDNA from healthy human tissues using isoform-specific primers. Arrows show the expected size for NM_001136123 (primers P1 and P3), NM_018121 (primers P1 and P2) and β -actin. **d** RT-PCR of NM_018121 using cDNA derived from eight different adult tissues indicates ubiquitous expression using primers P1 and P2 (Supplementary Table S14). **e** RT-PCR on patient or control cDNA obtained from whole blood extracts indicates an isoform-specific splice defect leading to disruption of NM_018121. Primers specifically amplify NM_018121 (P6 and P8, T1, PCR3), NM_001136123 (P6 and P7, T2, PCR2) or both NM_018121 and NM_001136123 (P4 and P5, T1+T2, PCR1). Black arrows indicate result for transcript NM_018121, absent in the affected individual although present in control sample. **F** Representative immunoblot analysis of cell extracts from U-2 OS cells transiently transfected with constructs expressing either WT SLF2 or the patient associated SLF2 variant p.(Gln1162His) tagged with GFP. SLF2 constructs were mixed with an equal amount of mCherry expressing vector as a transfection control. Experiments in panels c, d, e and f are representative of three independent experiments with similar results.

Supplementary Figure 4: Analysis of RAD18-SLF1/2-SMC5/6 complex interactions and recruitment to DNA damage

a & b Co-immunoprecipitation of SLF2 deletion mutant interacting proteins with SLF1 and RAD18. (left) Schematic of SLF2 deletion mutants. (right) U-2 OS cells transfected with SLF2 deletion constructs were subject to HA-streptavidin pulldown (DP) and immunoblotted with the indicated antibodies to determine binding of GFP-SLF1 and RAD18. **c** Co-immunoprecipitation of SLF2 minimal binding region (MBR) interacting proteins. (left) Schematic of SLF2 MBR constructs. (right) U-2 OS cells transfected with SLF2 MBR constructs were subject to HA-streptavidin pulldown and immunoblotted with the indicated antibodies. **d** Co-immunoprecipitation of SLF2 deletion mutant interacting proteins as in (a) with SMC6 and RAD18. **e** Representative images of U-2 OS cells transiently transfected with WT or mutant GFP-SLF2 constructs after laser micro-irradiation. **f** Representative images of U-2 OS cells transiently transfected with WT or mutant GFP-SMC5 constructs after laser micro-irradiation. Note that nuclear GFP signal is lost from p.(Arg425Ter) with pre-extraction. Cells in (e & f) were recovered for 1 hour post irradiation and CSK pre-extracted prior to fixation, staining and imaging (scale bar = 20 μ M). Experiments in panels a, b, c, d, e and f are representative of three independent experiments with similar results.

Supplementary Figure 5: Structural modelling of the SMC5 p.(Del372Arg) mutation.

(Left) Secondary structure model showing selected amino acid side chains from the X-ray crystal structure of a short section of *Saccharomyces cerevisiae* Smc5 (PDB: 3HTK) in complex with Nse2 (grey surface). An AlphaFold model for the relevant section of the Smc5 arm has been structurally superposed (AF-Q08204-F1) to extend the two helices towards the hinge (as this region is absent from the crystal structure). (Right) Secondary structure model showing the equivalent region from an AlphaFold model of human SMC5 (AF-Q81Y18-F1). Arg372 is located within a small, charged motif (369-RQRR-372) that sits near to a region of predicted disorder in the opposing helix; a similar motif can be found in budding yeast (365-RTKK-368). A hydrophobic residue (Ile744 and Leu728, in budding yeast and humans, respectively) serves to anchor the restarted (descending) helix. The directionality of each helix from the Smc5 arm (N- to C-terminus) is indicated by an arrow, heading either towards (ascending) or away (descending) from the hinge. Of note, the C-terminal tail of Nse2 emerges in close proximity to the predicted break in the descending helix.

Supplementary Figure 6: Structural modelling of the SMC5 p.(His990Asp) mutation.

a (top) Secondary structure models showing selected amino acid side chains from *Pyrococcus furiosus* RAD50 (*Pf.Rad50*) in un-liganded (left) and ATP-bound forms (right); PDB accession codes 1F2T and 1FTU respectively. The ATP-binding cassette (ABC) signature motif, containing Ser793, is additionally highlighted with carbon atoms coloured in yellow. The side chains of Phe791, Arg787 and Trp782 are repositioned as a result of ATP-binding and interaction with a second Rad50 monomer (not shown). **a** (bottom) Comparative view for the same region of human SMC5 (AlphaFold model, AF-Q81Y18-F1; UniProt entry SMC_HUMAN). Side chains for amino acids in equivalent positions to those shown in the top panel are shown in stick representation. His990 of human SMC5 is structurally equivalent to Phe791 of *Pf.Rad50* (carbon atoms coloured green and orange respectively) but is also within hydrogen-bonding distance of the side chain of Thr987 (black dotted line). Mutation of His990 to Asp (p.His990Asp) is likely to be tolerated, without any gross effects on protein folding as no major steric clashes are predicted by the change in amino acid identity [Mutagenesis Wizard, PyMOL]. However, its introduction would affect the overall charge and electronics of the region accepting the adenine moiety of bound ATP. In addition the p.(His990Asp) mutation would affect stacking/packing interactions with the side chains of both

His984 and Phe977 (by analogy to *Pf.Rad50*). **b** Summary of prediction outcomes from the DynaMut webserver: <http://biosig.unimelb.edu.au/dynamut>. The SMC5 p.(His990Asp) patient mutation is predicted to generate only small increases or decreases in $\Delta\Delta G$ and thus no gross effect on the overall protein fold. A moderate decrease in molecule flexibility is predicted, but this is limited to just the loop containing the affected amino acid (see inset molecular model, region coloured in dark blue).

Supplementary Figure 7: Efficiency of reagents used to target *slf2* and *smc5* in zebrafish larvae.

a Schematic of the *Danio rerio slf2* genomic locus (GRCz11). Filled rectangles denote coding exons; black lines indicate introns. Target position of single guide RNAs (sgRNA) and morpholinos (MO) used are indicated with vertical arrows. **b** Polyacrylamide gel image showing heteroduplex analysis of PCR products amplified from genomic DNA harvested at 2 dpf from control embryos and embryos injected with *slf2* sgRNAs plus Cas9 protein. Embryos revealed high mosaicism of frameshifting insertions and deletions at each respective target site (*slf2* sgRNA1: 82%; *slf2* sgRNA2: 70%). Asterisks indicate homoduplexes of WT PCR product. **c** Representative sequences generated from PCR products cloned into TOPO-TA vectors. Plasmids were purified from individual colonies and subjected to direct sequencing, revealing insertions and deletions in *slf2* F0 mutant larvae. Protospacer adjacent motif (PAM) is shown with red dashed box. **d** Representative sequences confirming an 8 bp deletion in *slf2*^{-/-} mutants. **e** qRT-PCR depicts 50% reduction in *slf2* mRNA level normalized to *β-actin*. F1-5' and F2-3' indicate two different primer sets complementary to the 5' and 3' regions of the *slf2* mRNA, respectively. n=2 independent experiments. **f** Schematic of the *Danio rerio smc5* genomic locus (GRCz11). Filled rectangles denote coding exons; black lines denote introns. Target position of single guide (sg) RNAs and MO used are indicated with vertical arrows. **g** Polyacrylamide gel image showing heteroduplex analysis of PCR products amplified from genomic DNA harvested at 2 dpf from control embryos and embryos injected with *smc5* sgRNA plus Cas9 protein. High mosaicism of frameshifting insertions and deletions at each respective target site is visible (*smc5* sgRNA1: 92%; *smc5* sgRNA2: 80%). Asterisks indicate homoduplexes of WT PCR product. **h** Representative sequences generated from PCR products (panel g) cloned into TOPO-TA vectors. Plasmids were purified from individual colonies and subjected to direct sequencing, revealing insertions and deletions in *smc5* F0 mutant larvae. Protospacer adjacent motif (PAM) is shown with red dashed box. Polyacrylamide gels in panels b and g were generated for screening purposes and so are representative of one experimental repeat.

Supplementary Figure 8: Loss of *slf2* and *smc5* in zebrafish give rise to microcephaly and aberrant craniofacial patterning

a Agarose gel images show exon exclusion of *slf2* exon 11 in morphants (MO) resulting in a 103 bp deletion (Δ) as determined by RT-PCR and sequencing. **b** Agarose gel images show semi-quantitative reduction of WT message in *smc5* MO as determined by RT-PCR. Agarose gels in **b** and **c** are representative of one experimental repeat. **c** RT-PCR product sequence confirmation of exon 11 skipping in MO as determined by cloning and sequencing of the lower *slf2* band in the morphant lane of (**a**). **d** RT-PCR sequence confirmation of exon 3 skipping in MO as determined by cloning and sequencing the *smc5* band in the morphant lane of (**b**). **e-h** Quantification of lateral head size (**e** & **g**) (left to right; 47, 42, 39, 37 embryos/condition were analysed from 3 independent experiments for panel **e**, and 27, 33, 20, 13 embryos/condition were analysed from 3 independent experiments for panel **g**), and ceratohyal angle measurements (**f** & **h**) (left to right; 19, 16, 24, 13 embryos/condition were analysed from 3 independent experiments for panel **f**, and 17, 16, 16, 24 embryos/condition were analysed from 3 independent experiments for panel **h**), of larvae injected with different doses (3 ng, 6 ng and 9 ng) of MO, or MO with co-injection of human WT *SLF2* or *SMC5* mRNA. Error bars represent standard deviation of the mean. Statistical differences were determined with an unpaired Student's t-test (two sided).

Supplementary Figure 9: Loss of *slf2* and *smc5* in zebrafish give rise to microcephaly and aberrant craniofacial patterning.

a Representative bright field lateral (top) and ventral images of the GFP signal in the anterior region of *-1.4col1a1:egfp* transgenic reporter larvae (bottom) showing controls, *slf2* morphants (MO) and *slf2* MO rescued with human WT *SLF2* mRNA, respectively. **b** & **c** Quantification of lateral head size (**b**) (left to right; 38, 34, 34 embryos/condition from 3 independent experiments) or ceratohyal angle measurements (**c**) (left to right; 27, 13, 22 embryos/condition from 3 independent experiments). **d** Representative bright field lateral (top) and ventral images of the GFP signal in the anterior region of *-1.4col1a1:egfp* transgenic reporter larvae (bottom) showing controls, *smc5* MO and *smc5* MO rescued with human WT *SMC5* mRNA, respectively. **e** & **f** Quantification of lateral head size (**e**) (left to right; 46, 45, 45 embryos/condition from 3 independent experiments) or ceratohyal angle measurements (**f**) (left

to right; 18, 24, 22 embryos/condition from 3 independent experiments). **g** Left, representative lateral bright field images; and right, representative ventral GFP signal showing in the mandible of *1.4col1a1:egfp* transgenic reporter larvae at 3 dpf. Images show head size (left) and craniofacial patterning (right) in controls, in *smc5* MO, MO rescued with human SMC5 WT mRNA, and MO complemented with p.(His990Asp) patient variant. Left, white dashed shape depicts head size measured; right, white dashed lines show the ceratohyal angle. Abbreviations: MK, Meckel's cartilage; CH, ceratohyal cartilage (indicated with arrowheads, respectively); CB, ceratobranchial arches (asterisks); MO, morpholino. Scale bar, 300 μ m, with equivalent sizing across panels. **h & i** Quantification of lateral head size (**h**) (left to right; 54, 36, 39, 33, 39, 40, 34 embryos/condition from 3 independent experiments) and ceratohyal angle measurements (**i**) (left to right; 34, 42, 49, 32, 33, 37, 21 embryos/condition from 3 independent experiments) of larvae injected with MO alone, co-injection of MO with human WT or variant encoding mRNA; p.(Arg733Gln) is a negative control (rs59648118; 16 homozygotes in gnomAD). For all panels: Statistical differences were determined with an unpaired Student's t-test (two sided). Error bars represent standard deviation of the mean. Scale bars, 300 μ m with equivalent sizing across panels.

Supplementary Figure 10: *slf2* and *smc5* depletion induces apoptosis and altered cell cycle progression in zebrafish larvae.

a Representative dorsal inverted fluorescent images indicating TUNEL positive cells in *slf2* MO at 2 dpf. The blue dashed box indicates the region of interest (ROI). **b** Quantification of TUNEL positive cells in controls and larvae injected with *slf2* MO with or without WT mRNA (left to right; 35, 29, 28 embryos/condition from 3 independent experiments). ROI used is shown in panel (a). **c** Representative dorsal inverted fluorescent images indicating pHH3 positive cells in *slf2* MO at 2 dpf. **d** Quantification of pHH3 positive cells in larvae injected with *slf2* MO with or without WT mRNA (left to right; 24, 25, 25 embryos/condition from 3 independent experiments). ROI used was the same as that shown in panel (c). **e** Representative dorsal inverted fluorescent images show TUNEL positive cells in *smc5* MO at 3 dpf. **f** Quantification of TUNEL positive cells in controls and larvae injected with *smc5* MO with or without WT mRNA (left to right; 32, 31, 29 embryos/condition from 3 independent experiments). **g** Representative dorsal inverted fluorescent images indicating pHH3 positive cells in *smc5* MO at 2 dpf. **h** Quantification of pHH3 positive cells in controls and larvae injected with *smc5* MO and WT mRNA

(left to right; 24, 23, 24 embryos/condition from 3 independent experiments). In all cases, embryos of the same developmental stage and similar magnification were assessed for all *slf2* or *smc5* conditions. Fluorescent staining in the ROI was quantified using the ImageJ (NIH) ICTN plugin. Error bars represent standard deviation of the mean. Scale bar in panels a, c, e, g: 30 μm with equivalent sizing across panels. In all cases, statistical differences were determined with an unpaired Student's t-test (two sided).

Supplementary Figure 11: Replication fork analysis of SLF2 and SMC5 patient-derived cell lines

a Representative immunoblot analysis of myc-SLF2 expression in SLF2 patient fibroblasts infected with lentiviruses encoding myc-tagged WT SLF2 or an empty vector. A nonspecific cross-reactive protein was used as a loading control. **b** Representative immunoblot analysis of SMC5 expression in SMC5 fibroblasts infected with lentiviruses encoding WT SMC5 or an empty vector. A nonspecific cross-reactive protein was used as a loading control. Immunoblotting analysis in panels a and b are representative of two independent experiments with similar results. **c & d** Replication fork velocity of ongoing forks in WT cells, SLF2 patient LCLs (A) or SMC5 patient LCLs (B). $n=3$ independent experiments. A minimum of 430 fork structures were counted. Red lines denote median values. A Mann-Whitney rank sum test was performed for statistical analysis. **e & f** DNA fibre analysis in untreated cells and cells exposed to replication stress in SLF2 patient-derived LCLs (e) or SMC5 patient-derived LCLs (f) was carried out. In untreated cells, the indicated cell lines were pulse-labelled with CldU for 20 min, and then pulse-labelled with IdU, for 20 min. For DNA fibres following MMC treatment, cells were incubated with 50 ng/ml MMC for 24 h prior to pulse-labelling with CldU and IdU. For DNA fibres following hydroxyurea (HU) treatment, cells were pulsed with CldU for 20 min, exposed to 2 mM HU for 2 h and then pulsed with IdU for 20 min. The percentage of stalled forks was quantified. $n=4$ independent experiments. A minimum of 650 fork structures were counted. A Student's t-test (two-sided, equal variance) was performed for statistical analysis. Error bars denote SEM.

Supplementary Figure 12: Generation of U-2 OS SLF2 CRISPR hypomorphic cell lines

a Schematic of the human *SLF2* genomic locus. Filled rectangles indicate coding exons; black lines denote introns. Positions of single guide RNAs (sgRNA) are highlighted by red text and the location of the protospacer adjacent motif (PAM) is indicated by blue text. **b** Table detailing SLF2 variants present

in U-2 OS SLF2 CRISPR HM clones cl.1 and cl.2. **c** Representative immunoblot analysis of SLF2 expression in U-2 OS SLF2 CRISPR HM cell lines infected with lentiviruses encoding myc-tagged WT SLF2 or an empty vector. GAPDH was used as a loading control. **d** Representative immunoblot analysis of myc-SLF2 expression in U-2 OS SLF2 CRISPR HM cell lines infected with lentiviruses encoding myc-tagged WT SLF2 or an empty vector. Endogenous c-Myc was used as a loading control. Immunoblotting analysis in panels c and d are representative of two independent experiments with similar results.

Supplementary Figure 13: Analysis of the ATR-CHK1 dependent replication stress response in SLF2 and SMC5 patient-derived LCLs

a & b DNA fibre analysis of SLF2 (a) and SMC5 (b) patient-derived LCLs was carried out as in (Supplementary Figure 11 e & f) and the percentage of new origins (IdU only) were quantified. A representative image is included. n=4 independent experiments. A minimum of 650 fork structures were counted. A Student's t-test (two-sided, equal variance) was performed for statistical analysis. Error bars denote SEM. **c-f** Representative immunoblot analysis for the indicated proteins in whole-cell extracts from SLF2 (c & e) or SMC5 (d & f) patient-derived LCLs subjected to treatment with 0.5 mM HU for 2 h (c & d) or 50 ng/ml MMC for 24 h (e & f). In all cases, immunoblotting analysis are representative of two independent experiments with similar results.

Supplementary Figure 14: Representative microscopy images of SLF2/SMC5 mutant cell lines exhibiting elevated levels of S-phase associated DNA damage

a Representative immunofluorescence microscopy images of EdU positive S-phase cells with 53BP1 foci quantified in Figure 6a. **b** Representative immunofluorescence microscopy images of mitotic cells with MiDAS quantified in Figure 6b. **c** Representative immunofluorescence microscopy images of 53BP1 bodies in CENPF negative G1 cells quantified in Figure 6c. **d** Representative immunofluorescence microscopy images of cells with micronuclei quantified in Figure 6d. **e** Representative brightfield microscopy images of different types of chromosomal aberrations quantified in Figure 6f-l, Figure 8e, Supplementary Figure S15a-b, Supplementary Figure 19c, Supplementary Figure S20c-d. In all cases, scale bars = 10 μ M.

Supplementary Figure 15: Genome instability in SLF2/SMC5 mutant cell lines is not exacerbated by exogenous replication stress

a & b Quantification of the average number of chromosomal aberrations (which includes chromatid/chromosome gaps, breaks, fragments and radials) in metaphase spreads from SLF2 (a) and SMC5 (b) patient derived LCLs before treatment or following exposure to 500 nM APH or 50 ng/ml MMC for 24 h. n=3 independent experiments. A minimum of 140 metaphases were counted. A Student's t-test (two-sided, equal variance) was performed for statistical analysis. Error bars denote SEM. **c & d** Quantification of the average numbers of sister chromatid exchanges in metaphase spreads from SLF2 (c) and SMC5 (d) patient derived LCLs treated as in (a & b). n=3 independent experiments. A minimum of 100 metaphases were counted. Red lines denote median values. A Mann-Whitney rank sum test was performed for statistical analysis.

Supplementary Figure 16: Levels of mosaic variegated hyperploidy in SLF2/SMC5 mutant LCLs

a Quantification of the number of chromosomes per metaphase in SLF2 patient-derived LCLs. n=3 independent experiments. A total of 300 metaphases were counted. **b** Quantification of the number of chromosomes per metaphase in SMC5 patient-derived LCLs. n=3 independent experiments. A total of 300 metaphases were counted. **c** Quantification of the average number of CENPA positive and CENPA negative micronuclei in SLF2 and SMC5 mutant fibroblast cell lines infected with lentiviruses encoding WT SLF2, WT SMC5, or an empty vector. n=3 independent experiments. A minimum of 185 micronuclei were counted. Student's t-test (two-sided, equal variance) was performed for statistical analysis. Error bars denote SEM. **d** Representative images of CENPA positive micronuclei. **e** Representative immunofluorescence microscopy images of mitotic cells from SLF2-P1 LCLs with multi-polar spindles quantified in Figure 7h. In all cases, scale bars = 10 μ M.

Supplementary Figure 17: Representative microscopy images of SLF2 and SMC5 patient LCLs exhibiting mosaic variegated hyperploidy and sister chromatid cohesion defects

a Representative bright field microscopy images of metaphases exhibiting mosaic variegated hyperploidy derived from peripheral blood of SLF2 and SMC5 mutant patients. **b** Representative bright field microscopy images of metaphases displaying railroad chromosomes derived from peripheral blood of SLF2 and SMC5 mutant patients. In all cases, scale bars = 10 μ M.

Supplementary Figure 18: SLF2 and SMC5 patient cells exhibit a unique chromosomal breakage phenotype.

Representative bright field microscopy images of metaphases displaying segmented chromosomes derived from peripheral blood of SLF2 and SMC5 mutant patients. In all cases, scale bars = 10 μ M.

Supplementary Figure 19: SLF2 and SMC5 patient cells exhibit increased levels of recombination intermediates

a Quantification of the percentage of S/G2 (CENPF positive) cells with >5 RAD51 foci in SLF2 and SMC5 mutant fibroblast cell lines complemented with either WT SLF2, WT SMC5, or an empty vector. A minimum of 850 CENPF positive cells in total were counted over 3 independent experiments for SLF2-P2, SMC5-P7 and SMC5-P8, and 4 independent experiments for SLF2-P1. Error bars denote standard error of the mean. For statistical analysis, a Student's t-test (two-sided, equal variance) was performed. **b** Representative immunofluorescence microscopy images of cells from panel a. Scale bars = 10 μ M. **c** The average number of telomeric SCEs (tSCEs) per chromosome end was quantified in WT, SLF2 and SMC5 patient-derived LCLs. The red line denotes the mean. n = 2 independent experiments. **d** Quantification of the level of chromosomal aberrations per metaphase (chromatid/chromosome gaps, breaks, fragments and chromosome radials) in complemented SLF2 and SMC5 mutant fibroblast cell lines infected with either an empty lentiviral expression vector, or a vector expressing WT RUSA. n=3 independent experiments. A minimum of 120 metaphases were counted. Error bars denote standard error of the mean. Student's t-test (two-sided, equal variance) was performed for statistical analysis. **e** Representative immunoblot analysis of HA-tagged RUSA expression in SLF2 and SMC5 mutant patient fibroblasts infected with lentiviruses encoding myc-tagged WT SLF2/SMC5 or an empty vector. GAPDH was used as a loading control.

Supplementary Figure 20: SLF2 and SMC5 mutant cells exhibit increased genome instability in the presence of G-quadruplex stabilising agents

a Quantification of the percentage of G1-phase (CENPF negative) cells with >10 53BP1 bodies in SLF2 and SMC5 mutant fibroblast cell lines expressing WT SLF2, WT SMC5, or an empty vector, with or without exposure to 250 nM CX5451 for 24 h. n=4 independent experiments. A minimum of 390 G1-

phase cells were counted. **b** Quantification of the average number of segmented chromosomes per metaphase in SLF2 and SMC5 patient-derived LCLs before or after exposure to 250 nM CX5461 for 24 h. n=6 independent experiments for untreated cells and n = 4 for CX5461 treated cells. A minimum of 350 metaphases were counted. **c** Quantification of the level of chromosomal aberrations (chromatid/chromosome gaps, breaks, fragments and chromosome radials) per metaphase in U-2 OS SLF2 CRISPR HM cell lines complemented with either WT SLF2 or an empty vector before or after exposure to 250 nM CX5461 or 1 μ M pyridostatin (PDS) for 24 h. n=3 independent experiments. A minimum of 100 metaphases were counted. **d** Quantification of the average number of chromosomal aberrations (chromatid/chromosome gaps, breaks, fragments and radials) in metaphase spreads from SLF2 and SMC5 patient derived LCLs either left untreated or exposed to 1 μ M PDS, 50 nM etoposide (ETOP) or 1 μ M BMH21 for 24 h. n=3 independent experiments. A minimum of 100 metaphases were counted. In all cases, a Student's t-test (two-sided, equal variance) was performed for statistical analysis. Error bars denote SEM.

Supplementary Tables:

Table S11. Primers used for SLF2/SMC5 in vivo modelling studies.

| Purpose | oligo name | Sequence |
|-------------------------------------------|---------------------------------|------------------------------------------|
| <i>slf2</i> sgRNA1 CRISPR/Cas9 | <i>slf2</i> sgRNA 1 | 5'-CAATATAGAAGAGCTGGAGG-3' |
| <i>slf2</i> sgRNA1 CRISPR/Cas9 efficiency | <i>slf2</i> sgRNA1 PCR primer F | 5'-AAATACCCATTTTTGCCAACAG-3' |
| <i>slf2</i> sgRNA1 CRISPR/Cas9 efficiency | <i>slf2</i> sgRNA1 PCR primer R | 5'-AGGATGACAGTTTTGGCTTGTT-3' |
| <i>slf2</i> sgRNA2 CRISPR/Cas9 | <i>slf2</i> sgRNA 2 | 5'-TCTTATTCCAGCAGAGACCG-3' |
| <i>slf2</i> sgRNA2 CRISPR/Cas9 efficiency | <i>slf2</i> sgRNA2 PCR primer F | 5'-TTCCTCACTCATCTCACAGACG-3' |
| <i>slf2</i> sgRNA2 CRISPR/Cas9 efficiency | <i>slf2</i> sgRNA2 PCR primer R | 5'-CCTGGACTAGTCATCGTGTTC-3' |
| <i>slf2</i> MO-induced suppression | <i>slf2</i> e11i11 sb MO | 5'-ATGAGAAAAGTGGCTGGTATTACCT-3' |
| <i>slf2</i> e11i11 sb MO efficiency | <i>slf2</i> e11i11 PCR primer F | 5'-ACAGTCAAAGTAAAGGGGAGGAC-3' |
| <i>slf2</i> e11i11 sb MO efficiency | <i>slf2</i> e11i11 PCR primer R | 5'-AAAAGACTGATGAACGATGCCC-3' |
| <i>smc5</i> sgRNA1 CRISPR/Cas9 | <i>smc5</i> sgRNA 1 | 5'-GTTGCAGGTTACGATCGGA-3' |
| <i>smc5</i> sgRNA1 CRISPR/Cas9 efficiency | <i>smc5</i> sgRNA1 PCR primer F | 5'-TGTGCTGAACATCAACCAGAG-3' |
| <i>smc5</i> sgRNA1 CRISPR/Cas9 efficiency | <i>smc5</i> sgRNA1 PCR primer R | 5'-AAACAAACGACGCTTGCATA-3' |
| <i>smc5</i> sgRNA2 CRISPR/Cas9 | <i>smc5</i> sgRNA 2 | 5'-AAAACATCTGTCCTGGGCCG-3' |
| <i>smc5</i> sgRNA2 CRISPR/Cas9 efficiency | <i>smc5</i> sgRNA2 PCR primer F | 5'-CAGCACGTACGATCACTCTGA-3' |
| <i>smc5</i> sgRNA2 CRISPR/Cas9 efficiency | <i>smc5</i> sgRNA2 PCR primer R | 5'-GCCAGACACAGTGGATGTGA-3' |
| <i>smc5</i> MO-induced suppression | <i>smc5</i> e3i3 sb MO | 5'-TGTA AAAACACATACTTACAGCTCT-3' |
| <i>smc5</i> e3i3 sb MO efficiency | <i>smc5</i> e3i3 PCR primer F | 5'-CCGGACCCAAACTGAACAT-3' |
| <i>smc5</i> e3i3 sb MO efficiency | <i>smc5</i> e3i3 PCR primer R | 5'-TCCTCCACTGCCTTCTGACT-3' |
| SMC5 mutagenesis | SMC5-p.R733Q-F | TGAAGAGGAAGAGCAAAAAGCAAGTACCA |
| SMC5 mutagenesis | SMC5-p.R733Q-R | 5'-TGGTACTTGCTTTTTGCTCTTCTCTTCA-3' |
| SMC5 mutagenesis | SMC5-p.H990D-F | 5'-GAATTA ACTCCTCATGATCAAAGTGGAGGTGAA-3' |
| SMC5 mutagenesis | SMC5-p.H990D-R | 5'-TTCACCTCCACTTTGATCATGAGGAGTTAATTC-3' |
| SMC5 mutagenesis | SMC5-p.R425*-F | 5'-GAAATAATTGATAAGTGAAGAGAGAGGGAAACT-3' |
| SMC5 mutagenesis | SMC5-p.R425*-R | 5'-AGTTTCCCTCTCTTCACTTATCAATTATTTTC-3' |
| SMC5 mutagenesis | SMC5-p.R372-del-F | 5'-TTGACCGACAGAGGATAGGTAATACCCGC-3' |
| SMC5 mutagenesis | SMC5-p.R372-del-R | 5'-GCGGGTATTACCTATCCTCTGTGCGGTCAA-3' |
| SMC5 construct sequencing | SMC5-seq1 | 5'-GCAAGAAGACGTCAACTCCA-3' |
| SMC5 construct sequencing | SMC5-seq2 | 5'-CGAGCAGATAAGGTTGGGTTT-3' |
| SMC5 construct sequencing | SMC5-seq3 | 5'-GGAATATGAAAATGTTTCGTCAGG-3' |
| SMC5 construct sequencing | SMC5-seq4 | 5'-TGGACGATCATATTGTACGTTTT-3' |
| SMC5 construct sequencing | SMC5-seq5 | 5'-CAGCAGAAGAAAAGTATGTGGTG-3' |
| SMC5 construct sequencing | SMC5-seq6 | 5'-ACAGTGATCTCTGAGAAGAACAAA-3' |
| SMC5 construct sequencing | SMC5-seq7 | 5'-GCAGTGTGCTGGTGAAGTTG-3' |
| SLF2 construct sequencing | SLF2-seq1 | 5'-AGAAGTTGGGTGCGTGGTT-3' |
| SLF2 construct sequencing | SLF2-seq2 | 5'-TTTGGCTAAATATTTGGAGGCTA-3' |

| | | |
|----------------------------------|------------------------|------------------------------|
| <i>SLF2</i> construct sequencing | <i>SLF2</i> -seq3 | 5'-TTCCCATGAATCAGAAGAGGA-3' |
| <i>SLF2</i> construct sequencing | <i>SLF2</i> -seq4 | 5'-CACTTGGAACACGGGAAAGT-3' |
| <i>SLF2</i> construct sequencing | <i>SLF2</i> -seq5 | 5'-GAGCAGGAGGCTTTCCTGTA-3' |
| <i>SLF2</i> construct sequencing | <i>SLF2</i> -seq6 | 5'-ATCATCCGAAACAGCCACTT-3' |
| <i>SLF2</i> construct sequencing | <i>SLF2</i> -seq7 | 5'-ATGCCAGACAGAGTTCAGG-3' |
| <i>SLF2</i> construct sequencing | <i>SLF2</i> -seq8 | 5'-TTTCCTGCCATTTCCATGT-3' |
| <i>SLF2</i> construct sequencing | <i>SLF2</i> -seq9 | 5'-AGTAGGCCGACAGTTCTGGA-3' |
| <i>actinb2</i> -RT-PCR | <i>actinb2</i> _F | 5'-CCACCATGTACCCTGGCATT-3' |
| <i>actinb2</i> -RT-PCR | <i>actinb2</i> _R | 5'-GTCACCTTCACCGTTCCAGT-3' |
| <i>slf2</i> mRNA expression | <i>slf2</i> -qPCR-F1 | 5'-TCTCCTGCAAAAGTCCAGTTC-3' |
| <i>slf2</i> mRNA expression | <i>slf2</i> -qPCR-R1 | 5'-GCCTCTCAGGACTTCGTCTG-3' |
| <i>slf2</i> mRNA expression | <i>slf2</i> -qPCR-F2 | 5'-ATGCGTCCTTCATCTCTGCT-3' |
| <i>slf2</i> mRNA expression | <i>slf2</i> -qPCR-R2 | 5'-TCTCTGGGCTGAGGGTAAGA-3' |
| <i>actinb2</i> mRNA expression | <i>actinb2</i> -qPCR-F | 5'-TTGTTGGACGACCCAGACAT-3' |
| <i>actinb2</i> mRNA expression | <i>actinb2</i> -qPCR-R | 5'-TGAGGGTCAGGATACCTCTCTT-3' |

Table S12. Primers used for sequencing of SLF2/SMC5

| SLF2 Sequencing Primers | Primer name | Sequence |
|--------------------------------|--------------------|---------------------------------|
| | SLF2-760F | 5'-AAGGAGCAAATGGAGCAGAGAA-3' |
| | SLF2-1624F | 5'-TGCGCTCAGAATATGGCACT-3' |
| | SLF2-2556F | 5'-GTCTGATGTAGCAGCTGTGTT-3', |
| | SLF2-2961F | 5'-TGA ACTCTCCAGTCATCCCCA-3' |
| | SLF2-1768R | 5'-GGCTTTATCTGAAGGTGCTGC-3' |
| | SLF2-2575R | 5'-ACACAGCTGCTACATCAGACA-3' |
| | SLF2-3437R | 5'-CTGGCGACCAAGTCTTTCAC-3' |
| | | |
| SMC5 Sequencing Primers | Primer name | Sequence |
| | SMC5-300F | 5'-ACCTGCTTTCATGGGACGAG-3' |
| | SMC5-975F | 5'-AGAAAAGGCAACAGATATTAAGGAG-3' |
| | SMC5-1563F | 5'-GGTTTTCTCAAAGAGGTTTCGTG-3' |
| | SMC5-1681F | 5'-GTTTTCTCAAAGAGGTTTCGTG-3' |
| | SMC5-2188F | 5'-GAGGAAGAGCGAAAAGCAAGT-3' |
| | SMC5-2322F | 5'-TGCTTTTCGCTCTTCCTCTTCA-3' |
| | SMC5-2486F | 5'-CCGCATCTTCACAACTCCGT-3' |
| | SMC5-687R | 5'-GCATGAGGTCTCGAGCTGTTT-3' |
| | SMC5-1194R | 5'-GGGCTGAAGATTCTCGCAGT-3' |
| | SMC5-1234R | 5'-TTCTCCTCTGTCCGTCAAGC-3' |
| | SMC5-3178R | 5'-TTTTGCAGGAGCTTTGGTGT-3' |

Table S13. Primers used for the generation of SLF2 and SMC5 deletion/mutation constructs

| SLF2 deletion constructs | Sequences of primer pairs |
|----------------------------------------|----------------------------------------------------------------------------------------------------|
| SLF2 Δ1 | 5'-TCCAGCACAGTGGCGGCCGCAACAGCTCCAGAAGCCTTAG-3' and 5'-CTAAGGCTTCTGGAGCTGTTGCGGCCGCCACTGTGCTGGA-3' |
| SLF2 Δ2 | 5'-AGAAGAATGATAGAGATCGAAATTCTGGCAATTCTGGCCA-3' and 5'-TGGCCAGAATTGCCAGAATTTTCGATCTCTATCATTCTTCT-3' |
| SLF2 Δ3 | 5'-GTGATGTGTTGCGCTTAGAAAACCTAGACAGTGATGAGGA-3' and 5'-TCCTCATCACTGTCTAGGTTTTCTAAGCGCAACACATCAC-3' |
| SLF2 Δ4 | 5'-CAGGAAATTC AATGCAGGTCTGTTTCGGATGATGTCAGT-3' and 5'-ACTGACATCATCCGAAACAGACCTGCATTGGAATTTCTCTG-3' |
| SLF2 Δ5 | 5'-AGATTTTTTTGACAACACAAAGGCAACTGAGACAGTGCCT-3' and 5'-AGGCACTGTCTCAGTTGCCTTTGTGTTGTCAAAAAAATCT-3' |
| SLF2 Δ6: | 5'-TGGGCATAAATGAACTCTCCTAGGGGCCCGTTTAAACCCG-3' and 5'-CGGGTTTTAAACGGGCCCTAGGAGAGTTTCATTTATGCCCA-3' |
| SLF2 Δ7 | 5'-GCCGAGGCATTAAATCCCCACCTGTCCCTGTGTTAAAGTG-3' and 5'-CACTTTAACACAGGGACAGGTGGGGATTTAATGCCTCGGC-3' |
| SLF2 Δ8 | 5'-CGTCTGCTTATCACTATGTCCCAATTTTTTCAACTTCC-3' and 5'-GGAAGTGTGAAAAAATTGGGACATAGTGATAAGCAGACG-3' |
| SLF2 Δ9 | 5'-GGAAAGAAAGTGAAGATTCACAGCTGGTCCCTAATTGGAC-3' and 5'-GTCCAATTAGGGACCAGCTGTGAATCTTCACTTTCTTTCC-3' |
| SLF2 Δ10 | 5'-ACAACCTCCTGTGGTTGGTATGTTTCTCATTCTTTTTCTTC-3' and 5'-GAAGAAAAAGAATGAGAACATACCAACCACAGGAGGTTGT-3' |
| SLF2 Δ11 | 5'-CACTGAAAAGAAAATAAGGTCCCCAATCAGAATTGGAGA-3' and 5'-TCTCCAATTCTGATTGGGGACCTTAGTTTTCTTTTCAGTG-3'. |
| | |
| MBR1 | 5'-GAACATGCGGCCGCTTCAATCAGTATACCTTG-3' and 5'-CGCTCTAGAGCCTAACTAATTCACCGACTAA-3' |
| MBR2 | 5'-GAACATGCGGCCGCTTCAATCAGTATACCTTG-3' and 5'-CAGCATTCTAGACGCTAAGAATCTGGTACCCA-3'. |
| | |
| SLF2 and SMC5 mutant constructs | Sequences of primer pairs |
| SLF2 p.Ser815Ter | 5'-TGTTTCGGATGATGTGAGTTCATACAGACTG-3' and 5'-CAGTCTGTATGAACTCACATCATCCGAAACA-3' |
| SLF2 p.Arg336Lysfs: | 5'-AATTCCTGAAAAAAGAAAAAGGAACTCTG-3' and 5'-CAGAGTTCCTTTTTCTTTTTTTCAGGGAATT-3' |
| SLF2 p.ΔSer907Phefs | 5'-TCCTGAAACCAACATTTTAAATG-3' and 5'-AAAAAATTGGCTTATAAGATGAATC—3' |
| SLF2 p.Asn861Ile | 5'-GTGTTTTTTCATTATGGGGATTGATTTTAG-3' and 5'-AGCTGCTACATCAGACAATG-3' |
| SLF2 .ΔAla1085_Arg1110 | 5'-AAACACTTTGTGCTACTC-3' and 5'-CTGCTTTTCAAGTTCTAAATG-3' |
| SLF2 p.Aps783Serfs | 5'-TCAGATTTTTTTGACAACAC-3' and 5'-TGTTTTTCCCGATTTAAGAATAAG-3' |
| | |
| SMC5 p.Arg425Ter | 5'-AATTGATAAGGGAAGAGAGAGG-3' and 5'-ATTTTCGCCTTACATAATG-3' |
| SMC5 p.ΔArg372 | 5'-GAGAATAGGTAATACCCGC-3' and 5'-TGTCGGTCAAGCTCTTCA-3' |
| SMC5 p.His990Asp | 5'-AACTCCTCATGATCAAAGTGG-3' and 5'-AATTCATGCAGTTGAGTAC-3' |

Table S14. Primers used for RT-PCR expression studies

| Experiment | Primer name | Identifier | Sequence |
|---------------------------|--------------------|-------------------|-------------------------|
| Expression studies | | | |
| RT-PCR | SLF2_ex16_common_F | P1 | GTGCAGATGAAGCCTTCTGA |
| RT-PCR | SLF2_1173_ex20_R | P2 | GGTACCCAGAAGTCATGAAGC |
| RT-PCR | SLF2_1186_ex19_R | P3 | TGAAGAGTGCCATTCAGCAA |
| RT-PCR | SLF2-E1-FOR | P4 | CGCGCTGCCATCTGAGACCC |
| RT-PCR | SLF2-E3-REV | P5 | GGACAGGCTGCTCCTGCTGC |
| RT-PCR | SLF2-E14-FOR | P6 | GGACAGGCTGCTCCTGCTGC |
| RT-PCR | SLF2-I19-REV | P7 | GGTGCCTGAACTCTGTCTGGGC |
| RT-PCR | SLF2-E20-REV | P8 | TGAAGAGTGCCATTCAGCAAACT |